UNIVERSITY OF CALIFORNIA, SAN DIEGO

Graphene/Silicon Schottky Junction Based Solar Cells

A dissertation submitted in partial satisfaction of the requirements for

the degree Doctor of Philosophy

in

Material Science and Engineering

by

Serdar Yavuz

Committee in charge:

Professor Prabhakar R. Bandaru, Chair

Professor David P. Fenning

Professor Javier Garay

Professor Olivia A. Graeve

Professor Donald J. Sirbuly

2018

The Dissertation of Serdar Yavuz is approved, and it is acceptable in quality and form for publication on microfilm and electronically:

Chair

University of California, San Diego

2018

DEDICATION

Dedicated to 301 beautiful and hardworking souls who died on 13 May 2014, an explosion at a coal mine in Soma, Manisa, Turkey.

TABLE OF CONTENTS

LIST OF ABBREVIATIONS

AA: Active area

ALD: Atomic Layer Deposition

CVD: Chemical vapor deposition

PECVD: Plasma enhanced chemical vapor deposition

PCE: Power conversion efficiency

FF: Fill factor

TCE: Transparent conductive electrode

TOPcon: Tunnel oxide passivated contact

PERC: Passivated emitter and Rear Cell

PERL: Passivated emitter, Rear Locally-doped

PERT: Passivated emitter, Rear Totally-doped

LIST OF SYMBOLS

Φ_b: Schottky barrier height

W: Work function

η: Efficiency

τ: Lifetime

λ: Wavelength

χ: Electron affinity

q: Electronic charge

k_b: Boltzmann constant

R_s: Series resistance

R_{sh}: Shunt resistance

A*: Richardson constant

J: Current density

I: Current

V: Voltage

T: Temperature

LIST OF FIGURES

LIST OF TABLES

ACKNOWLEDGEMENTS

Before beginning this thesis, I would like to express my gratitude to people who contributed to its creation.

Firstly, I would like to acknowledge and thank my advisor Professor Prabhakar R. Bandaru for his guidance, support and sharing his wisdom during the course of my PhD. I would like to thank my committee members for their helpful comments and suggestions, especially Professor David P. Fenning for valuable feedback and discussions. I also would like to thank my previous supervisor, Professor Sungho Jin for his support.

I would like to special thank Aybuke Gul Turker for her enormous support, encouragement as well as help with sample preparation, data collection and analysis. I am grateful for the tremendous help during my PhD.

I would like to acknowledge and thank the following individuals for their help and contributions to this study: Cihan Kuru for sharing his experience with solar cell fabrication process; Elizabeth Caldwell for reflectance measurements; Erick M. Loran, Yun Goo Ro for electrical measurements set up; Alireza Kargar, Duyoung Choi, Cyrus Rustomji; for useful discussion; Bandaru Lab members; Mehmet F. Canbazoglu, Nirjhar Sarkar, Peng Chen, Bei Fan, Hidenori Yamada, Anna Alexander, Rajaram Narayanan, Roisul Galib, Zichen Zang, Abishek Satisha for group meeting discussions; my housemate Jesse Lu, for discussing the n-/p-doping strategies for graphene at 3:00AM in the morning.

I would like to thank Calit2 staff at UCSD; Sean Park for sharing his thin film deposition expertise and wisdom, Larry Grissom for the help with ALD, PECVD deposition tools and their operation procedure.

Last but not least, I would like to thank so much my family for their enormous help, trust, and encouragement as well as continues support throughout my life.

Chapter 3, in part, has been published in Nanoscale in 2016 which titled “Graphene oxide as a p-dopant and an antireflection coating layer, in graphene/silicon solar cell” by Serdar Yavuz, Cihan Kuru, Duyoung Choi, Alireza Kargar, Sungho Jin and Prabhakar R. Bandaru. The dissertation/thesis author was the primary investigator and author of this paper.

Chapter 4, in part, has been submitted to Solar Energy Materials and Solar Cells which titled “Enhanced power conversion efficiency in graphene/silicon solar cell, through the electrical carrier and interface engineering” by Serdar Yavuz, Ernesto Magana, Aybuke Turker, David P. Fenning and Prabhakar R. Bandaru. The dissertation/thesis author was the primary investigator and author of this paper.

Chapter 5, in part, has been submitted to Nano Letters which titled “Improved conversion efficiency and stability, through the use of aluminum oxide, in an n-graphene/p-silicon solar cell” by Serdar Yavuz, Erick M. Loran, Nirjhar Sarkar, David P. Fenning and Prabhakar R. Bandaru. The dissertation/thesis author was the primary investigator and author of this paper.

VITA

2009 Bachelor of Science, Ataturk University

2013 Master of Science, Rize University

2018 Doctor of Philosophy, University of California, San Diego

PUBLICATIONS

1. Improved conversion efficiency and stability, through use of aluminum oxide, in an n-graphene/p-silicon solar cell; **Serdar Yavuz**; Erick M. Loran, Nirjhar Sarkar, David P. Fenning, Prabhakar R. Bandaru, submitted,

2. Enhanced power conversion efficiency of graphene/n-silicon solar cell, through electrical carrier and interface engineering; **Serdar Yavuz**, Ernesto Magana, Aybuke Turker, David P. Fenning, Prabhakar R. Bandaru, submitted.

3. Graphene oxide as a p-dopant and an antireflection coating layer, in graphene/silicon solar cell; **Serdar Yavuz**, Cihan Kuru, Duyoung Choi, Alireza Kargar, Sungho Jin, and Prabhakar R. Bandaru,; Nanoscale, 2016, 8,

4. Enhanced Power Conversion Efficiency of Graphene/Silicon Heterojunction Solar Cells Through NiO Induced Doping; Cihan Kuru,; **Serdar Yavuz,**; Alireza Kargar,; Duyoung Choi,; Chulmin Choi,; Cyrus Rustomji,; Sungho Jin,; Prabhakar R Bandaru,; Journal of Nanoscience and Nanotechnology, 2016, 16, 1190

5. High-performance flexible hydrogen sensor made of WS_2nanosheet-Pd nanoparticle composite film, Cihan Kuru,; Duyoung Choi,; Alireza Kargar,; Chin Liu, **Serdar** ;**Yavuz,**; Chulmin Choi,; Sungho Jin,; Prabhakar R. Bandaru,; Nanotechnologhy, 2016,

6. Solution-Processed $CoFe_2O_4$ Nanoparticles on 3D Carbon Fiber Papers for Durable Oxygen Evolution Reaction, Alireza Kargar,; **Serdar Yavuz,**; Tae Kyoung Kim,; Chin- Hung Liu,; Kuru, Cihan; Rustomji, Cyrus S; Jin, Sungho; Bandaru, PrabhakarR;, ACS Applied Materials & Interfaces, 2015, 7

7. MoS_2 Nanosheet-Pd Nanoparticle Composite for Highly Sensitive Room Temperature Detection of Hydrogen., Kuru, Cihan; Choi, Chulmin; Kargar, Alireza; Choi, Duyoung Kim; Young Jin, Liu; Chin Hung; **Yavuz, Serdar**; Jin, Sungho; Advanced Science, 2015, 2

8. The effects of external electric field on mass attenuation coefficient of some semiconductors; **Yavuz**,**Serdar;** Master's thesis, Department of Physics, Rize University, Rize-Turkey, 2011. Presented as a Masters' Thesis.

ABSTRACT OF THE DISSERTATION

Graphene/Silicon Schottky Junction Based Solar Cells

by

Serdar Yavuz

Doctor of Philosophy in Materials Science and Engineering

University of California, San Diego, 2018

Professor Prabhakar R. Bandaru, Chair

After experimental discovery in 2004, graphene is one of the most extensively studied materials in last 15 years. The sp^2 bonded carbon atoms in honeycomb geometry in the atomic thickness leads to use of graphene in many applications including but not limited to sensors, field effect transistor, batteries, photo detectors, super capacitors, diodes. In particular, the highly conductive, highly transparent (97.7%) and mechanical flexibility of graphene indicated its use as a transparent conductive electrode (TCE). As a new emerging material for TCE applications, the incorporation of graphene with well-studied silicon leads to a new photovoltaic area:

Graphene/Silicon (Gr/Si) solar cell. Over the course of 8 years, the efficiency has been improved up to 17%.

After a brief introduction in chapter 1 and 2, chapter 3 introduces a promising alternative as incorporation of two-dimensional materials for Gr/Si solar cell. It is shown that applying graphene oxide via a simple spin coating process increases the efficiency of solar cell by a factor of three. A detail analysis of factors that contributions PCE enhancement are discussed. This chapter highlights the use of graphene oxide as an antireflection coating in Gr/Si solar cell.

In chapter 4, the highest efficiency Gr/Si solar cell is presented. Through a detail analysis and addressing the efficiency limiting parameters, a more effective doping along with an engineered design is discussed. The experimental studies and related discussions of the highest efficiency graphene/n-silicon (Gr/n-Si) solar cell is highlighted.

In chapter 5, It is demonstrated that the modifying the work function of graphene through an n doping allows us to use graphene as an electron extraction layer. A detail analysis and effective doping methodologies yielded the highest efficiency Gr/p-Si solar cell obtained so far. In addition, it is demonstrated that the one of most critical aspect of Gr/Si solar cells, stability, can be address through the use of aluminum oxide.

In chapter 6, a future direction for the possible efficiency improvements of Gr/Si solar cells by incorporating new doping strategies and materials for graphene is discussed. A strategy following the foot prints of p-n junction counterparts is provided for future studies.

CHAPTER 1: SOLAR CELLS

1.1 Introduction

The energy demand of world increases so rapidly that the natural resources such as fossil fuels and coal cannot fulfill the demand. In addition, those resources are limited and we have relied on them after the industrial revolution. Using those resources over the past two century resulted in a significant problem for the future of world: carbon emission which is the main contributor of greenhouse gasses. A promising alternative for energy production was emerged in the last century: photovoltaic solar cells. Using sunlight as a natural resource, which is the most abundant energy source, made solar cells an ideal alternative as an energy production platform.

Solar cells convert sunlight into electricity. By doing so, they produce electricity without releasing any harmful byproduct which makes them more attractive for the world's future energy demand. In addition, solar cells can be used anywhere that sunlight can reach, from any rural part of the world to the space. Indeed that makes solar cells even more promising by avoiding many complications of the transportation of electricity form a power plant to a house. While technological progress in the solar cell manufacturing as well as the scientific contributions through higher solar cell efficiency reduced the cost of solar panels significantly, they are still operating below their potential. Therefore, improving the efficiency of solar cells as well as reducing the manufacturing cost is critical to make solar cells more affordable.

1.2 Efficiency of solar cell

Solar cells are designed to produce electricity when exposed to sunlight. When photons absorbed, the electron hole pairs are generated and collected through an external circuit. Thus, the efficiency of solar quantifies as the ratio of obtained electrical energy to the input solar

energy. In such as energy conversion system, the power is defined as the product of current (I) and the electrical potential of system (V), there is a point where the product of those two gives the highest power, which is the maximum power point of solar cell and represented with mpp abbreviation. Maximum power that can be obtained in a solar cell is graphically presented in Figure 1.1.To convert as much sunlight into the electricity, a solar cell is operated at its maximum power so that a general term the power conversion efficiency (PCE) or simply efficiency (η) is used for simplicity and it is given by

$$\eta = \frac{P_{mpp}}{P_{in}} \qquad (1.1)$$

Where P_{in} is the incident solar power. The efficiency is the most important output of any solar cells. Independently confirmed and the most efficient solar cells reported in literature for various materials are listed in Table 1.1.[1]

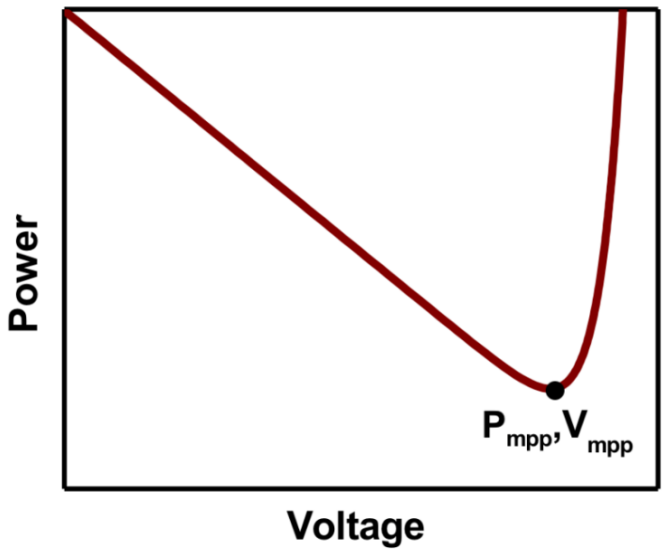

Figure 1.1: Power –Voltage curve of a typical solar cell.

Table.1.1: The most efficient solar cells and corresponding output parameters under standard testing conditions.

Solar Cell	J_{sc}(mA/cm^2)	V_{oc} (V)	FF (%)	PCE (%)
Crystalline GaAs	29.68	1.12	86.5	28.8
Crystalline Si	42.65	0.738	84.9	26.7
Crystalline InP	31.15	0.939	82.6	24.2
Multicrystalline Si	41.08	0.674	80.5	22.3
CdTe	30.25	0.875	79.4	21.0
Perovskite	24.92	1.125	74.5	20.9
Amorphous Si	16.36	0.896	69.8	10.2

1.3 *J-V* curves of solar cell

As an alternative to current (*I*), a more universal term "current density" (*J*) which is the normalized current per area is mostly used in solar cells, and *I-V* curve of solar cell often called as *J-V* curve. While efficiency is the most important output of a solar cell, it is beneficial to describe the efficiency with other parameters to understand how it can be made more effective. The three parameters that made up of efficiency are: the open circuit voltage, V_{oc}, where the current density is zero, the short circuit current density, J_{sc}, the maximum current density at the absence of applied potential, and the fill factor, *FF*. Figure 1.2 represents a typical *J-V* curve of a

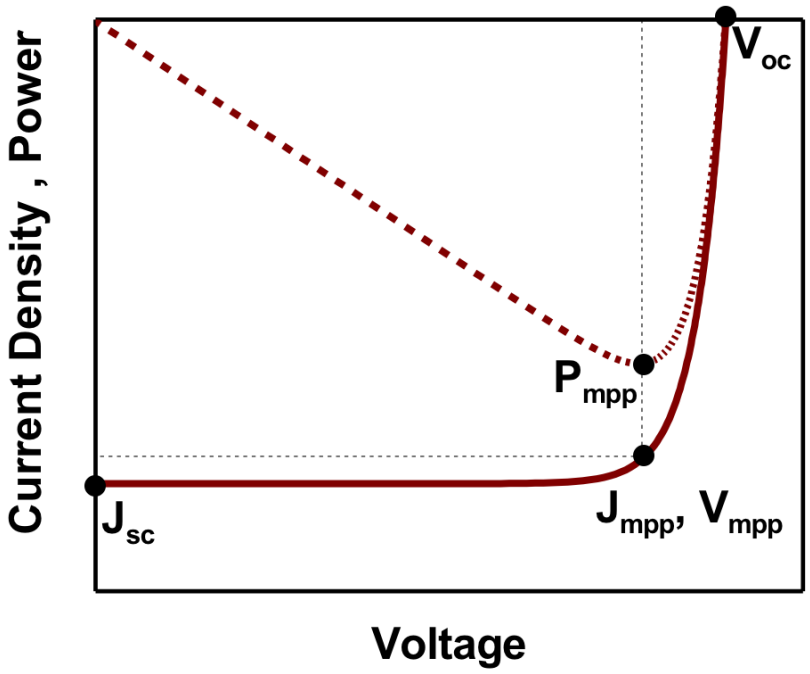

Figure 1.2: Current density (*J*)- voltage (*V*) curve (solid line) of solar cell and related output parameters. As a reference Power-V curve of solar cell is shown.

solar cell in which related output parameters are marked on the Figure. After defining the output parameters, the efficiency given in Equation 1.1 can be redefined as

$$\eta = \frac{V_{oc} J_{sc} FF}{P_{in}} \qquad (1.2)$$

Figure 1.2 also plots the Power-Voltage curve of solar cell with dash line. It can be seen that there are two parameters that corresponds to the maximum power point (mpp) of solar cell: current density at mpp (J_{mpp}) and voltage at mpp (V_{mpp}). Therefore the equation 1.1 can be rewritten in terms of *J* and *V*

$$\eta = \frac{P_{mpp}}{P_{in}} = \frac{V_{mpp} J_{mpp}}{P_{in}} \qquad (1.3)$$

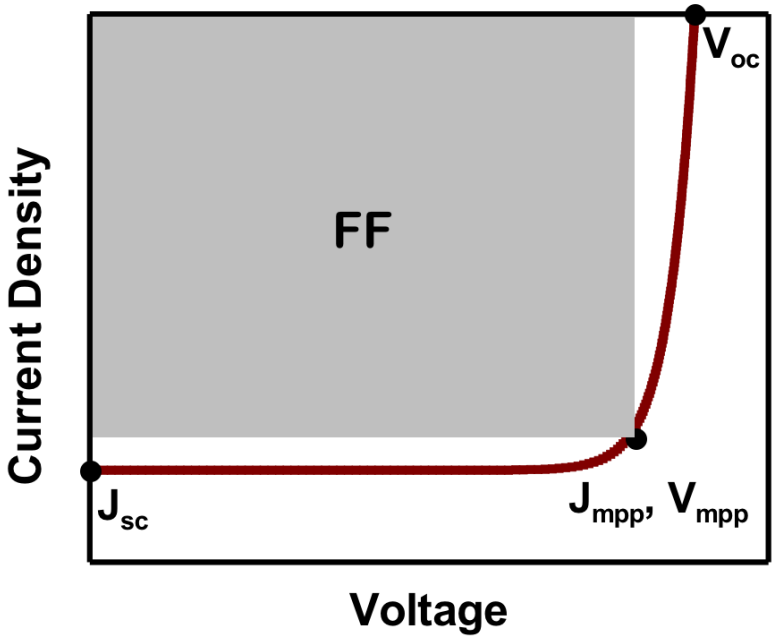

Figure 1.3: Graphical fill factor (FF) of a solar cell.

Now, using Equation 1.2 and 1.3, a mathematical expression for the *FF* can be obtained:

$$FF = \frac{V_{mpp} J_{mpp}}{V_{oc} J_{sc}} \qquad (1.4)$$

Graphically, *FF* can be described as the "*squareness*" of the *J-V* curve or it is also referred as the "*biggest rectangle"* that can fit under the *J-V* curve, as shown in Figure 1.3. In this thesis, the *FF* of graphene/silicon solar cells, which was one of the limitations of this PV cells, will be discussed in detail (Chapter 4).

In this thesis, *J-V* curves of solar cells are presented based on two different measurement conditions: (i) *J-V* curve under standard illumination, 100mW/cm^2, A.M 1.5G, and (ii) dark *J-V* curve that is carried out in dark room at the absence of illumination. Both measurements are carried out at room temperature (25°C).

1.4 Photo generated current

When there is no illumination, a solar cell acts like a diode and the *J* that flows across the solar cell is given by ideal diode equation:[2]

$$J = J_s \left[\left(exp \frac{qV}{k_b T} \right) - 1 \right] \qquad (1.5)$$

Where, q is the electronic charge, k_b is the Boltzmann constant, V is the applied voltage, T is the temperature and J_s is the saturation current density. There are several assumptions in Equation 1.5 which is detailed in literature.[3] Under illumination, the photo generated carriers (electron-holes) in photoactive material are creates a current that flows through the solar cell to the electrical contacts. This current called photo/light generated current (J_L) and the diode equation modifies as:

$$J = J_L - J_s \left[\left(exp \frac{qV}{k_b T} \right) - 1 \right] \qquad (1.6)$$

Although, the Equation 1.5 is very helpful and can be solved for J_{sc} and V_{oc} by assuming J_L is equal to the J_{sc}, it is not completely true for a real solar cell since the resistance of solar cell is neglected. A more general equation including the component of resistance needs to be included. Thus, Equation 1.6 can be extended as:

$$J = J_L - J_s exp \left(\frac{q(V + JR_s)}{k_b T} \right) + \frac{V + JR_s}{R_{sh}} \qquad (1.7)$$

Here, R_s is the series resistance and R_{sh} is the shunt resistance of solar cell. While Equation 1.6 cannot provide an explicit expression for FF, several derivations have been demonstrated[4–6] to

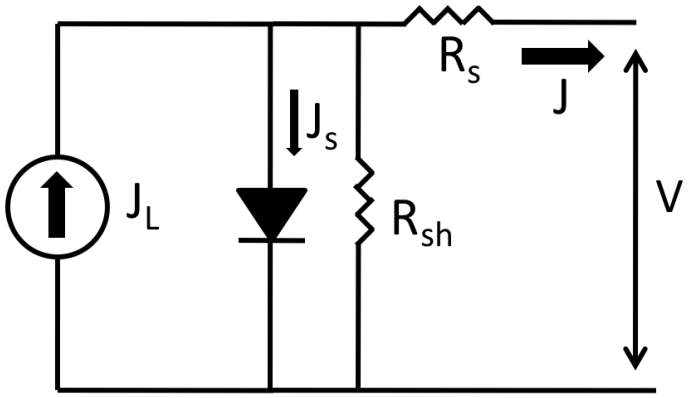

Figure 1.4: An equivalent circuit of a basic solar cell under illumination.

correlate the *FF* to R_s and R_{sh}. Ideally, an R_s as low as and an R_{sh} as high as possible is desirable for a solar cell. A schematic circuit equivalent of solar cell including R_s and R_{sh} is presented in Figure 1.4. The effect of R_s and R_{sh} on solar cells *FF* is presented in Figure 1.5. As can be seen J_{sc} and V_{oc} are not affected by R_s and R_{sh} unless R_s and R_{sh} are too high and too low, respectively.

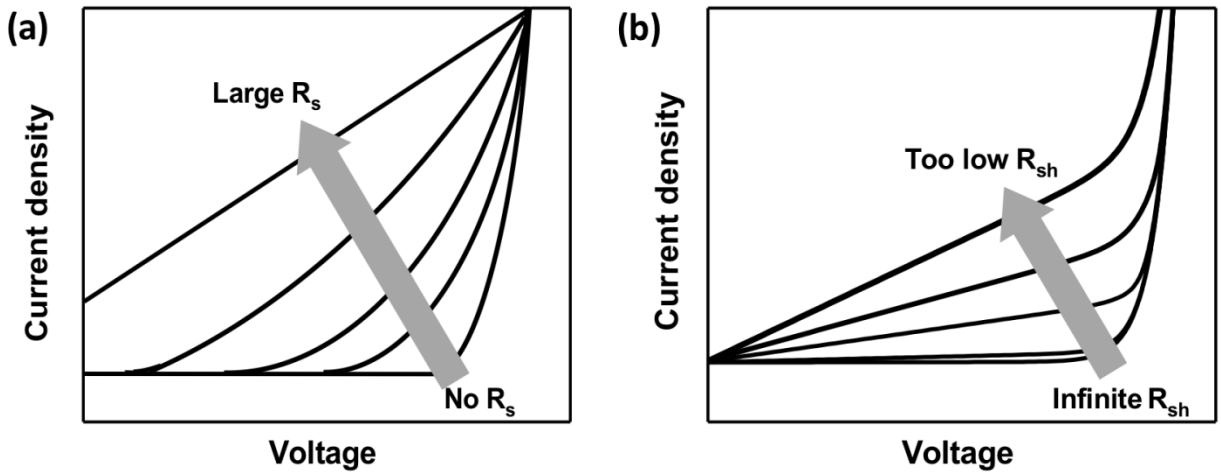

Figure 1.5: (a) *J-V* curve of solar cell as a function of R_s, the direction of arrow indicates increasing R_s. (b) Evolution of the *J-V* curve with respect to $R_{sh,}$ the direction of arrow shows the decreasing R_{sh}.

1.5 Summary

While significant improvement in the efficiency of solar cells as well as cost reduction in manufacturing have been realized over the last three decades, the increasing energy demand and our dependence of electricity keeps growing. Therefore, improving the efficiency of solar cells and/or reducing the cost to make them more applicable is a necessity for our future. In addition to current and commercially available solar cells, there is a tremendous ongoing research for possible solar materials and new solar cells designs. Within that scope, this thesis focuses on a possible alternative that can contribute the energy production through a solar cell which was emerged in 2010[7] as a graphene/silicon solar cell.

CHAPTER 2: GRAPHENE/SILICON SCHOTTKY JUNCTION SOLAR CELLS

2.1 Graphene as a transparent conductive electrode

Atomic thickness of single layer graphene (SLG) provides exceptional transparency with over 97% transmittance at the wavelength range from 300nm to over 1000nm. Combining this transparency with superior conductivity[8] as high as 10^6S/cm suggested its possible application as a transparent conductive electrode (TCE). In addition, mechanical flexibility of graphene is an advantageous compared to brittle TCE used in industry such as indium-tin-oxide (ITO). Due to above mentioned reasons, graphene was considered as a suitable alternative to replace the ITO. Although, the sheet resistance of SLG is around an order of magnitude higher than that of industrial TCEs, the modification of electrical characteristic has shown to be promising for such applications. While obtaining a large scale of SLG sheet was a significant issue, a remarkable improvement for large area graphene synthesis and its first TCE application in a device was shown in 2010.[9] These scientific progress suggested its use for photovoltaic applications.

2.2 Schottky junction

A Schottky junction forms when a metal and a semiconductor that have adequate potential energy barrier in between are brought together. This energy barrier is called Schottky barrier and it forms at the metal–semiconductor (MS) interface and called as MS-Schottky junction. Due to simple and cost-effective fabrication procedure, MS junction solar cells have been studied extensively in early 1970.[10] However, the efficiency of solar cells was limited due to the low barrier height and it is often reported that the Fermi level at the interface is independent from the work function of metal which limited the tunability of Schottky barrier.[11] Inserting a thin (< 3nm) oxide/insulator layer between the metal and semiconductor, so called

MIS junction, significantly improved the efficiency.[12,13] It was concluded that the thin oxide layer creates an inversion layer at the interface and the first generation of those types called metal-insulator-semiconductor, inversion layer (MIS-IL).[14] Improved surface passivation techniques along with the introducing diffused emitter yielded efficiency over 20% in the first years of twenty first century.[15]

While the low cost manufacturing was appealing for MIS-IL solar cell, the open circuit voltage of solar cell was limited to the barrier height. Therefore the overall efficiency was significantly low compared to p-n junction counterparts. Progress in the fabrication process significantly reduced the cost of p-n junction solar cell and photovoltaic research mostly focused on p-n junction solar cells.

2.3 Graphene/Silicon Schottky junction based solar cell

Combined with the high conductivity, overlapping the valance band maximum with conduction band minimum at K point which indicates a zero bandgap material, suggested that graphene can be considered as metal. In that case, incorporating graphene with a semiconductor implies a Schottky junction formation. Here, the difference between the work function of graphene (W_{Gr}) and electron affinity of semiconductor (X_s) creates a built in potential (V_{in}) which can separate the electron hole pair generated in semiconductor upon photon absorption. Since the work function of graphene and Fermi level of semiconductor should be at equilibrium, the Schottky barrier height is given with the electrostatic potential differences of W_{Gr} graphene and semiconductor, say Si (X_{Si}):

$$\Phi_b = W_{Gr} - X_{Si} \qquad (2.1)$$

As X_{Si} is constant, a higher W_{Gr} would provide a higher barrier. Since the junction should be operating at equilibrium, the Φ_b causes a band bending creating a built in potential (V_{in}) as shown below. Correlation between the Φ_b and V_{in} can be express as follows:[16]

$$\Phi_b = V_{in} + e^{-1} n k_b T ln\left(\frac{N_C}{N_D}\right) \quad (2.2)$$

Where, N_C is the density of states in conduction band and N_D is the doping concentration of semiconductor. As the second term in equation 2.2 is constant, V_{in} scales up linearly with the Φ_b. The Φ_b can be extracted from the dark *J-V* measurements of solar cell using the thermionic emission model in the form of:[17]

$$J = J_s\left[\left(exp\frac{eV}{nk_bT}\right) - 1\right] \quad (2.3)$$

in here J_s; the saturation current density is defined:

$$J_S = A^* T^2 exp\left(\frac{\Phi_b}{k_b T}\right) \quad (2.4)$$

where, A^* as the effective Richardson's constant, Φ_b as the Schottky barrier height, n is the diode ideality factor, k_b is the Boltzmann constant, and T is the temperature. From *ln(J)-V* plot at the absence of illumination (dark *J-V* measurements), Φ_b can be estimated from J_s.

How does Φ_b correlate the open circuit potential (V_{oc}) of solar cell? While Φ_b is obtained from *J-V* measurements, V_{in} can be estimated from the capacitance versus voltage (C-V) measurements in the form of;

$$C^{-2} = 2\left(\frac{(V_R + V_{in}}{eN_D\varepsilon_s\varepsilon_0}\right) \quad (2.5)$$

where V_R is the reverse bias potential. It can be seen from the Equation 2.5, C^{-2} linearly changes with V_R. Therefore, a plot of C^{-2} vs V_R provides a linear line where the intercept of *x* axis gives the V_{in}. The extracted values of V_{in} from C-V measurements indicated a good correlation with V_{oc}.[16] From equation 2.2, since Φ_b scales up with V_{in}, it should also change linearly with the V_{oc}. Indeed, form the literature of Gr/Si solar cells, a plot of Φ_b as a function of V_{oc} indicates a linear dependence as highlighted in Figure 2.1. While the V_{oc} of Gr/Si may be affected by other parameters such as surface recombination, bulk lifetime, current density, series resistance and so on, it can be clearly seen that a higher Φ_b yields a higher V_{oc} and subsequently improves the PCE of Gr/Si solar cells.

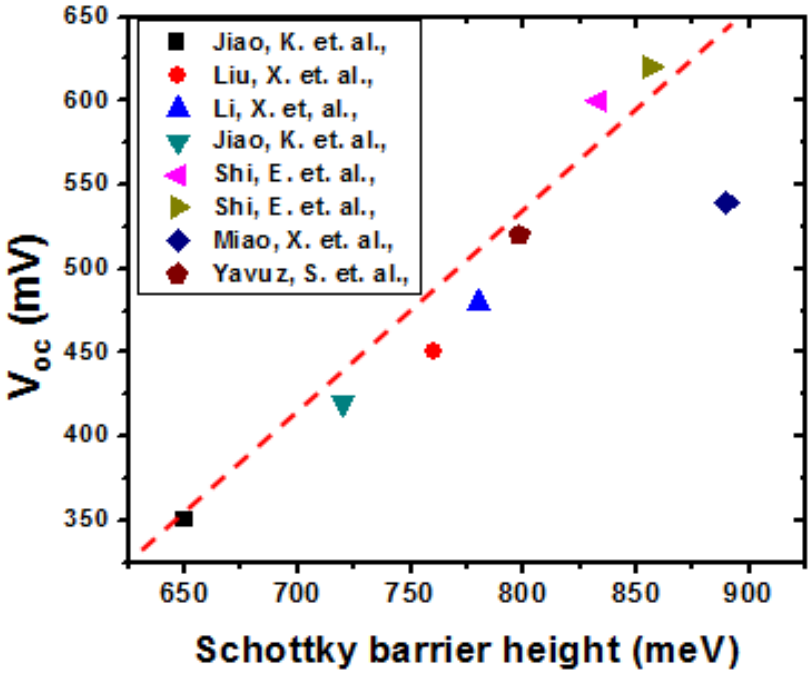

Figure 2.1: Correlation between the V_{oc} and Schottky barrier height (Φ_b) of Gr/n-Si solar cells from the literature is presented.[7,16,18–21] A linear dependence (with small variations) indicates that higher Φ_b provides a higher V_{oc}.

2.4 Doping of graphene for photovoltaic applications

As a 2-dimensional material with an atomic thickness, Gr provides an ideal platform to alter/modify its electrical and optical properties.[22]This tunable electrical characteristic enables graphene (Gr) to be used both as an electron and a hole extraction layer in organic and inorganic photovoltaic devices.[21,23] For example, it is shown that bis(trifluoromethanesulfonly)-amide (TFSA)[24] and nitric acid (HNO_3)[25] may *p*-dope the graphene while TiO_x[26] could serve as an *n*-dopant. In here, p- doping, say through HNO_3, is promoted by pulling electrons from graphene which induces hole doping to graphene while TiO_x has been shown to donate electrons to graphene implies an n-doping. From electrostatic point of view, hole doping will increase the work function of graphene (W_{Gr}) while n-doping would reduce the W_{Gr}. By modifying the W_{Gr} through doping, graphene can be incorporated with both n-Silicon and p-Silicon. For the former case, graphene will serve as an hole extraction layer for generated electron-hole pairs. In the later case, graphene collects the electrons created in silicon. In both cases, the performance of solar cell depends on the Φ_b as described above. Therefore, increasing or (/reducing) the W_{Gr} of graphene for n-Si (/p-Si) solar cell is necessity to create a higher Φ_b.

In addition to inducing electron-holes to graphene, the W_{Gr} can be modified with respect to incorporated material. In general, a material with a higher work function than that of Gr is a p-type dopant as previously demonstrated with Au (~5.4eV),[19,25] graphene oxide, (~5.3eV)[21,27] and NiO (~5.4eV-6eV)[28,29] while a material with lower work function such asTi (4.3eV),[30] polyethylenimineethoxylate (PEIE ~4.1eV),[31,32] TiO_2 (~4.15eV),[33] n-dopes the graphene. Applying above mentioned doping approaches indicated that W_{Gr} can be tuned from ~5.1eV to ~3.25eV. The effect of p- and n-doping on the W_{Gr} with respect bare/undoped graphene is presented in Figure 2.2.

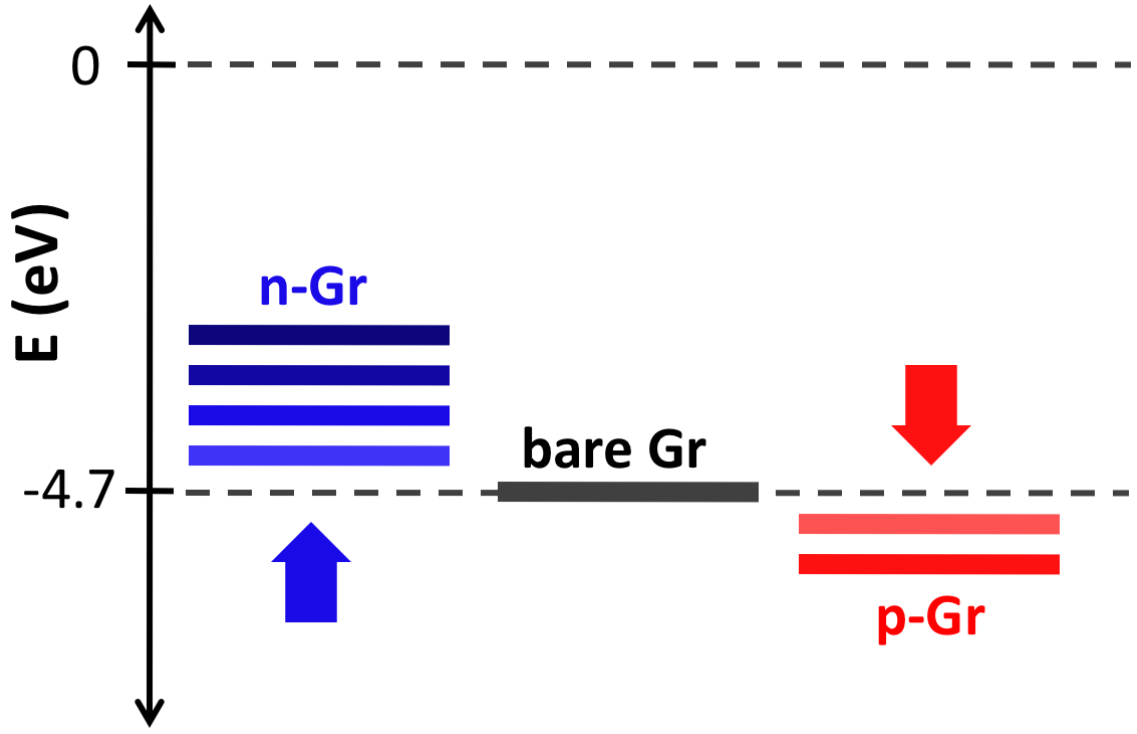

Figure 2.2: A schematic representation of the work function of graphene (W_{Gr}) and its relative change with doping is shown. Blue color represents n-doping/electron inducing to Gr while red color represents the p-doping/hole inducing to Gr.

Since the doping of graphene and its effect on Gr/Si solar cells is discussed throughout this thesis, a well-established technique is used to characterize the type of doping through Raman spectroscopy analysis. In this thesis, Raman spectroscopy analysis are carried out with Reinshaw inVia Raman spectrometer, equipped with 514nm laser beam with a spot size ~1 um. Measurements are carried out at room temperature. A typical Raman spectrum of single layer graphene on a SiO_2/Si substrate using 514 nm laser is shown in Figure 2.3. The type of doing which is established as the main criteria through the shift of 2D peak in literature[34–37] as well as some other factors such as broadening of peaks, intensity ratio will be used to identify the effect of doping. As a basis the doping type through the shift of 2D peak is indicate in Figure 2.3 with

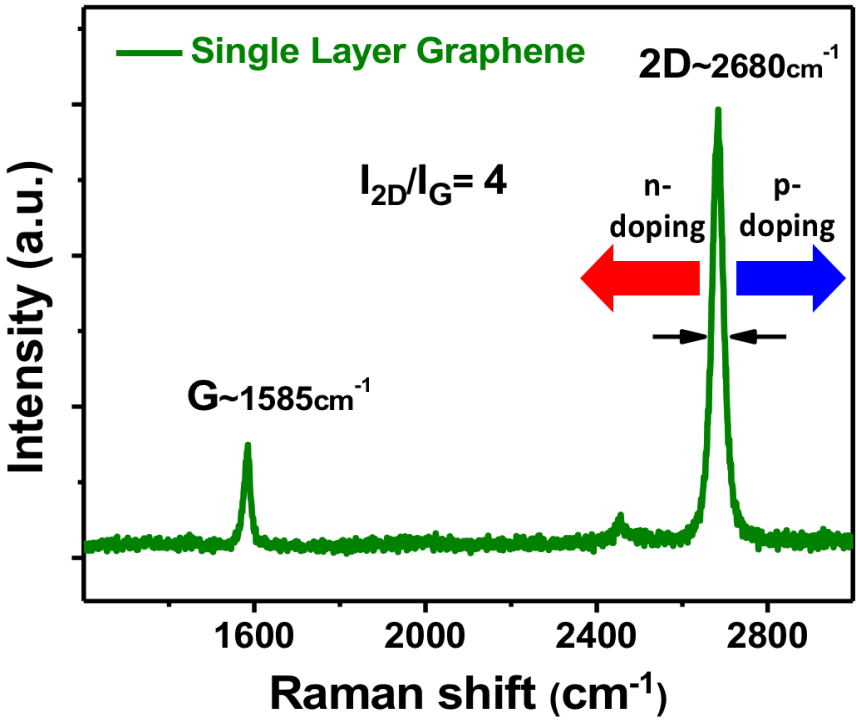

Figure 2.3: A typical Raman spectrum of single layer graphene on SiO_2/Si substrate.

corresponding arrows. Since graphene from different commercial companies are used in this study, a small variation in the Raman spectrums of bare/pristine graphene that might be due to the growth method is observed. However, all Raman analysis and interpretations are reported using the control sample of corresponding experiment.

2.5 Summary

After first demonstration of graphene silicon Schottky junction solar cell with a power conversion efficiency of ~1.5% in 2010,[7] modification of electrical properties of graphene indicated that PCE of ~17% for Gr/n-Si solar cell which will be discussed in Chapter 3 and 12.5% for Gr/p-Si solar cell (Chapter 4) can be obtained experimentally. Such a significant PCE improvement within the eight years is promising for further PCE enhancement in the near future.

Compared to p-n junction counterparts, simple and cost effective device fabrication that does not required high temperature process (Gr/Si, T<400°C whereas p-n Si T>700°C) is one of the advantageous of Gr/Si solar cells. Although the PCE of Gr/Si is still low (at ~17%) compare to the p-n junction solar cells to date, having a single atom thick emitter on top of silicon can be beneficial as compared to the p-n junction counterparts. It is well known that highly doped emitters are responsible for the efficiency limit of solar cells due to the Auger recombination.[38,39] By avoiding such limitation through the use of graphene, a higher PCE compared p-n junction counterparts might be obtained.

In chapter 6, possible directions for further PCE improvements in Gr/Si solar cell will be discussed in details. After reveling the whole nature of graphene and its opti-electrical limitations, employing the well-studied and understood optimization steps of p-n junction counterparts can indicates the efficiency limits of Gr/Si solar cells.

CHAPTER 3: GRAPHENE OXIDE AS A P-DOPANT AND AN ANTI-REFLECTION COATING LAYER, IN GRAPHENE/N-SILICON SOLAR CELL

3.1 Introduction

In this chapter, incorporation of two carbon based two-dimensional (2-D) materials for solar cell is introduced. The use of graphene oxide (GO) on top of Gr/n-Si solar cells and its contribution to PCE as well as stability of solar cell is discussed. The details of three fold of PCE enhancement via a simple and cost effective methodology by analyzing the *J-V* curves are investigated. Contributions through the use of GO are demonstrated through the Raman Spectroscopy analysis and reflectance measurements.

3.2 Graphene oxide as an encapsulation layer

Graphene has been one of the most intensively researched materials, over the past decade,[40] for various applications incorporating batteries,[41] supercapacitors,[42] transistors,[43] photo detectors,[44] sensors.[45,46] Unique characteristics of graphene, incorporating high transparency (97.7% for single layer graphene), in addition to high electrical conductivity (10^6 S/cm), and mechanical flexibility have suggested the use of graphene as a transparent electrode for solar cells.[8,47] Indeed, the first graphene/*n*-Silicon (Gr/Si) Schottky junction based solar cell with an efficiency of 1.5% was demonstrated in 2010.[7] Various methods have since been proposed to further increase the efficiency of Gr/Si solar cells through acid doping,[16] reducing the sheet resistance of the graphene,[48,49] and texturing the underlying silicon surface for efficient light harvesting.[25,50] While the developed methodologies improved the PCE up to 10%, the stability of the Gr/Si devices, while maintaining high efficiency, is still a major issue, *e.g.*, due to the observed loss of acidic doping as well as the oxidation of the underlying silicon. Moreover,

existing methods aimed at improving efficiency involve multiple steps including surface passivation, doping of the graphene, and applying an anti-reflection coating (ARC) layer, often through diverse layers.[20,49]

Considering that the stability of the solar cell devices was a major issue, we initially sought to tackle this specific problem through using an oxidation barrier facilitated through a graphene oxide (GO) coating. GO was particularly chosen due to its stability in ambient air,[27] and high transmittance in the electromagnetic spectrum, ranging from the ultra-violet to the near-infra-red regimes.[51] We have also found, subsequently, that GO can function both for doping graphene and through the use of suitable thickness, as an ARC layer. As will be shown later, GO coating yields superior performance and enhanced environmental stability for Gr/Si solar cells. For instance, a three-fold enhancement in the efficiency along with device stability over a 20 day period, which seems to among the most durable reported thus far for Gr/Si solar cells, was observed.

3.3 Experimental

The Gr/Si solar cells were fabricated through well-known lithographic processes. Briefly, an *n*-type Si (resistivity: 0.5Ωcm-1Ωcm) wafer was covered with a 300 nm silicon oxide (SiO_2) layer deposited by plasma enhanced chemical vapor deposition (PECVD).A 9 mm^2(3 mm x 3 mm) window was defined by photolithography. Subsequently, gold/titanium (Au/Ti) and aluminum (Al) were sputtered to provide Ohmic contacts at the front and back-side, respectively. A buffered oxide etch (BOE: with NH_4F/HF in a 6:1 ratio) was employed to remove the top SiO_2 layer through the Au/Ti window. SiO_2 removed window is used as the device active area (AA) Figure 3.1 shows a schematic of lithography process.

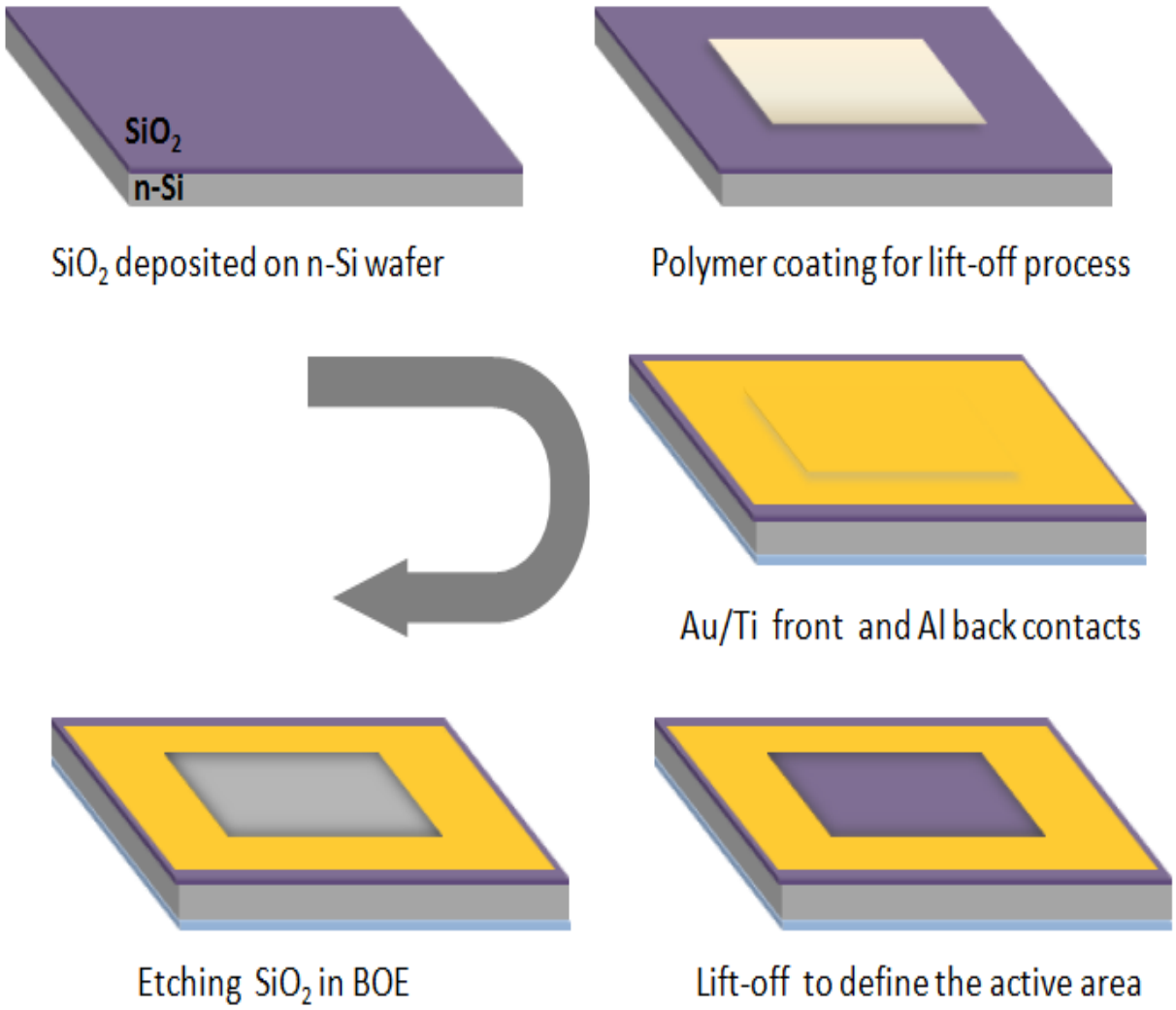

Figure 3.1: A schematic of typical sample preparation and defining the active/working area of solar cell is briefly shown. A simple lithography process for device fabrication is one of the promising advantageous of Gr/Si solar cells.

Single layer graphene synthesized through Chemical Vapor Deposition (CVD) on Cu foil was obtained from ACS Materials. PMMA was spin coated on Gr/Cu foil for a mechanical support for the transfer of graphene. Cu foil was than etched in 0.1M ammonium persulfatefor 6 hours and free floating PMMA/Gr was transferred in DI water onto the samples via wet transfer process.[21] A schematic of graphene transfer process is shown in Figure 3.2.

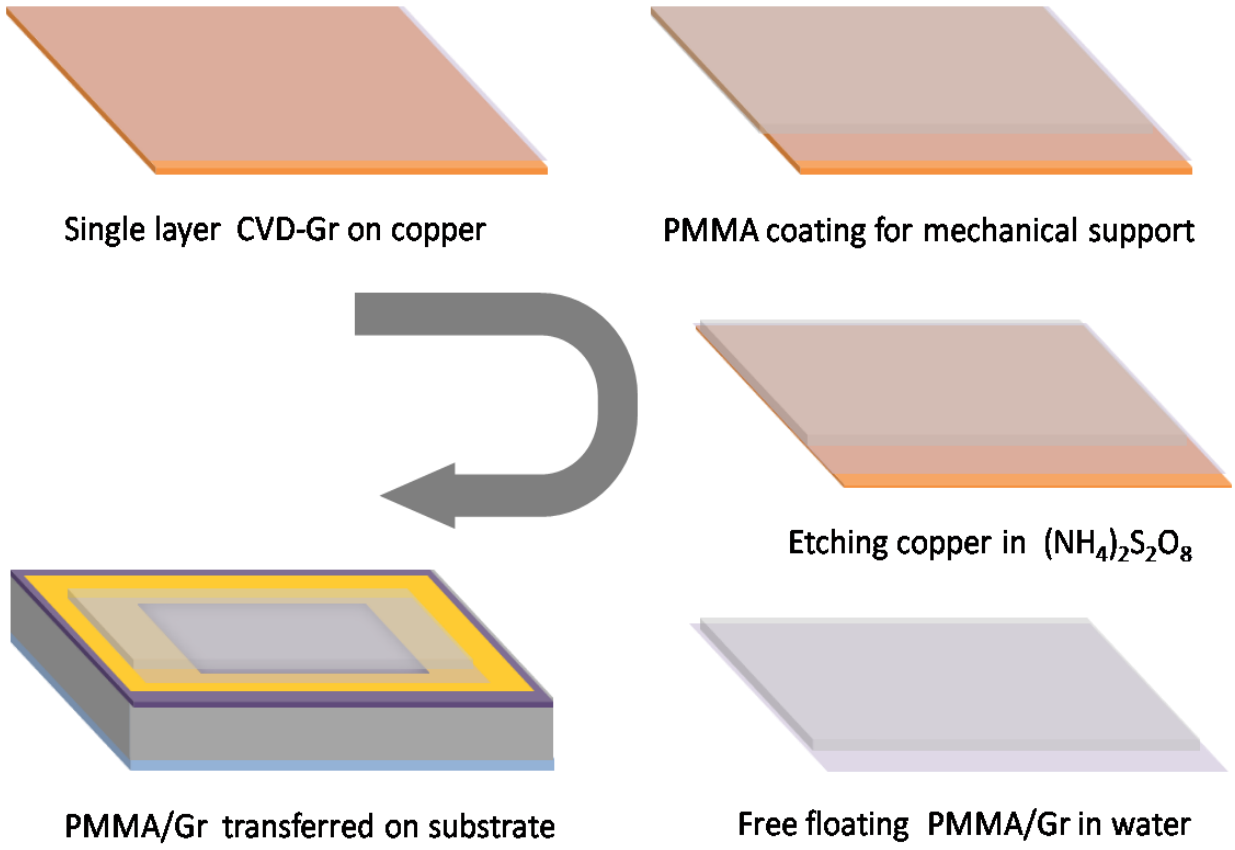

Figure 3.2: A schematic representation of graphene (Gr) placement (PMMA/Gr) on solar cell through the wet transfer process is shown. Following this process, PMMA is etched in acetone followed by annealing.

After Gr transfer, samples were left in ambient air overnight to dry, followed by removing PMMA through treatment with acetone for 30 minutes and isopropyl alcohol for 1 min. Subsequently, samples were annealed 1 hour at 400°C under H_2/N_2 gas flow (10sccm) to improve the Gr/Si junction contact.[20] Graphene oxide (GO), synthesized using a modified Hummer's method, was dispersed in deionized water with a concentration of 1mg/mL.[52] Well-dispersed, highly stable GO solution was spin coated on Gr/Si solar cell for film, confirmed with scanning electron microscopy (SEM) analysis. The schematic of solar cell under illumination which is illustrated in Figure 3.3a along with the actual device as displayed in Figure 3.3b.

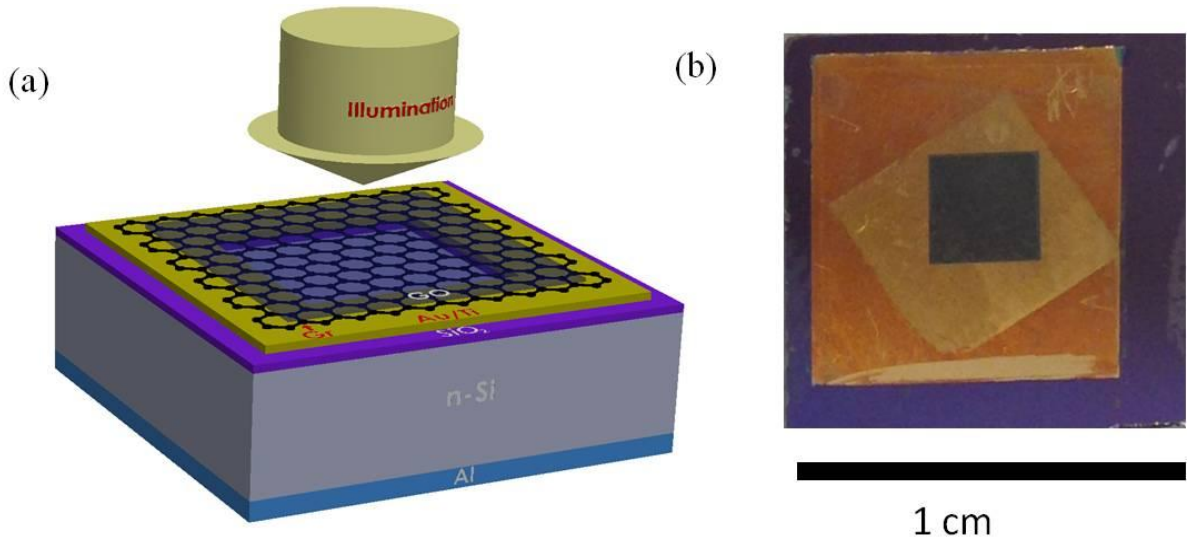

Figure 3.3: (a) A schematic of GO/Gr/Si solar cell. (b) Optical image of the solar cell.

3.4Results and Discussion

Current density (J) – Voltage (V) measurements were carried out through illumination (using AM1.5 standard at 100 mW/cm^2) for bare and GO coated devices: Figure 2a.The open circuit voltage (V_{oc}), the short-circuit current density (J_{sc}), and fill-factor (FF) of bare Gr/Si solar cell were measured to be 0.440 V, 27.2 mA/cm^2, and 29%, respectively, resulting in PCE of 3.6% (blue line). After GO coating, the V_{oc}, J_{sc}, and FF of sample (red line) increase to 0.512 V, 38.4 mA/cm^2, and 53%, respectively, boosting the PCE of 10.6%,- a factor of three higher than that of the bare Gr/Si solar cell. External Quantum Efficiency (EQE) measurements, as indicated in Figure 3.4d, shows a comparison of bare Gr/Si solar cells with the GO coated Gr/Si solar cells. For the wavelength in the range of 400 nm – 900nm the EQE of bare Gr/Si solar cell was around 70%, comparable to the state-of-the-art.[16,53]However, the EQE of GO coated solar cells was increased to ~90%, with a corresponding enhancement of the J_{sc} to ~ 37 mA/cm^2 (from ~ 29 mA/cm^2 for the Gr/Si basis). In here, a monochromator (Newport, CS260), equipped with a

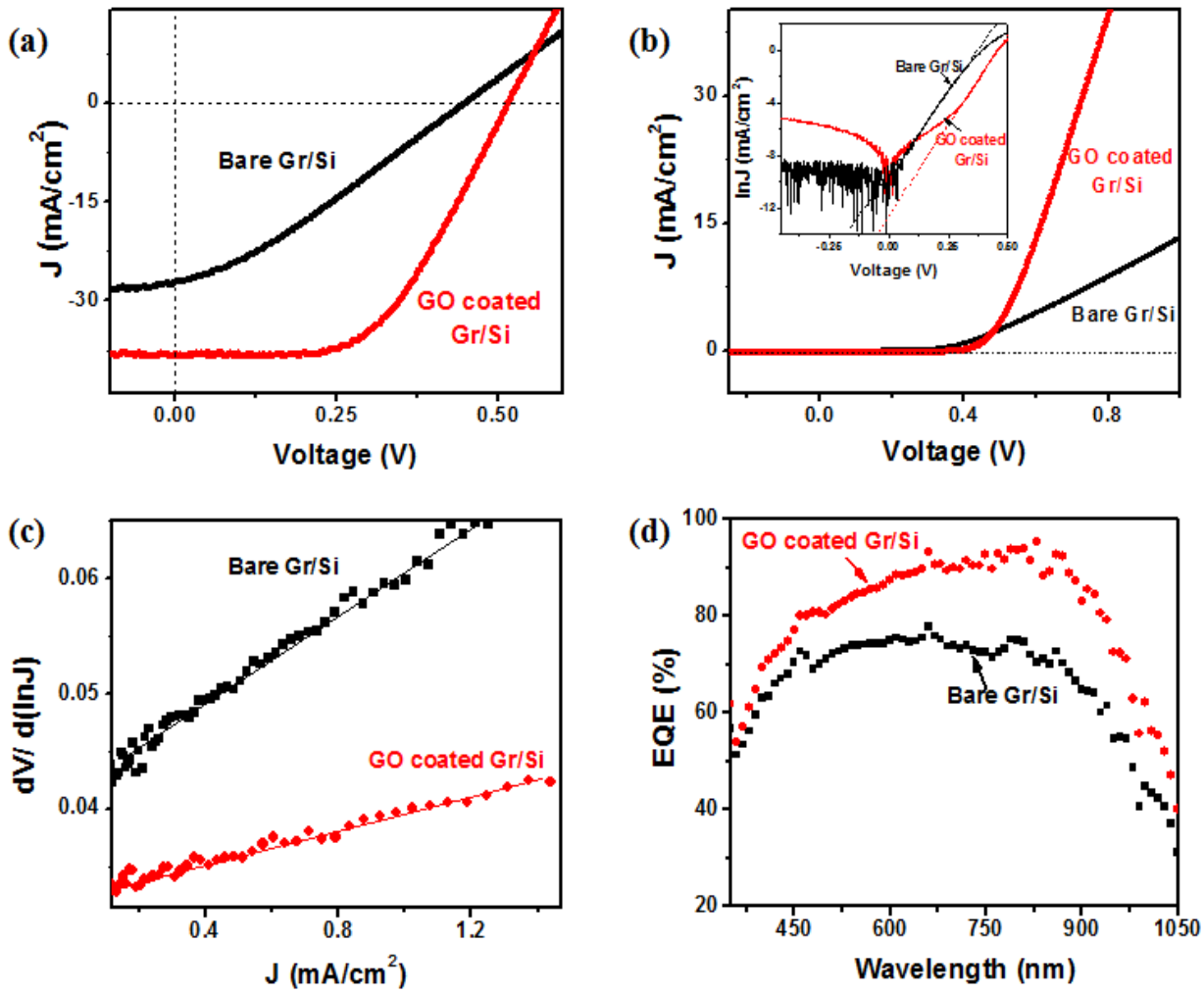

Figure 3.4: (a) *J-V* characteristics of bare Gr/Si and GO coated Gr/Si solar cells under illumination. (b) Dark *J-V* curves or solar cells. Inset figure shows the *ln(J)-V* graph that used for Φ_b calculations. (c) *d(V)/d(ln(J))* versus *J* curves of corresponding solar cells. (d) EQE plots of bare Gr/Si and GO coated Gr/Si solar cells.

solar simulator, was used for external quantum efficiency (EQE) measurements, as a function of wavelength. The response was calibrated by a silicon photodiode (Newport, 818-UV). EQE, as defined through the ratio of the number of collected electrical carriers (as measured by the electrical current) *to* the incident photon intensity (measured through a photodiode) on the solar

Table 3.1: Output parameters of the *J-V* curves presented in Figure 3.4a

	J_{sc}(mA/cm^2)	V_{oc} (V)	FF (%)	PCE (%)
Bare Gr/Si	27.4	0.440	29	3.6
GO coated Gr/Si	38.4	0.512	53	10.6

cell. The maximum J_{sc} that can be obtained from a silicon solar cell is ~43.2 mA/cm^2 under standard testing conditions. The J_{sc} values were obtained through:

$$J_{sc} = \int EQE(\lambda) x \lambda x E(\lambda) x \frac{\lambda}{1240} d\lambda \qquad (3.1)$$

Where, EQE(λ) obtained from the measurements, E(λ) is the standard solar spectrum and λ *is* the wavelength. Through the analysis of such results, we propose that the beneficial effect of GO arises from two reasons: (i) the doping of Gr by GO coating, which increases the work function of graphene (W_g)**,** and improves the conductivity, and (ii) the functioning of the GO as an anti-reflection coating (ARC) layer.

We first consider the rationale for the doping of the Gr by the GO. To extract the Schottky barrier height (Φ_b), series resistance (R_s), and diode ideality factor (n), *J-V* measurements carried out in dark room (Figure 3.4b). From the dark ln(*J*)-*V* curve, Figure 3.4b inset figure, the Φ_b of Gr/Si and GO/Gr/Si cells were estimated through a diode equation of the form[54]:

Table 3.2: Extracted Schottky parameters (Φ_b, R_s, and n) of bare Gr/Si and GO coated Gr/Si solar cells presented in Figure 3.4

	Φ_B (eV)	R_s (Ω)	n
Bare Gr/Si	0.791	17.3	1.65
GO coated Gr/Si	0.868	9.5	1.42

$$J = J_s[exp(qV/nkT) - 1], \quad \text{where} \quad J_s = A^*T^2 exp(q\Phi_b|kT) \tag{3.2}$$

Here J_s is the saturation current density, q is the elementary electronic charge, n is the ideality factor, k is the Boltzmann constant, T is the temperature, and A^* is the Richardson constant (112 A/cm^2/K^2 for n-Si). The Φ_b of the Gr/Si and GO/Gr/Si samples were estimated to be 0.791eV and 0.868eV, respectively. A 77meV increase of Φ_b is in accord with the experimentally observed 72mVincrease in the V_{oc}, indicating a possible influence of the GO coating on the W_g. Additionally, from the dark *J-V* curve analysis, the R_s was seen to be lowered by ~ 50%to 9.5 Ω for the GO layer coated Gr/Si cells (compared to 17.3 Ω for the bare Gr/Si cells), contributing to the *FF* increase: Figure 3.4c. From equation 3.2, we deduce:[54]

$$\frac{d(V)}{d(\ln(J))} = RA_{eff}J + \frac{n}{\beta} \tag{3.3}$$

Here, RA_{eff} is the slope, β is q/kT, and n/β is the intercept related to the diode ideality factor, n. While an ideal diode, would have n = 1, it was seen that the n improved[16,55] for the GO coated cells to ~ 1.42 (compared to ~ 1.65 for the bare Gr/Si cells). Schottky junction parameters of bare

Gr/Si and GO coated Gr/Si solar cell are summarized in table 2.2. It was also interesting to note that the *J-V* characteristics seem to be altered in a manner similar to that reported for nitric acid (HNO_3) based doping of Gr.[20] Through experimentation, we have confirmed that such acid treatment indeed increased the V_{oc} and *FF* from 0.442 to 0.510 V and 29% to 52%, respectively, resulting in increased *PCE* from 3.6% to 7.6%, similar to that observed through the GO coating. In here, using of HNO_3 reduces the sheet resistance of graphene through p-doping and improves the collection of carriers leading a higher V_{oc} and *FF*. However, the J_{sc} was not enhanced. Figure 3.5 shows the *J-V* characteristic of HNO_3 doped and GO coated Gr/Si solar cell as compared to the bare Gr/Si solar cell.

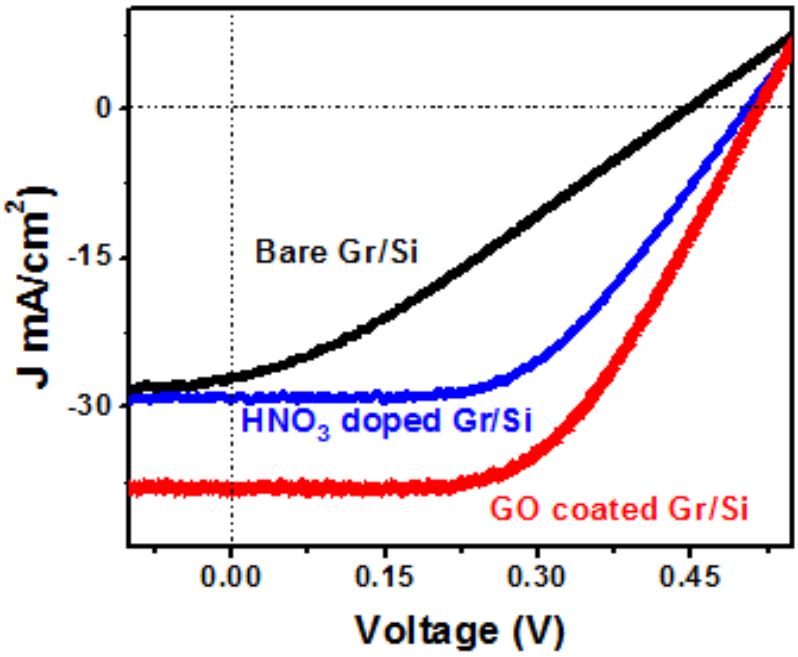

Figure 3.5: A comparison of the *J-V* curves of HNO_3 doped and GO coated Gr/Si solar cells with respect to bare Gr/Si solar cell are presented. While both treatment implies similar V_{oc}, the enhanced J_{sc} observed in GO coated solar cell indicates the beneficial effects of GO through the ARC layer.

Generally, in a Schottky junction based diode ,the difference between the W_g and the electron affinity of *n*-Si (χ_{Si}) causes a built-in potential (V_{bi})and a concomitant electric field to separate electron-hole pairs generated in Si on photons absorption: Figure 3.6a. A schematic of the hypothesized energy band diagram of the Gr/Si solar cell, upon doping the Gr, say through the GO, is indicated in Figure 3.6b. Note that *p*-doping through the GO further increases the W_g of graphene, with an enhancement of the Φ_b and the V_{bi} and the photon to electrical carrier conversion efficiency. Moreover, the increased number of holes in the W_{Gr}, due to *p*-doping, would also reduce the sheet resistance of the Gr and contribute to a greater *FF*.

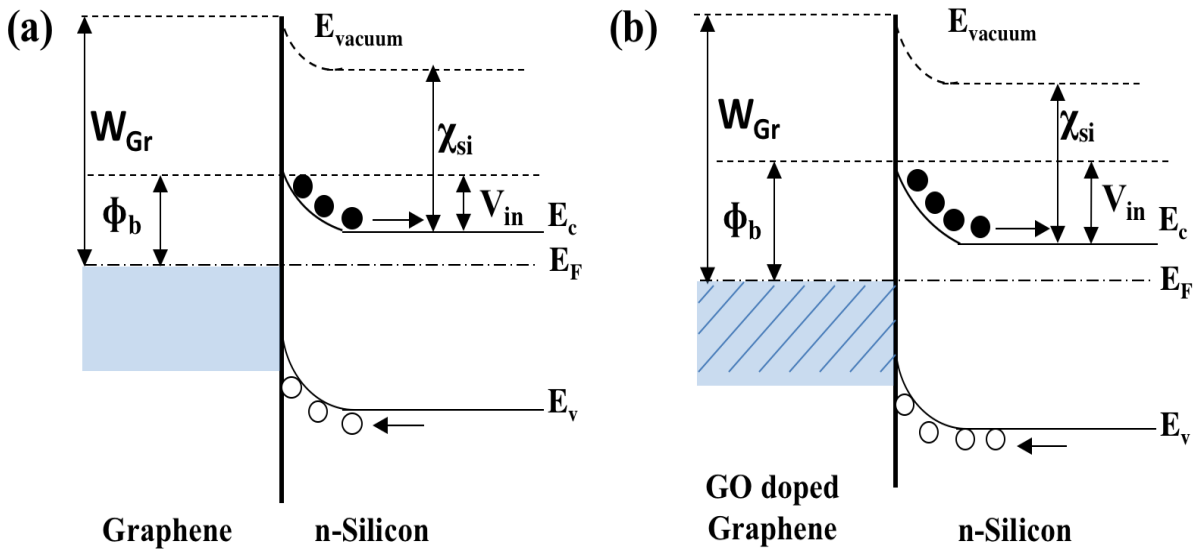

Figure 3.6: (a) A schematic of the hypothesized energy band diagram of the Gr/Si solar cell, (b) Upon p-doping the Gr, say through the GO, is indicated. An increase in band bending due to a higher work function of graphene is highlighted.

The possible doping of Gr by GO coating was also verified through Raman spectroscopy.As indicated in Figure 3.7, the D- (1352 cm^{-1}), G-(1598 cm^{-1}), 2D- (2702 cm^{-1}), and 3S- (2945 cm^{-1}) peaks are representative of synthesized GO/oxidized graphite. The D *to* G-

peak intensity ratio I_D/I_G is around 0.92, consistent with previously reported values.[56,57]The doping of the Gr is indicated through a peak shift as well as through a change in the peak width as indicated in chapter 2.As indicated in chapter 2, blue shift of both the G and the 2D peaks of Gr indicates *p*-doping whereas red shift of 2D peak is an indication of*n*-doping.[30]It can be seen in Figure 3.7a that upon GO coating, a significant blue shift of 2D peak is realized. However, the G peak of GO coated Gr overlaps the G-peak of GO, hence no significant blue shift has been observed for G peak. To analyze G peak more carefully, Raman analysis of GO on $SiO_2$is obtained as indicated in Figure 3.7b. Through the peak analysis, using two sets of data, we obtained the inset figure.

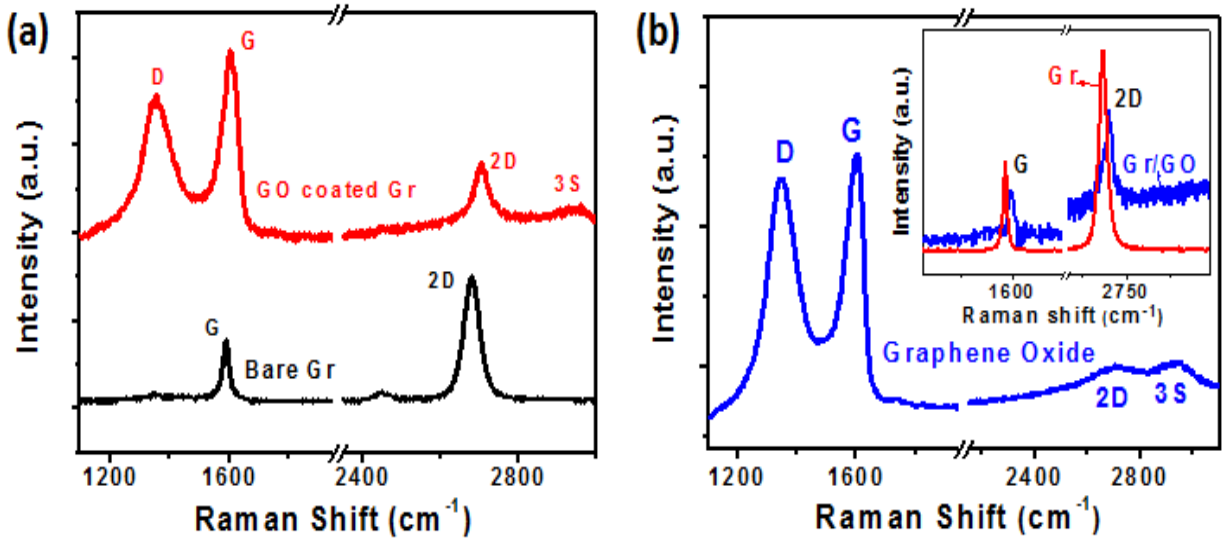

Figure 3.7: (a) Raman spectrums of bare graphene (black line) and GO coated Gr (red line) are presented. Blue shift of 2D peak upon GO coating can be realized. The G peak of Gr overlaps with the G peaks of GO. (b) Raman spectrum of GO is shown which is used as a reference and through peak analysis the G peak shift in the Gr upon GO coating is revealed as shown in inset figure of (b).

As seen in Figure 4.7b inset figure, a considerable blue shift (24 cm^{-1}) of the 2D peak of GO coated Gr (2709 cm^{-1}) as compared to the position of the peak in the bare Gr (2685 cm^{-1}) indicates enhanced *p*-doping in the former.[58,59] A blue shift of 11cm^{-1} was also observed for the G peak upon GO coating. As indicated earlier,

We next examined the rationale for the use[60,61]of GO as an ARC, which was hypothesized as further contributing to the *PCE* of the Gr/Si solar cells. If the GO coating thickness (d_o) was of the order of $\lambda/4n_{GO}$, where λ is the free space wavelength and n_{GO} (the refractive index of the GO coating) is the geometric mean of the refractive indices of the silicon and air, it would constitute an ideal ARC layer.[62,63]To evaluate the possibility of GO functioning as an ARC, reflectance measurements were carried out on the GO/Gr/Si cells (using a Lambda 1050 UV/Vis/NIR Spectrophotometer). Figure 3.8a shows the reflectance measurements (in diffuse and specular configurations) of bare Si, GO coated Si, and GO coated Gr/Si samples. For calibration, the bare Si sample has a reflectance around 35% at λ =600nm (black line), consistent with the literature.[64] After coating with GO layer (red line), the reflectance was reduced to ~15%at the same wavelength. It is feasible that the GO coating reduces the loss of light from the silicon, resulting in better light harvesting which creates more electron-hole pairs and consistent with the increase in J_{sc}.For the GO/Gr/Si solar cell (blue line), the reflectance was further reduced to ~12%, consistent with the expected absorption inGr.[51]The lowest reflectance of the GO coated Si (14.5%) and GO coated Gr/Si (11.5%) has been observed around 700 nm and 750 nm, respectively. The ARC layer thickness at these wavelengths would correspond to ~ 88 nm and ~ 94 nm, respectively. The thickness values, concomitant with the refractive index variation, where n_{GO} was of the order of 2, were further confirmed through ellipsometry measurements: Figure 3.8b. Moreover, the highest EQE (~90%), *e.g.*, see Figure3.4d, which was observed

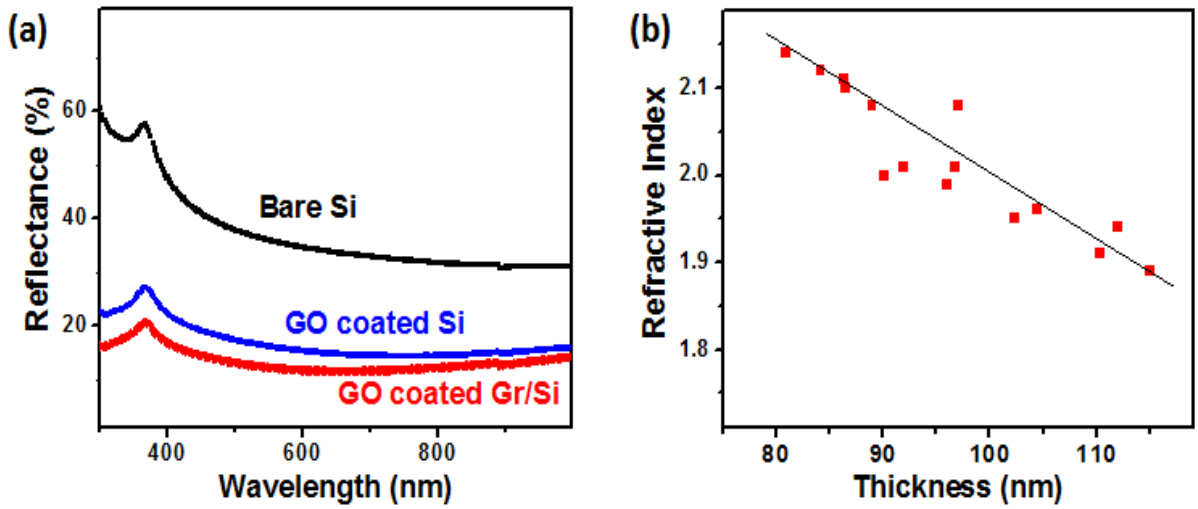

Figure 3.8: (a)Reflectance measurements of bare Si, GO coated Si and GO coated Gr/Si samples are presented which shows a significant reduction upon GO coating. (b) Refractive index as a function of film thickness is shown.

around 785 nm, seems to correspond well to the lowest reflectance value brought about by the ARC characteristics of the GO layer

It is notable that the ARC effect of the GO persists over a relatively large wavelength range (from 300 nm – 1000nm).Such a broadband response may arise due to the flake-like structure of GO mimicking a broad range of roughness in addition to the wide stoichiometry that may be present in the GO. Additionally, the refractive index of the GO would be expected to change with the porosity of the coating layer, which would be a function of the thickness: Figure 3.8b.[65]We carried out atomic force microscopy (AFM) and SEM analysis on GO coated solar cell: Figure 3.9a. AFM images revealed the surface roughness of GO which seems to be around 25nm in which might be the reason for such a wide broadband response. In addition, the flake-like structure of GO, which can be seen in both AFM and SEM images presented in Figure 3.9b might cause internal reflection. Moreover, the thickness of GO was confirmed with SEM

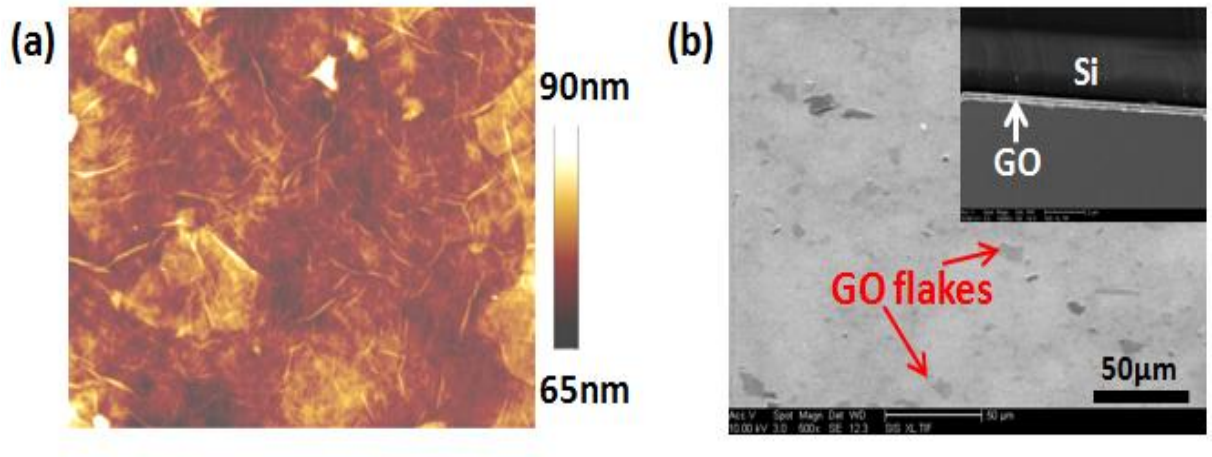

Figure 3.9: Surface characterization of GO coating. (a) Top-down atomic force microscopy image of GO coating reveals the flak-like structure of GO and surface roughness. (b) Scanning electron microscopy image of GO coating on Gr/Si. Inset figure shows the cross-sectional image of GO coated Gr/Si solar cell.

analysis in Figure 3.9b inset. The influence of porosity of the GO on the optical response would be a promising topic of investigation,[63] with relevance to its influence on the ARC efficiency.

As the original hypothesis, related to the use of GO, was to enhance the stability of the Gr/Si solar cells, the devices (without encapsulation) were placed in the ambient and tested over multiple days to examine the stability: Figure 2.10. As a basis, it was noted that the uncoated Gr/Si solar cells exhibit a~40% decrease of the *PCE* after ~ 10 days, presumably due to silicon oxide formation at the graphene-silicon interface Figure 2.10a.Such a degradation mechanism is based on an observed *s*-shape kink in *J-V* curves, which was previously attributed to the oxide formation,[66]due to exposure of the Si through defects in the overlaid Gr, and which considerably reduces the *FF*. Evolution of related solar cell parameters, such as V_{oc}, J_{sc}, and *FF* are highlighted in Figure 3.10b. Alternately, GO coated Gr/Si solar cells were much more stable,

showing negligible (~1%) decrease in the *PCE*. Figures 3.10c and Figures 3.10d shows the corresponding *J-V* characteristics and the variability of the performance and efficiency parameters (such as the V_{oc}, J_{sc}, and *PCE*), respectively during a 20-daytesting period. It was also

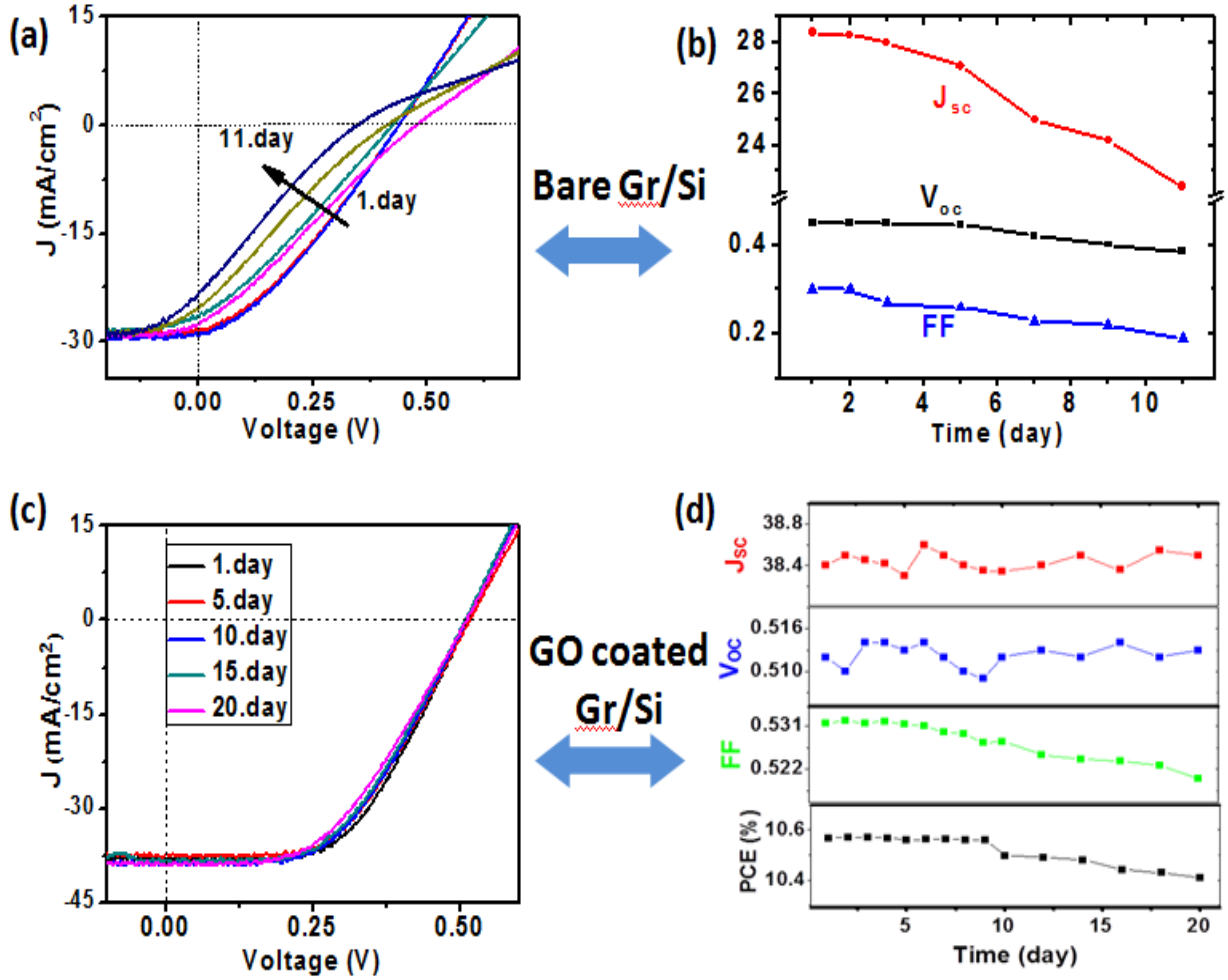

Figure 3.10: *J-V* Comparison of stability for bare and GO coated Gr/Si solar cells. (a) Evolution of the *J-V* curves of bare Gr/Si solar cell over the testing period of 11 days is shown. (b) Corresponding *J-V* parameters of bare Gr/Si as function of time. (c) *J-V* characteristic of GO coated Gr/Si solar cell during the 20 days of testing period. (d) Related *J-V* parameters of GO coated solar cell as a function of time.

observed that the *FF* was reduced at most by ~ 2% (Figure 3.10d). Generally, a more uniform GO coating[27] would be expected to further enhance the corrosion resistance of the Gr/Si solar cells, through reducing the Si exposure to the ambient. In addition, thickness of GO can be adjusted so that it can address the peak intensity of solar spectrum. In turn, a higher Jsc can be obtained through better harvesting of light.

3.5 Conclusion

In summary, we have reported that single layer Gr/Si solar cell efficiency of 10.6% can be obtained through a simple and cost-effective GO spin coating. While the original intent of using GO was to enhance the stability of the Gr/Si solar cell through reducing the propensity of oxidation of the underlying Si, we have seen significant additional benefits. For instance, GO has also shown to serve to*p*-dope the Gr/Si solar cell, contributing to a reduced sheet resistance. Additionally, we have shown, for the first time, that an optimal thickness of the GO could function as an ARC layer for the solar cell, further increasing the J_{sc} and the EQE. The stability of the GO coated solar cell seems to be unprecedented from a comparison with literature[20,49,67]. Future work would focus on further increasing the overall efficiency and the *FF*, and investigating means to further reduce the sheet resistance of the graphene.

Chapter 3, in part, has been published in Nanoscale in 2016 which titled “Graphene oxide as a p-dopant and an antireflection coating layer, in graphene/silicon solar cell” by Serdar Yavuz, Cihan Kuru, Duyoung Choi, Alireza Kargar, Sungho Jin and Prabhakar R. Bandaru. The dissertation/thesis author was the primary investigator and author of this paper.

CHAPTER 4: ENHANCED POWER CONVERSION EFFICIENCY OF GRAPHENE/N-SILICON SOLAR CELL, THROUGH ELECTRICAL CARRIER AND INTERFACE ENGINEERING

4.1 Introduction

While GO coating significantly improved the PCE of Gr/n-Si solar cell and its stability, the overall efficiency is still low. A general comparison of the solar cell parameters with respect to p-n junction counterparts implies that the low *FF* and V_{oc} are the main limiting factors of Gr/n-Si solar cell. While most of the p-n junction solar cells have the *FF* of ~80% and over 700mV V_{oc}, most of the Gr/Si solar cells were reported with around 65% *FF* and less than 550mV V_{oc}. In this chapter, a possible direction to improve the *FF* and V_{oc} of solar cell will be discussed. In addition, a significant p-doping of graphene due to the air exposure has been revealed which is shown to be as effective as chemical doping. A back surface passivation is introduced to Gr/Si solar cell which significantly improved the PCE over earlier reports. Finally, an engineered device active area to minimize the resistance related losses has been discussed. In a schematic study, it is shown that applying those approaches address the low *FF* of Gr/Si solar cells. In addition to highest *FF* of 78%, a significant V_{oc} improvement up to 593mV results in record PCE of 16.9%, to date.

4.2 Addressing the low fill factor of graphene silicon solar cell

The unique energy dispersion of graphene (Gr)[68,69] motivates its use for photovoltaic (PV) applications. Graphene exhibits resonant absorption over all the energies relevant to solar radiation, coupled with high optical transparency[47] – particular to its single atomic layer thick two-dimensional characteristic. Additionally, the superlative flexural rigidity[70] of Gr, placed on suitable substrates, may be used for the next generation of portable electronics. However, the

difficulty of controlling *p*- and *n*-doping of the Gr, at the present time, implies that initial PV application of graphene could be evaluated through Schottky junction based solar cells, where the graphene is adjacent to a *p*- or *n*-doped Silicon. Moreover, the use of a single atomic layer on one side of a junction could considerably reduce the penalties associated with heavy (/light) doping[39], such as Auger (/surface) recombination[38], which has been implicated in reducing the efficiency of nanostructured[71] Si solar cells.

We report that such a layout of Gr on Si, as a Schottky junction, while optimizing the efficiency of carrier extraction, is indeed a promising route for obtaining high efficiency PV cell architectures. In such a junction, as described earlier the difference between the work function of Gr (= W_{Gr}) and the electron affinity of *n*-Si (= χ_{Si}) creates a built-in potential (V_{bi}). When photons with energy greater than the bandgap of Si (~1.1 eV) are absorbed, the generated electron (e^-)-hole (h^+) pairs are separated due to the V_{bi}, with the electrons collected at the back-contact to the Si, while holes are transported to the front Gr side, as indicated in Figure 3.6. The overall *input* optical to *output* electrical power conversion efficiency (PCE) is promoted through enhancement of the (i) V_{bi}, (ii) the electron mobility in the Si and hole mobility in the graphene, iii) reduced number of defects and carrier recombination centers, (iv) a large transmission coefficient of the respective $e^-$and h^+ collecting contacts, in addition to (v) optical design, such as through the use of texture, anti-reflection coatings, *etc*. Through careful consideration of these parameters, we have obtained a record PCE of ~ 16.9%, and we outline schemes to extend this even further.

The key performance characteristics[72] of solar cells such as the V_{oc}, J_{sc}, and *FF* were studied. A large V_{bi} enhances separation of the photo-electrons and photo-holes and, for the Gr/Si junction cell, may primarily be controlled through increasing the W_{Gr} in the absence of Fermi-

level pinning at the Gr/Si interface. A *p*-doped Gr, with a Fermi energy (E_F) lowered below the Dirac point, is used here on top an *n*-type silicon substrate. In this context, earlier work indicated that treatment of Gr by oxidizers such as trifluoromethanesulfonic acid (TFSA) and nitric acid (HNO_3) yielded a PCE of Gr/Si solar cell of ~ 9%.[24,25] It is then relevant to consider the extent to which the W_{Gr} could be tuned and the concomitant increase in the V_{oc}. The W and the doping should be modulated such that seamless carrier passage (*e.g.*, h^+ into the Gr) could be ensured. The charge at the Gr-silicon interface, say, due to defects and associated carrier recombination, could also enhance the surface recombination velocity and diminish the V_{oc}. In our work, we investigated various Gr doping strategies for with an aim of obtaining the largest V_{oc}.

The maximum V_{oc} that may be attained is reduced by various non-radiative recombination processes, *e.g.*, due to surface or interface defects, material impurities, *etc.* To investigate the possibility of reducing the influence of surface defects, we deploy a thin SiO_x layer between the *n*-Si and the electrical contact to the back-surface to passivate the surface and subsequently enhance the PCE of Gr/Si solar cell, through enhancing effective minority carrier lifetime. The use of the passivating SiO_x layer forming a tunnel oxide passivated contact (*i.e.*, TOPCon), has been previously described in Si PV cell literature.[73–75] The thickness of the passivation layer must be carefully optimized as a very thin layer may not be adequate for effective passivation, while too thick a layer would interfere with the efficient collection of carriers. Moreover, increasing SiO_x thickness reduces the saturation current (J_s) and yields a higher V_{oc} but may also hinder carrier tunneling to the contacts.[76]

In addition, *parasitic* attributes of a typical PV cell such as the series resistance (R_s) – from the constituent Si and the Gr, as well as the contact resistance at the front and back surfaces – together with the shunt resistance (R_{sh}) decrease the *FF* and must be controlled. Moreover, the

sheet resistance of the graphene would also need to be reduced, with respect to maintaining a large ratio of the electrical conductivity and the optical conductivity.[77] For the Gr, a reduced R_s may be accomplished through doping, so as to yield a carrier-mobility product of $>10^{16}$ $V^{-1}s^{-1}$, and a related sheet resistance of the order of 10Ω/□. Considering this aspect, we probed the influence of the Gr doping as well as active PV area in reducing the R_s.

The maximum J_{sc} that may be attained is proportional to the number of incident photons (solar power density) and is diminished through non-optimal light trapping and reflection losses. Consequently, we studied the influence of uniform anti-reflection coatings (ARC) to ensure light trapping in the PV cell. Ideally, the refractive index of the ARC (n_{ARC}) should be a geometric mean[78] of the respective refractive indices of the ambient air (n_{air} ~ 1) and the underlying Gr (n_{Gr} ~ 2.4), which is of the order of 1.5. It was previously found that a poly-methyl methacrylate (PMMA) polymer coating could be used for this purpose, where it was shown to be effective at enhancing the J_{sc} in Gr/Si and CNT/Si solar cells.[79,80] The PMMA thickness would be~ 90 nm, optimized to a value[63] of ~$\lambda/4n_{ARC}$, where λ corresponds to the free space wavelength of ~ 550 nm, corresponding to the peak intensity of the solar spectrum, and n_{ARC} (~ 1.5) is the refractive index of the PMMA.

4.3 Experimental

To experimentally characterize the relevance of such intrinsic and extrinsic aspects, we fabricated Gr/Si Schottky junction PV cells. For the Si substrate side, an *n*-type Si (0.5-1Ω-cm) wafer was first subjected to a standard RCA cleaning procedure. Subsequently, the wafers were treated with a dilute hydrofluoric acid (5 wt%), and immersed in 68 wt% nitric acid (HNO_3) to

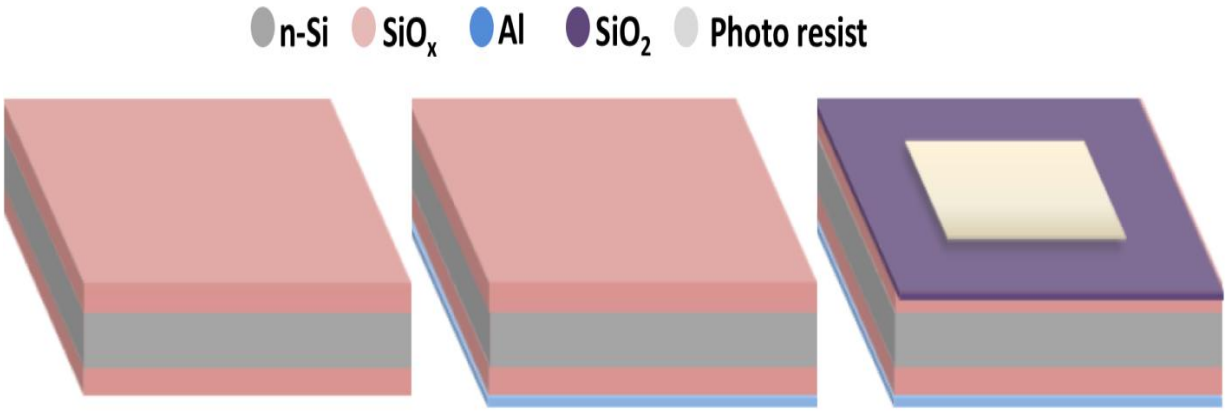

Figure 4.1: A schematic illustration of applied passivation in HNO_3. From left to right, SiO_x growth followed by Al back contact and thick PECVD-SiO_2 deposition. Than the standard procedure described in chapter 3 is performed.

form a thin SiO_x layer.[73–75] Aluminum (~300 nm) was sputtered as a back contact onto the SiO_x/Si as well as protection layer for SiO_x during sample fabrication. Figure 4.1 illustrates the applied SiO_x passivation and sealing process. Samples without the back SiO_x passivation layer were also prepared for reference. After sealing the back surface of wafers, the experimental procedure described in Chapter 3 is followed up to annealing of fabricated devices. It should be noted that the BOE removes the SiO_x from the front surface of devices. Therefore, there is no front surface passivation and any intentional oxide at the graphene/silicon interface. Following annealing step, all wafers kept in ambient conditions for the air exposure of Gr which will be discussed in detail. HNO_3 treatment for Gr doping was performed by exposing samples to HNO_3 vapor around~15 second at room temperature. PMMA, as an ARC, was spin coated on the HNO_3 treated solar cells for 60 second at 5000 rpm. The Gr/Si PV cells were tested under AM1.5 G illumination (using a Newport 66905 solar simulator), particularly AM1.5G corresponding to an incident power density of 1000 W/m^2, with the current measured by

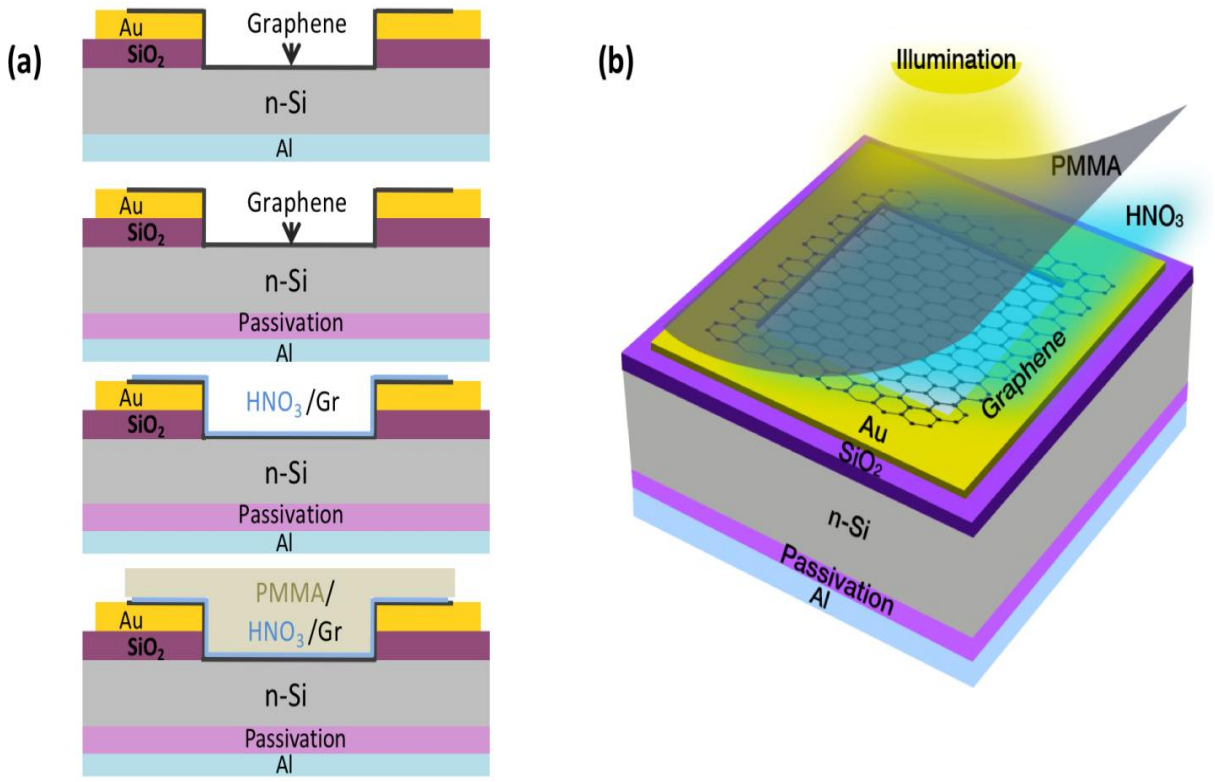

Figure 4.2: Schematic images of solar cells. (a) Cross sectional image of solar cells represents as synthesized control (Gr/Si), passivated (Gr/Si/SiO_x), HNO_3 doped (HNO_3/Gr/Si/SiO_x) and PMMA coated (PMMA/HNO_3/Gr/Si/SiO_x) solar cells from top to bottom (b). A schematic of the final device (PMMA/HNO_3/Gr/Si/SiO_x) is shown.

calibrated photodiodes (Newport 818-UV). A schematic of fabricated solar cell along with a cross sectional representation is given in Figure 4.2

4.4 Results and discussion

It has been previously reported that Gr is *p*-doped when exposed to the ambient air due to the presence of atmospheric oxygen[81,82], which induces hole doping and contributes to an increase in W_{Gr}, as described in first Chapter. It was observed that such a doping, indeed,

significantly improves the PCE of solar cells. The corresponding *J-V* curves, as a function of time of air exposure are indicated in Figure 4.3a. We noted that after 24 hours, the PCE of device reaches its highest value and saturates. No significant PCE variation observed upon further ambient exposure. Further analysis and fitting of the *J-V* curves to a one-diode model[17] indicated an increase of the Schottky barrier height with air-doping. It was observed that the Φ_b increased from an initial value of 567meV to 798meV over the 24-hour period, as show in Figure 4.3b. The increase is in close accord with the observed 221 mV increase of the V_{oc} in Figure 4.3a. The *J-V* characteristics of the Gr/Si PV cells stabilized after 24-hour of air exposure and characteristics after 24 hours of air exposure will be reported in the rest of the work. The variation of the *J-V* characteristics, as well as that of the PCE and the V_{oc} with time is indicated in. The average PCE observed was of the order of 8.9% for air-doped Gr/Si solar cells, in accord with previous reports.[24,25]

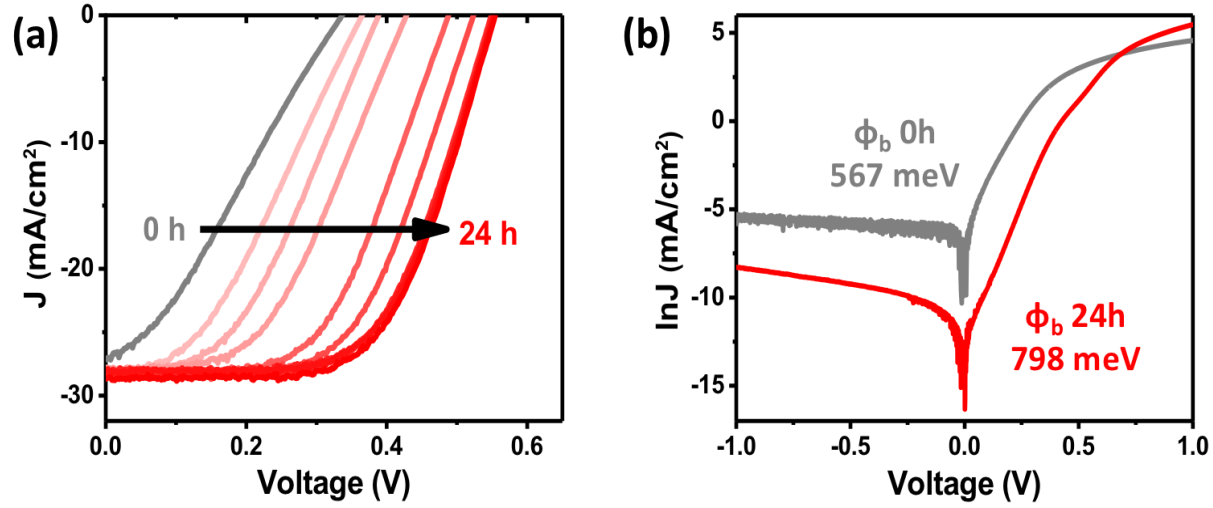

Figure: 4.3: (a) Evolution of *J-V* characteristic of Gr/Si solar cell with the ambient exposure (t= 0h to t= 24h). (b) Dark *ln(J)-V* curve of solar cell shows the low saturation current density after 24 hours of ambient exposure. Related Φ_b of solar cells are shown in the graph.

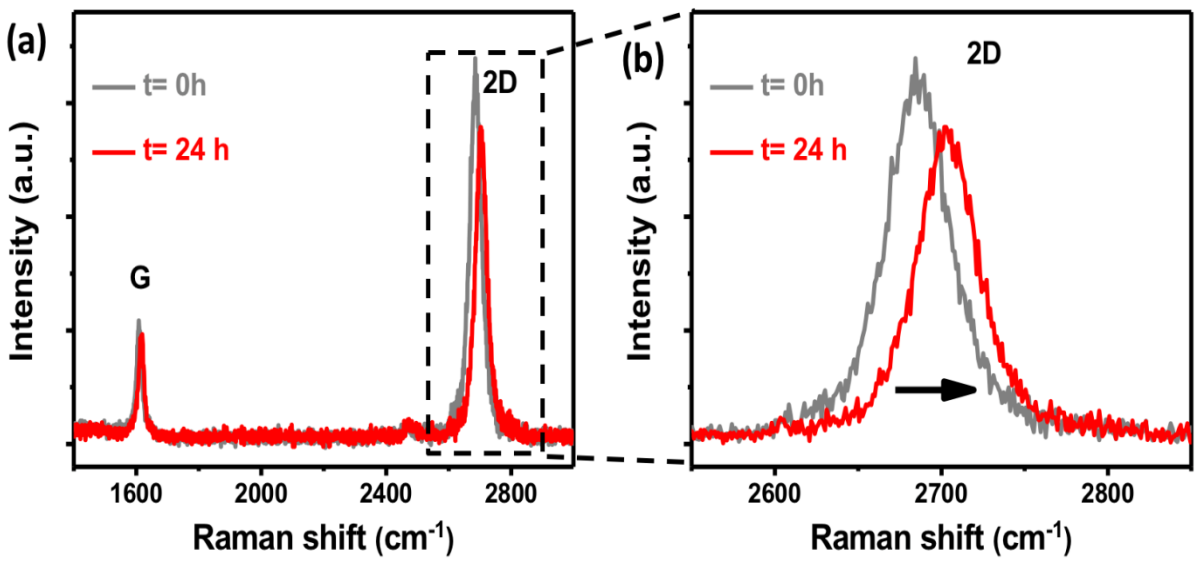

Figure 4.4: (a) Raman spectrum of bare Gr (t= 0h after annealing) and air exposed (t= 24h) Gr. (b) 2D peaks are highlighted indicating a blue shift of air exposed Gr

The *p*-doping nature of the Gr, through such ambient doping, was evidenced via Raman spectroscopy through a blue shift[30,81] of the *G*- and *2D*- peaks, as indicated in previous chapter. Figure 4.4a shows the Raman spectrum of Gr for after annealing (which is referred as t=0h) and 24 hour of air exposure time (t=24h). A clear blue shift in both peaks indicates the p-doping in addition to broadening of peaks. Figure 4.4b highlights the 2D peaks of related Gr. In addition to shift, a lower intensity and broader peak is in accord with the earlier reports.[36] One might suggests that such a doping might introduces due to a possible native oxide formation or reduced defects at the interface when graphene was placed on the Si. We annealed our saturated (PCE stabilized after 24hour) samples again to remove any possible absorbed species. As shown in literature, if such a doping is due to the absorbed species, annealing should reverse the doping.[81] After annealing at 400°C, it was observed that PCE of solar cells diminished to the initial value. However, exposure the ambient conditions indicated the recovery of solar cells PCE: Figure

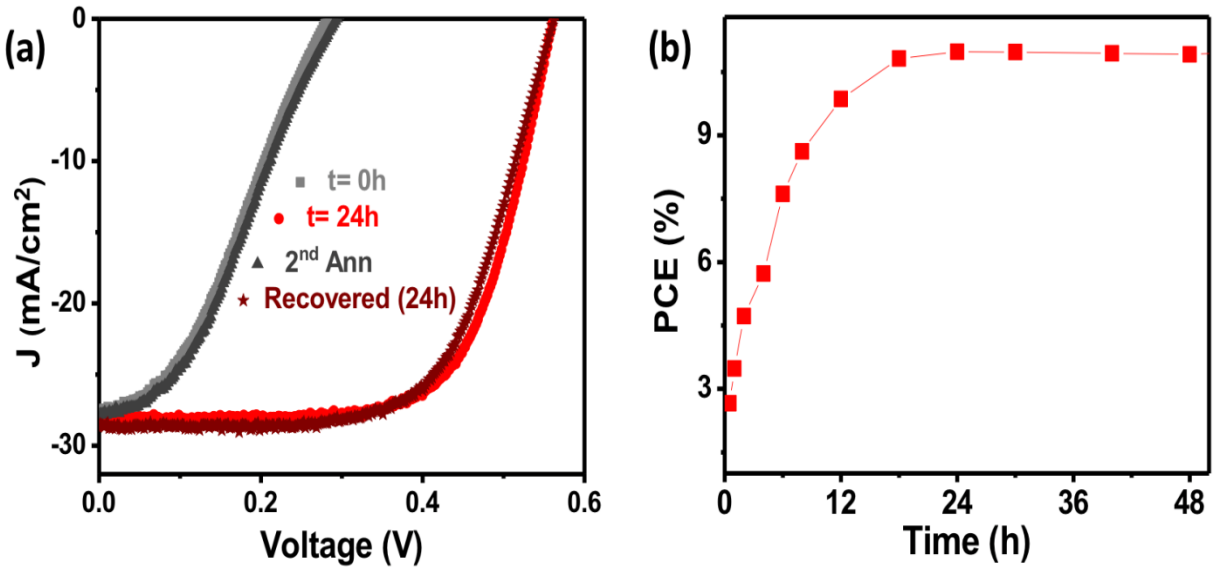

Figure 4.5: (a) *J-V* measurements indicated that p doping due to the air exposure and it can be reversed upon annealing. (b) PCE evolution of solar cell with air exposure time. No significant variation observed after 24 hours of exposure.

4.5a. Such an experiment confirms that observed doping is due to ambient exposure and it can be reversed. Figure 4.5b shows the PCE evolution of solar cell with time. 24 hours of air exposure applied to all reported samples and further treatments were performed after air exposure.

An increase of the PCE to ~ 11% was obtained through the use of the SiO_x passivation layer, placed between the Si and the electrical contact at the back-surface of the Gr/Si PV cell. We first consider the effect of passivation on minority carrier lifetime *via* quasi-steady state photoconductance measurements using Sinton Instruments WCT-120 tester. Figure 4.6a shows the lifetime of bare and passivated (Si/SiO_x) silicon wafers. Minority carrier (h^+) lifetime measurements, indicated that the effective h^+ lifetime was increased to ~75 μs due to an ~ 2 nm thick SiO_x passivation layer (compared to a value of ~5 μs for a reference bare *n*-Si wafer[83]). The

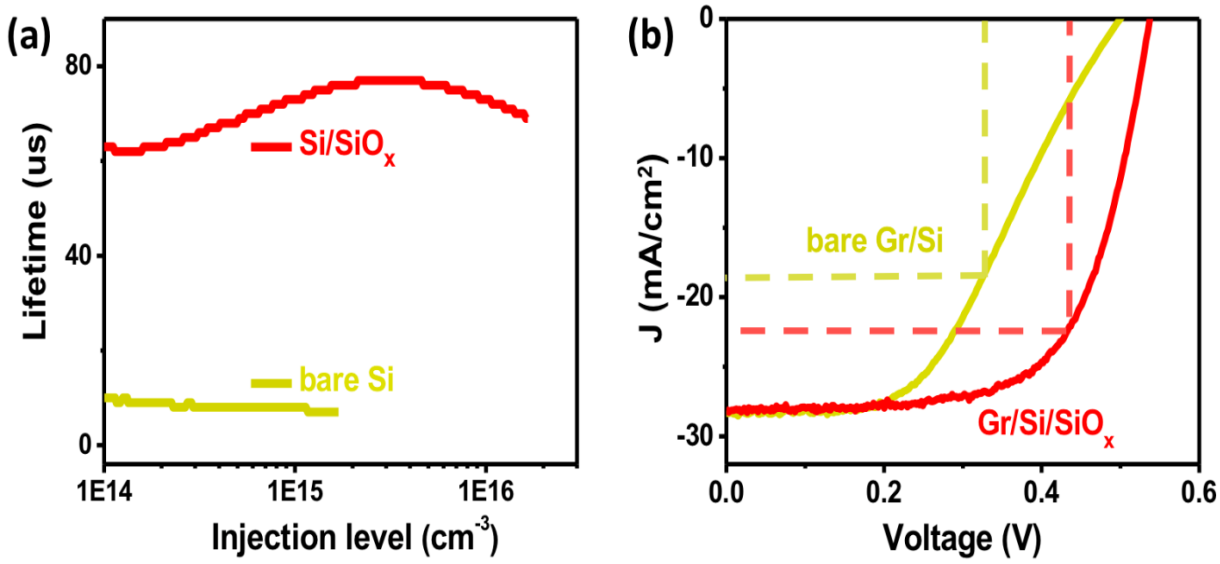

Figure 4.6:(a)Minority carrier lifetime as a function of injection level (excess carrier density) of bare silicon and passivated silicon (b) *J-V* curves of solar cell comparing the bare (Gr/Si) and passivated (Gr/Si/SiO_x) solar cells. Corresponding dash lines indicates the relative FF enhancement.

injection-dependence of the lifetime indicated that SRH (Shockley-Read-Hall) recombination in the bulk was dominant at carrier injection level densities corresponding to AM1.5G illumination.[84] A concomitant improvement in the *FF* and V_{oc} (of ~ 25 mV) due to the passivation layer was also observed as shown in Figure 4.6b, the typical *J-V* curves of Gr/Si and Gr/Si/SiO_x solar cells under illumination. It can be seen that introduction of passivation layer improved the *FF* and V_{oc} of solar cell due to the reduced surface recombination.

Since the surface of wafer presents defects such as disruption of crystal lattice, and includes impurities, dangling bonds, etc., it introduces electronic energy levels inside the bandgap. These energy levels, which also referred as surface states, provide many recombination sites for the carriers. Therefore, applying a dielectric layer to passivate those states is a necessity

to reduce the carrier losses at the interface.[76,85] Here we attributed the improved *FF* and V_{oc} to reduced recombination at the back contact of solar cell through the SiO_x passivation layer.

In order to obtain highest current density, a relatively high doped photoactive material is desirable for solar cell. However, it is important to note that high doping results in lower minority carrier lifetime (τ), that is, created electron-hole pairs will recombine quickly before reaching the corresponding electrode. Lifetime of the carriers in a material is given;

$$\frac{1}{\tau_{eff}} = \frac{1}{\tau_b} + \frac{1}{\tau_s} \qquad (4.1)$$

where, τ_{eff} is the effective lifetime, τ_b and τ_s are bulk and surface lifetime, respectively. Here, τ_b consists of radiative recombination, Auger recombination, and Shockley-Read-Hall recombination.[86] It can be seen from the Equation 4.1 that surface recombination plays an important role on the lifetime of carriers. Considering that most of the collected electron hole pairs are close to the surface of wafer, it is crucial to reduce the surface recombination to obtain maximum carrier lifetime. Therefore, applying an insulator layer to passivate the defects at the surface of wafer is required to improve the collection of carriers which subsequently improve the PCE of solar cells.[73,87,88]

We investigated the *optimal* thickness of the passivation layer to mediate between too little of a passivation effect and reduced current collection efficiency at large thicknesses, respectively. To this end, we varied the thicknesses of SiO_x (grown through HNO_3 as oxidizing agent[74,75,89]) in the range of 1 nm to 4 nm. From the resulting *J-V* curves, as in Figure 4.7a, it was observed that a 2 nm (± 0.2 nm) SiO_x thickness yields the highest PCE. The *FF* was also the

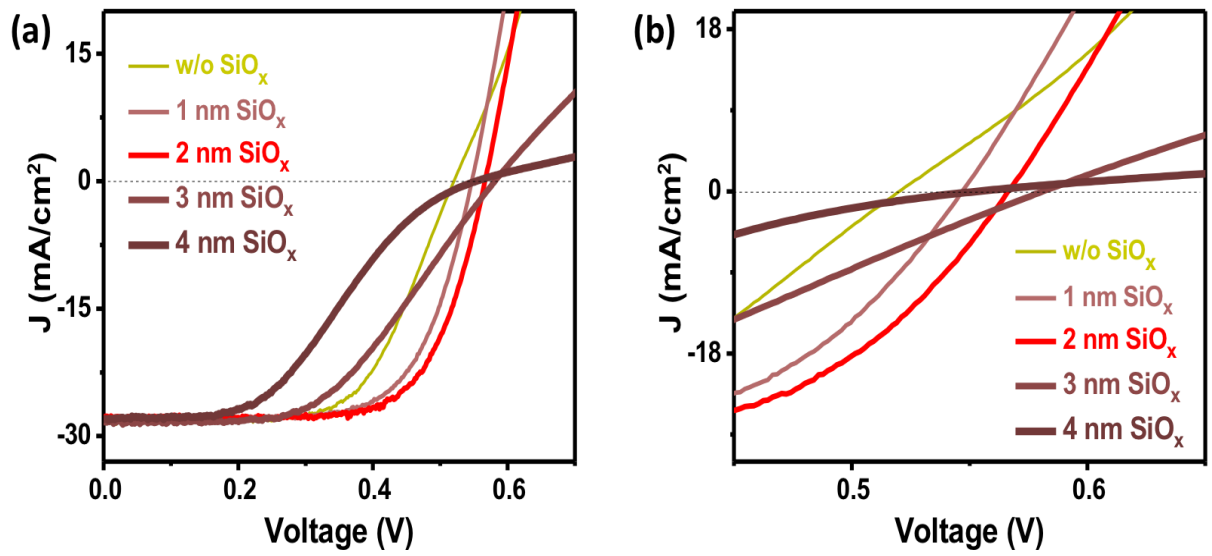

Figure 4.7: (a) *J-V* curves of solar cells with different passivation (SiO_x) thicknesses are used for passivation optimization. (b) Highlighted region of *J-V* curves at forward bias (0.45V to 0.65V) indicating a V_{oc} enhancement with increased thickness up to 3nm.

largest at ~ 2 nm of oxide thickness. It was previously noted[66] that with the use of thicker oxide layers, *S*-shaped kinks[3] are manifested in the *J-V* curves, presumably due to the formation of subsidiary diodic barriers, say at the back as well as in the front. This can be clearly seen in Figure 4.7a, for the 3nm and 4nm SiO_x thicknesses result in S-shape kink in *J-V* curves. No significant change was observed in the J_{sc}. It was noted that such optimal thickness values are in accord with earlier studies on metal-insulator-semiconductor junctions[90,91] and silicon based solar cells.[73] It was also noted that Voc is increasing with increasing oxide thickness until 3nm, as highlighted in figure 4.7b. We attributed that the increasing oxide thickness might reduce the leakage current and yield a higher V_{oc}. The diode *ideality factor* was obtained through standard procedures[17], and seen to be reduced to ~ 1.3 for Gr/Si/SiO_x (*cf.*, from ~ 1.5 for Gr/Si PV cells)

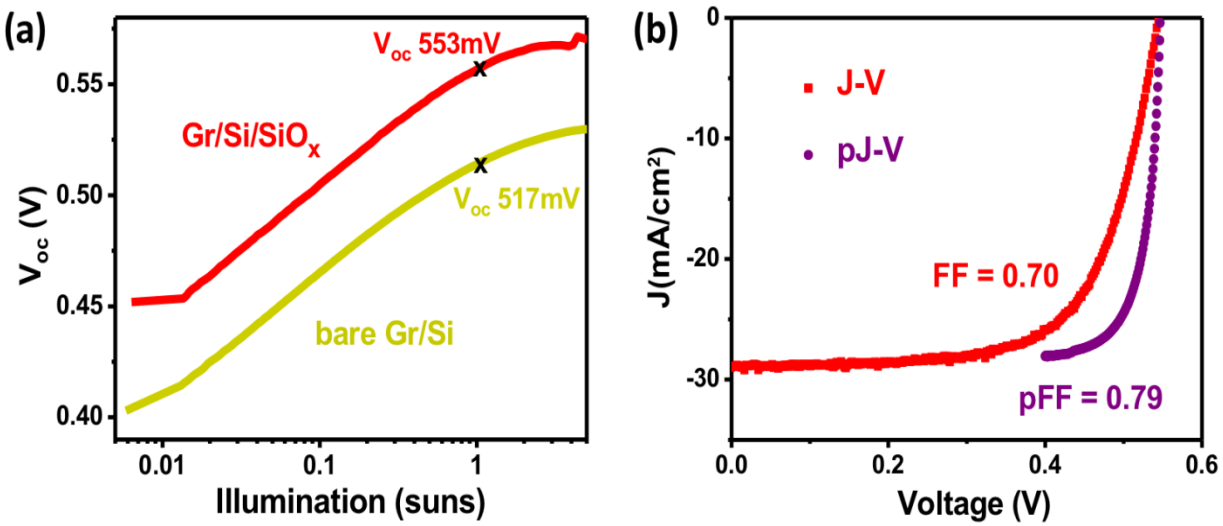

Figure 4.8: (a) Suns-Voc measurements for Gr/Si and and Gr/Si/SiO_x shows the attainable $_{Voc}$ as a function of illumination intensity. Higher Voc in Gr/Si/SiO_x indicates the beneficial effect of passivation. (b) *J-V* curves of Gr/Si/SiO_x solar cells obtained from two different measurements. The purple curve represents the *J-V* curve at the absent of series resistance indicates the effect of R_s on *FF*.

Such gains in the PV characteristics, brought about by the SiO_x passivation, and related to the J_{sc}, *FF* and the V_{oc} yields an overall increase of the PCE to ~ 11% which is the *highest efficiency for chemical doping-free Gr/Si solar cell to date*.

The variation of the V_{oc} as a function of the illumination intensity (in units of *Suns*) comparing bare Gr/Si and Gr/Si PV cells with the passivation layer: Gr/Si/SiO_x, is shown in Figure 4.8a. Such a measurement was carried in the absence of electrical current flow through the device and consequently series resistance effects are irrelevant. The V_{oc} of Gr/Si/SiO_x PV cells was clearly higher and suggests the beneficial influence of passivation. We also superpose the *pseudo J-V* and the measured *J-V* curves for the Gr/Si/SiO_x samples in Figure 4.8b. Here, the

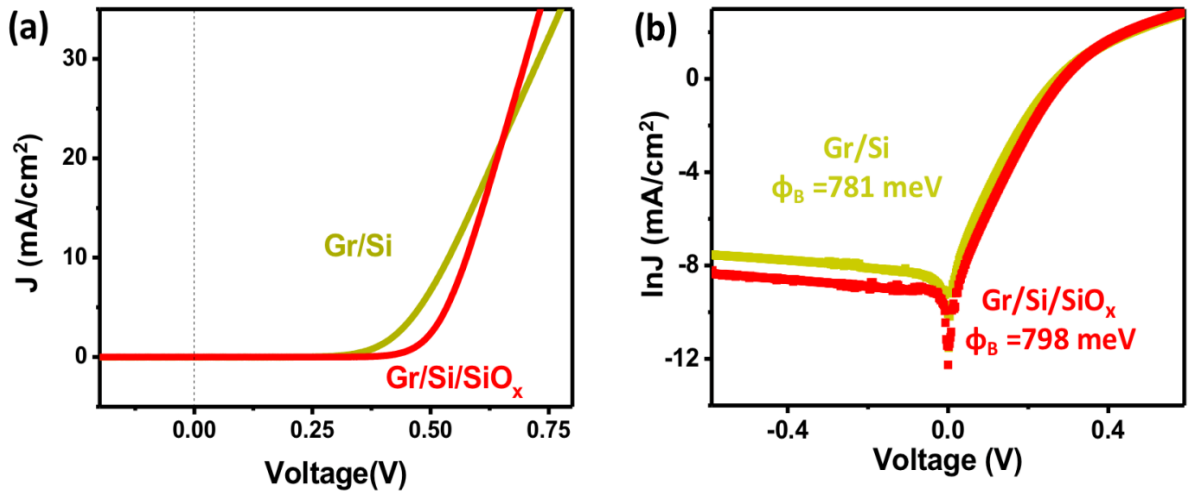

Figure 4.9: (a) Dark *J-V* curve of bare and passivated solar cells. (b) *ln(J)-V* curve of corresponding solar cells used to estimate the Φ_b. Related Φ_b are indicated in figure.

*pseudo*FF = FF/(1-R_sJ_{sc}/V_{oc}) from which the R_s was estimated to be ~ 0.94 Ωcm^2. From the dark J-V analysis as shown in Figure 4.9, it was estimated that Φ_b of passivated solar cell is higher than the bare solar cell. As can be seen in Figure 4.9b, J_s was lower due to the introduction of the SiO_x and contributes to an improved V_{oc}.[73,92]

The influence of the R_s as related to the lateral charge flow in the Gr, was studied through varying the active area (*AA*) of the Gr/Si/SiO_x PV cell. Five different values of the *AA* of Gr/Si/SiO_x solar cells, ranging from 2.25 mm^2 to 16.0 mm^2, were prepared with an optimized 2 nm SiO_x thickness: Figure 4.10: J-V curves of these solar cell under illumination are presented if Figure 4.10a, along with the actual devices presented in Figure 4.10c. It was noted that that the length corresponding to an *AA* of ~ 2.25 mm^2 corresponds to ~1.5 mm, comparable with the finger spacing of *p-n* junction solar cells.[93,94] It was observed at the very outset that the *FF* of solar cells significantly decreases with increasing *AA*, due to the increased R_s.[7,20] The highest *FF* and PCE are observed for the 2.25 mm^2 sample. From *J-V* analysis, in the *dark*, and using the

relation[17,95]: $d(V)/d\,(\ln J) = R_sAJ + n(k_BT/e)$, we estimated that the R_sA increases from 1.3 Ω-cm^2 to 14.1 Ω-cm^2 with an increase in the *AA* from 2.25 mm^2 to 16.0 mm^2 as shown in Figure 4.10b. Much of the R_s variation may be due to the relatively higher sheet resistance of the used Gr (measured at ~700Ω/□, by four-point probing) compared to state-of-the-art[66] emitter resistance

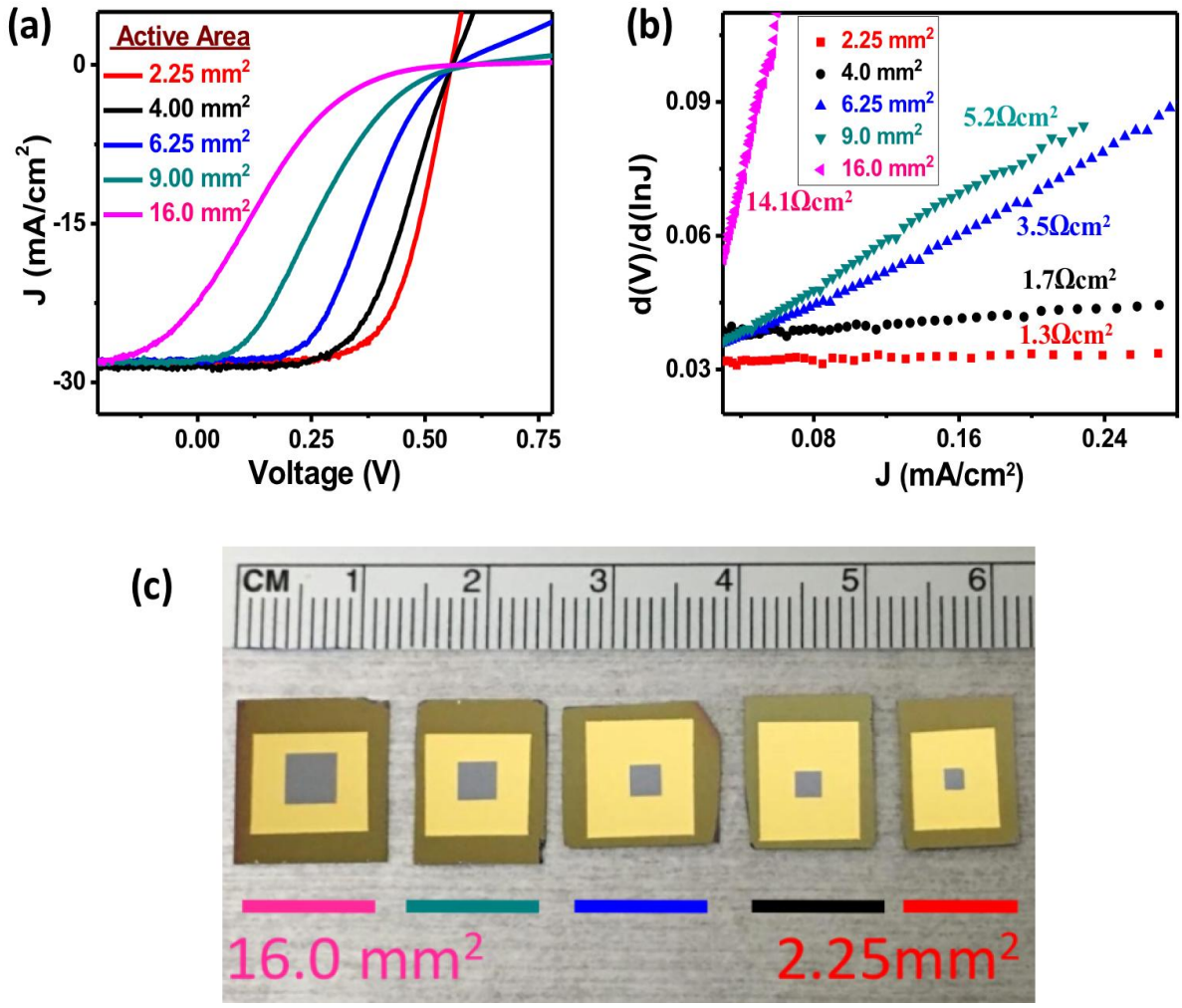

Figure 4.10: Optimization of solar cell active area (AA). (a) *J-V* curves of solar cells with different active areas ranging from 2.25mm^2 to 16.0mm^2. (b) *d(V)/d(ln(J))-J* plots of cells with different AA indicate the related R_s of solar cells. (c) Optical images of solar cells with different active areas that labeled with corresponding color.

values of the order of 120 Ω/□. As there was an insignificant change in the V_{oc}, we conclude that the enhanced PCE was primarily promoted by the *FF* enhancement and related to the R_s.

To reduce R_s further, we subjected the Gr/Si/SiO_x to nitric acid treatment,[24,96] where the Gr sheet resistance was measured to be further reduced to ~ 210 Ω/□. The corresponding R_s of the 2.25 mm^2 PV cell was reduced from 3.2 Ω-cm^2 to 1.3 Ω-cm^2 after ambient doping, with a further reduction to ~1.1Ω-cm^2 due to acid treatment. From such engineered architectures, using passivation layers coupled with *AA* optimization and ambient/acid based oxidation, a *FF* of 0.78 was obtained and noted to be the *highest* value to date for Gr/Si PV solar cell to date, along with a V_{oc} of ~ 593 mV and $J_{sc}$of ~ 28.5mA/cm^2, leading to a further increase of the PCE to ~13.1%.

A *record* PCE of ~16.9% was achieved in the Gr/Si/SiO_x solar cell by deploying PMMA as an ARC coating onto the graphene. The use of ~90 nm thick PMMA increased the J_{sc} from ~ 28.5mA/cm^2 to ~ 38.1mA/cm^2 with a V_{oc} of 0.593 V. The comparison of the *J-V* characteristics of the ARC layer coated Gr/Si/SiO_x PV cells with the earlier prototypes, are shown in Figure 4.11a, with the relevant output parameters of solar cells summarized in Table 4.1. Measurements were performed to record the resultant increased external quantum efficiency (EQE): Figure 4b. An EQE around 90% in the visible wavelength regime was achieved. In our experiments, we aimed to *specifically* enhance the EQE at the peak intensity of solar spectrum (~ 550 nm), through the use of 90nm thick PMMA (with refractive index of 1.5). In support, we carried out diffuse reflectance measurements with an integrating sphere on the PMMA coated Gr/Si solar cell, where a minimum reflection (of ~6%) was obtained at λ~ 550 nm: Figure 4.12. Note that the lowest reflectance corresponds to an EQE of ~ 90% at the wavelength region as reported. Around 3% loss in the EQE is attributed absorption of graphene in corresponding wavelength.

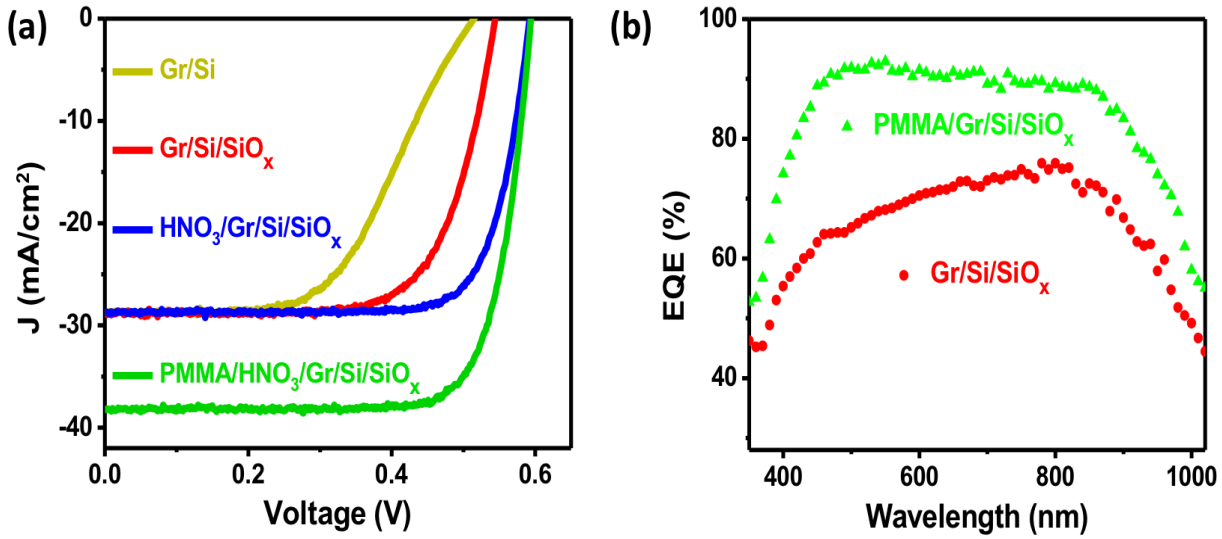

Figure 4.11: (a) Evolution of *J-V* curves upon applied methodologies. (b) EQE curves of $Gr/Si/SiO_x$ and $PMMA/Gr/Si/SiO_x$ indicates the enhanced current density upon PMMA coating.

Table 4.1:*J-V* parameters of solar cells shown in Figure 4.11(a)

	J_{sc}(mA/cm^2)	V_{oc} (V)	FF (%)	PCE (%)
Gr/Si	28.5	0.520	59	8.9
Gr/Si/SiO_x	28.5	0.549	70	11.0
HNO_3/Gr/Si/SiO_x	28.5	0.592	78	13.1
PMMA/HNO_3/Gr/Si/SiO_x	38.1	0.593	75	16.9

The lower EQE in the smaller wavelength regime may be due to parasitic absorption or recombination at the Gr/Si interface in the front, concomitant to lower light penetration depths.[88] The decrease of the EQE at larger wavelengths, beyond ~ 850 nm is likely related to the

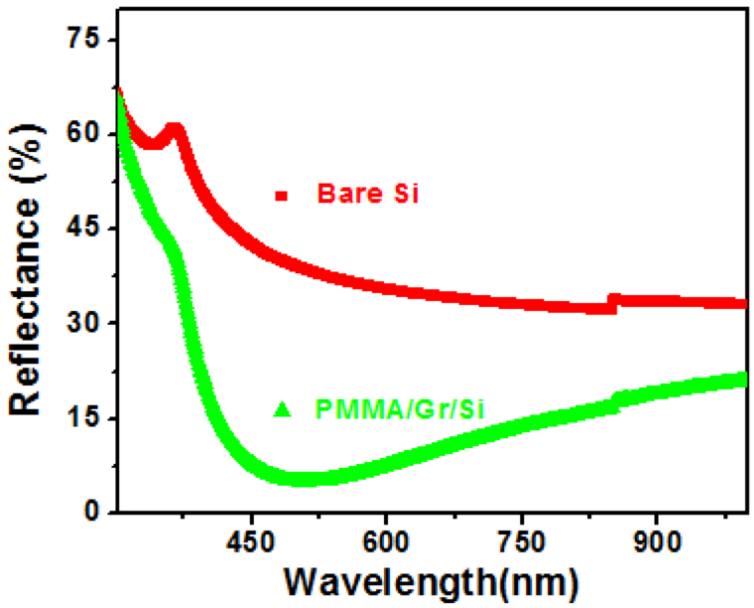

Figure 4.12: Reflectance measurements indicate the reduced reflection upon PMMA coating. Note that the lowest reflectance (λ ~550nm) corresponds to the peak intensity of solar spectrum.

recombination in the bulk. In the absence of the ARC, the EQE was ~70% in visible region. Note that, although the short wavelength (from 400nm to 600nm) response of our ARC free solar cell lower, introduction of ARC, specifically at that wavelength region, resulted in the highest EQE of ARC solar cell.

We carried out the Suns-V_{oc} measurements for our PMMA/HNO_3/Gr/Si/SiO_x solar cell as presented in Figure 4.13. It indicates an increase[20] of the achievable V_{oc} to 0.618 V for the ARC coated devices– a gain of 25 mV, which could be expected due to the enhanced J_{sc}. Since such a measurement carried out at the absence of series resistance, it reveals that our solar cell efficiency is also limited with the series resistance. Subsequently, it is observed that the FF our solar cells slightly reduced attributed the resistance related losses. However, the J_{sc} of our final device (with PMMA) is one of the highest reported thus far.[21,66,67]

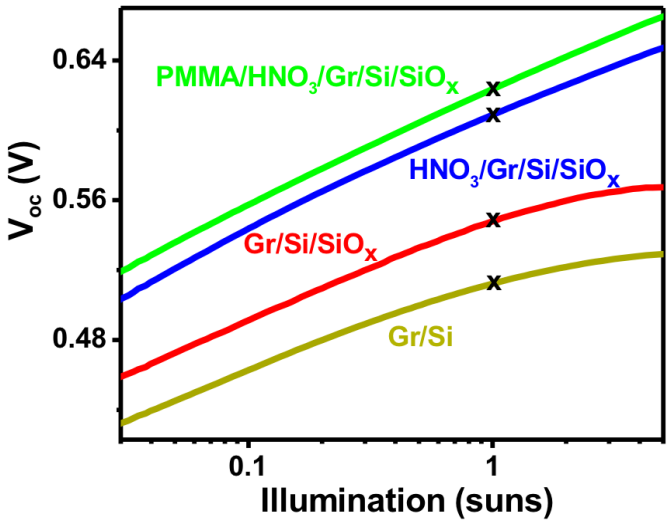

Figure 4.13: Suns-Voc measurements of solar cells presented in Figure 4.7a shows the attainable V_{oc} of solar cells at the absence of R_s.

While our work indicates record efficiency for a Gr/Si solar cell, even further improvements are possible. For example, it was remarked earlier that the PCE would be promoted through enhancement of the V_{bi} – which in turn may be related to an increased W_{Gr}. For instance, when the W_{Gr} is increased to correspond to the top of the valence band of the Si, *i.e.* ,to ~ 5.2 eV,[66] seamless hole transfer from the Si to the graphene may be expected. The subsequent efficient h^+ transport in the Gr would be facilitated through defect free material and facilitated through a small intrinsic sheet resistance. The latter aspect is presently considered a major issue restricting the widespread usage of graphene for electrical contacts, and needs to be more carefully studied. Moreover, the h^+ lifetime could be increased by an order of magnitude to ~ 1 ms, through using higher purity starting wafers or through impurity gettering[97], which would translate to an increase[88] of ~ 10% in the J_{sc} as well as the *FF*. Moreover, while back surface passivation was emphasized, further PCE enhancement may be achieved through front-surface passivation as well. Indeed, the trajectory of efficiency increase may follow the course of Si-

based heterojunction solar cell, with a PCE over 26%, leveraging exceptional surface passivation by a-Si.[88]

4.5. Conclusion

In summary, a Gr/Si PV cell with a record PCE of 16.9% was demonstrated. This was achieved through several stages of careful interfacial and surface control. For example, employing a selected thickness of passivation layer (SiO_X) at the back-surface of the cell was observed to enhance the *FF* and V_{oc}, by increasing photo-excited carrier lifetime. While exposure of the top Gr surface of the PV cell to ambient air yields a measure of *p*-doping contributing to the V_{oc}, further modulation of the resultant work function of Gr through acid treatment was found necessary to achieve the highest efficiency. A proper layout of the active area of the exposed Gr lowered the parasitic series resistance, with a maximum in the *FF* observed with an area of ~ 2.25 mm^2 corresponding to a length scale of ~1.5 mm, which was comparable to the electrode-finger spacing of commercial *p-n* junction silicon solar cells. We have indicated methodologies to further increase the efficiency of Gr/Si based PV cells, while avoiding issues such as Auger or surface recombination, to a point where they could compete with and perhaps even surpass conventional Si *p-n* junction solar cells.

Chapter 4, in part, has been submitted to Solar Energy Materials and Solar Cells which titled "Enhanced power conversion efficiency in graphene/silicon solar cell, through the electrical carrier and interface engineering" by Serdar Yavuz, Ernesto Magana, Aybuke Turker, David P. Fenning and Prabhakar R. Bandaru. The dissertation/thesis author was the primary investigator and author of this paper.

CHAPTER 5: IMPROVED CONVERSION EFFICIENCY AND STABILITY, THROUGH THE USE OF ALUMINUM OXIDE IN AN N-GRAPHENE/P-SILICON SOLAR CELL

5.1. Introduction

As described in chapter 2, one of the most attractive characteristics of graphene is the adjustable work function through doping which provides a broader platform for its applications. Due to the atomic thickness of graphene, which enables nanoscale contact path, a significant research has been carried out for graphene based field effect transistor (FET)[98–100] fabrication. Through these investigations, it is revealed that modulation the electrical characteristics of graphene can change the transistor type such as from p-type to n-type. This suggests that graphene can be used both as a hole extraction layer and an electron extraction layer by adjusting the underlying material. In chapter 3 and chapter 4, role of graphene as a hole extraction layer have been discussed by placing it on top of n-silicon. In this chapter, role of graphene as an electron extraction layer will be discussed in a graphene/p-silicon solar cell.

5.2 Graphene as an electron extraction layer in graphene/p-silicon solar cells

The tunability of the electrical and optical properties[22] enable graphene (Gr) to be used as both an electron and hole extraction in organic and inorganic photovoltaic devices.[21,23] For example, it is shown that bis(trifluoromethanesulfonly)-amide (TFSA)[24] and nitric acid (HNO_3)[25] may *p*-dope the graphene while TiO_x[26] could serve as an *n*-dopant. Such modifications lead to the formation of Schottky junction between Gr with an underlying silicon (p-type/n-type). The work function of graphene (W_{Gr}), for this purpose, can be significantly altered through p- (/n-) doping for higher (/lower).[31] In the Schottky junction, the difference between the work function of Gr and the electron affinity (χ) of semiconductor creates a build in potential (V_{in}) which

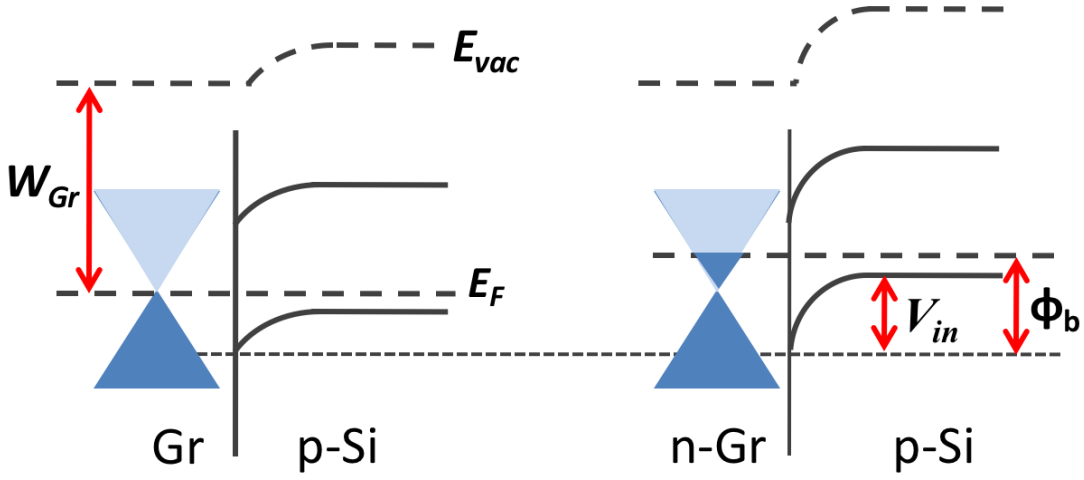

Figure 5.1: Hypothesized band diagram of Gr/p-Si solar cells. Figure on the right shows the bare/untreated Gr/p-Si solar cell. Left figure shows the evolution of Schottky junction parameters with n-doping of graphene.

separates the electron-hole pairs upon photon absorption: Figure 5.1. A lower W_{Gr} say through n-doping implies a higher V_{in} and a higher Schottky barrier height (Φ_b) with respect to *p*-Si (Figure 5.1, left diagram) with a consequent larger open circuit voltage (V_{oc}). A concomitant effective carrier separation would also yield a larger electrical current, e.g. the short circuit current density (J_{sc}) relevant for solar and a significant power conversion efficiency (PCE) of an n-Gr/p-Si solar cell.

However, compared to PCE of up to 17% in p-graphene/n-Silicon (p-Gr/n-Si) Schottky junction solar cells, the efficiency of n-graphene/p-Silicon (n-Gr/p-Si) solar cell is still lower (~10%) due to: (1) low Schottky barrier between the W_{Gr} (~4.7eV) and electron affinity of p-Si ($\chi_{p\text{-}Si}$~5.2eV), (2) natural p-doping of graphene when exposed to ambient oxygen.[81,82] To overcome these two main challenges, a significant n-doped Gr is required to ensure a high Schottky barrier height. It is also important to consider that such doping (*i*) should not sacrifice

the optical transmittance of graphene, (*ii*) should be stable for device performance, and (*iii*) be compatible with graphene based solar cell fabrication. Chang et al., has experimentally demonstrated that the W_{gr} can be reduced to ~3.25eV when treated with cesium fluoride (CsF).[31] This implies that the Φ_b could be larger in n-Gr/p-Si at compared to the p-Gr/n-Si case where the barrier height is ~1eV (W_{gr}- $\chi_{n\text{-}si}$(~4.1eV)), promising a larger V_{oc} and PCE in the former situation. Indeed, a significant PCE enhancement in n-Gr/p-Si solar cell from ~0.1% to ~10% reported through the use of TiO_x, which was posited to function as an electron donor to Gr, reducing the W_{gr}.[79]

In this part, we will investigate whether further improvements in the PCE are possible through tuning W_{gr} through effective n-doping. We will show that hydrofluoric acid (HF) treatment improves the PCE of Gr/p-Si solar cell bay a factor of sixty compared to a control un-treated-graphene/p-Si solar cell. Significant enhancement in J_{sc}, V_{oc} and *FF* upon HF treatment were observed. Raman spectroscopy analysis was used to confirm the n-doping of Gr. We additionally propose, for the first time, use of atomic layer deposited (ALD)-AlO_x as an anti-reflection coating (ARC) layer as well for encapsulation to prevent solar cell efficiency degradation. It was also interesting to note that the AlO_x may contribute to n-doping of the Gr. These innovations contributed to achieving a record PCE of 12.5% which is the highest value reported for an n-Gr/p-Si solar cell, to date

5.3 Experimental

Gr/p-Si solar cells were prepared through standard photolithography processing. Briefly, a 200nm PECVD SiO_2 deposited on top of the flat surface of p-Si (1-10Ωcm, single side polished) followed by the patterning of active area. Subsequently, Au/Ti and Al were deposited

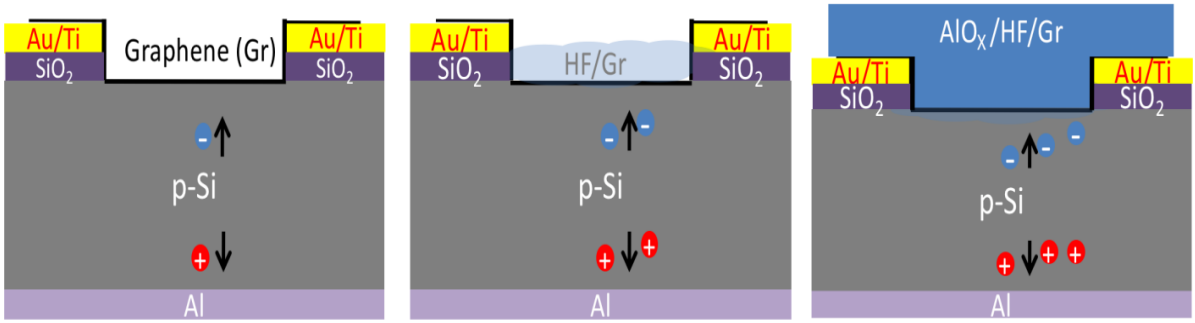

Figure 5.2: As synthesized solar cell (bare Gr/p-Si) solar cells and applied methodologies from left to right.

at the front side and the back side, respectively, for electrical contacts. A buffer oxide etch (BOE) (1:6 ratio) was used to remove the SiO_2 through the patterned window (1.5x 1.5mm). A CVD-grown single layer graphene (SLG) was transferred onto the top via a PMMA assisted wet transfer process[70] and dried in the ambient. The PMMA was then removed, using acetone and isopropanol. The Gr/p-Si sample was than annealed at 400C under H_2/N_2 gas flow to improve the contact between graphene and underlying Si, as previously considered.[20,101] Subsequently, the samples (Set A) were exposed to HF vapor at room temperature. In another set of samples (Set B), 80 nm ALD-AlO_x was deposited on top of the Gr as an antireflection coating (ARC) layer: Figure 5.2.

5.4 Results and Discussion

We first analyze the effect of HF treatment on the performance of Gr/p-Si solar cell, belonging to Set A. From a comparison, in Figure 5.3a, the PCE of bare Gr/p-Si solar cell was ~0.1% with J_{sc}, V_{oc} and FF of 6 mA/cm^2, 0.195V, and 10%, respectively. However, the HF treated has a substantially improvement in corresponding parameter values of 26.2mA/cm^2, 0.390V, and 0.58% of J_{sc}, V_{oc}, and FF, respectively, yielding a substantial boosts in the PCE

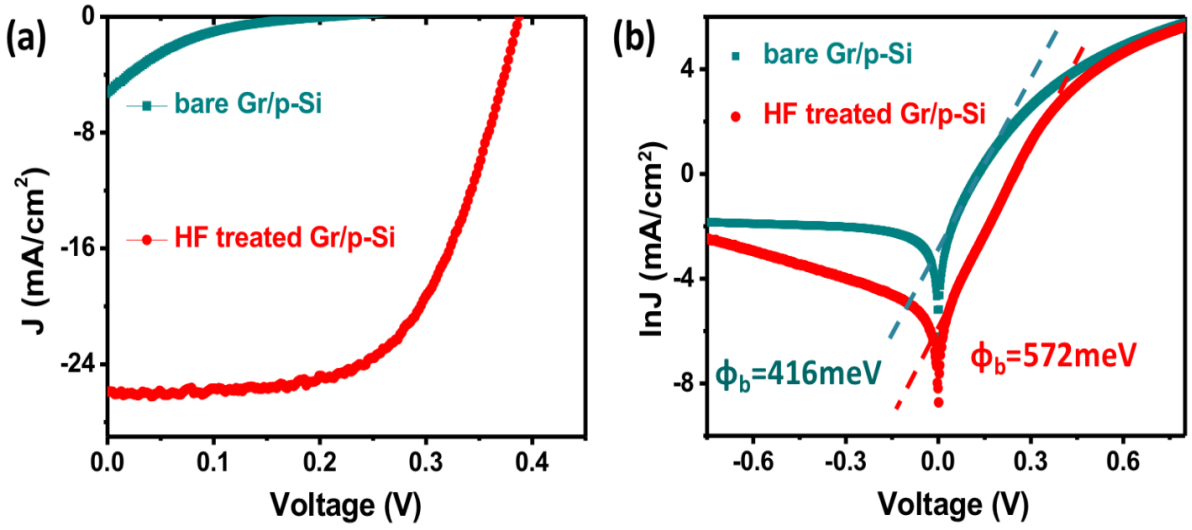

Figure 5.3: (a)*J-V* curve of bare Gr/Si and HF treated Gr/p-Si solar cells are presented (b)Corresponding dark *ln(J)-V* curve of solar cells.

from ~0.1% to 6%. We attribute this improvement mainly to increase in V_{oc} from a higher Schottky barrier (larger the Φ_b) due to the HF treatment. Such an observation was made through comparative analysis of *J-V* analysis at the absence of illumination (dark *J-V*). From the analysis of dark *J-V* curves of untreated and HF treated Gr/p-Si solar cells and incorporating a thermionic emission model[17] as described in previous chapter, in the form of:

$$J = J_s\left[\left(exp\frac{eV}{nk_bT}\right) - 1\right] \qquad (5.1)$$

where;

$$J_S = A^*T^2 exp\left(\frac{\varphi_b}{k_bT}\right) \qquad (5.2)$$

Here, J_s as the reverse saturation current density, A^* as the effective Richardson's constant, Φ_b as the Schottky barrier height, n is the diode ideality factor, k_b is the Boltzmann constant, and T is the temperature. From dark $ln(J)$-V graph presented in Figure 1d and using the Eqns. (1) and (2), the Φ_b was estimated to increase from 416 meV to 572 meV upon HF treatment. Such an increase in the Φ_b suggests that HF treatment may have reduced W_{Gr}. The larger Φ_b would facilitate the efficient separation and consequent collection of generated carriers leading a higher J_{sc} as hypothesized earlier.

The HF treatment may have also affected the Gr/p-Si interface, through removing the native oxide on the Si on which Gr was placed. While it has been discussed that a thin oxide can provide a better interface in the case of Gr/n-Si solar cells,[24,66] e.g., through passivation of the trap states (/dangling bonds) at the interface, and reducing the carrier recombination sites, it is not apparent whether similar reasoning would be applicable to p-Si. Alternately, non-stoichiometric interfacial oxide (SiO_x) may p-dope the graphene, and consequently lowering the related Φ_b.

We carried out Raman spectroscopy analysis on the bare Gr (as control sample) and HF treated graphene: as seen Figure 5.4. The G and 2D peaks at around 1585cm^{-1} and 2680cm^{-1}, respectively, are the two well-known characteristic peaks of Gr,[30] and form the basis for analysis. The peak intensity ratio: I_{2D}/I_G of ~2.4 indicates the single layer graphene. An observed blue (/red) shift in both G and 2D peaks is used to indicate the p- (/n-) type doping, corresponding to a shortening (/lengthening) of the C-C bonds.[102] Figure 5.4a shows the Raman spectroscopy of un-treated Gr on glass. It was seen that subsequent to HF treatment, the G peak shifts to 1579cm^{-1}, while 2D peak appears at 2660cm^{-1}, indicating an n-doping [17,18] Additionally, a wider 2D peak

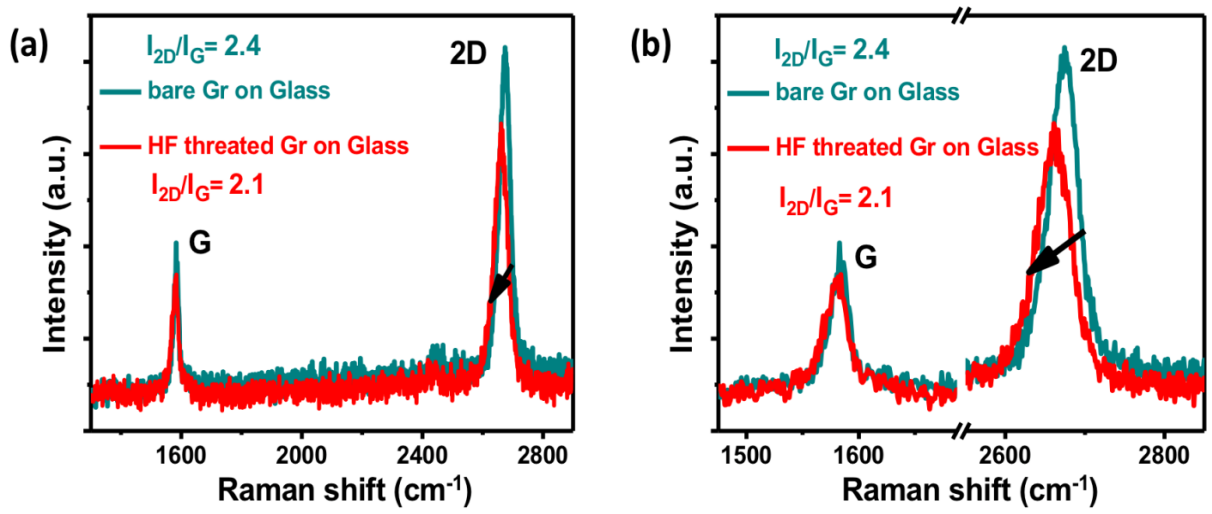

Figure 5.4: (a) Raman analysis of bare Gr on glass as control sample and HF treated Gr on glass are presented. (b) Extended peaks indicate the n-doping upon HF treatment.

width (increasing from 39cm^{-1} to 51cm^{-1}) as well as the reduced intensity ratio of I_{2D}/I_G from 2.4 to 2.1 seems to be in accord with the earlier reports of n-doping of graphene.[30,103]

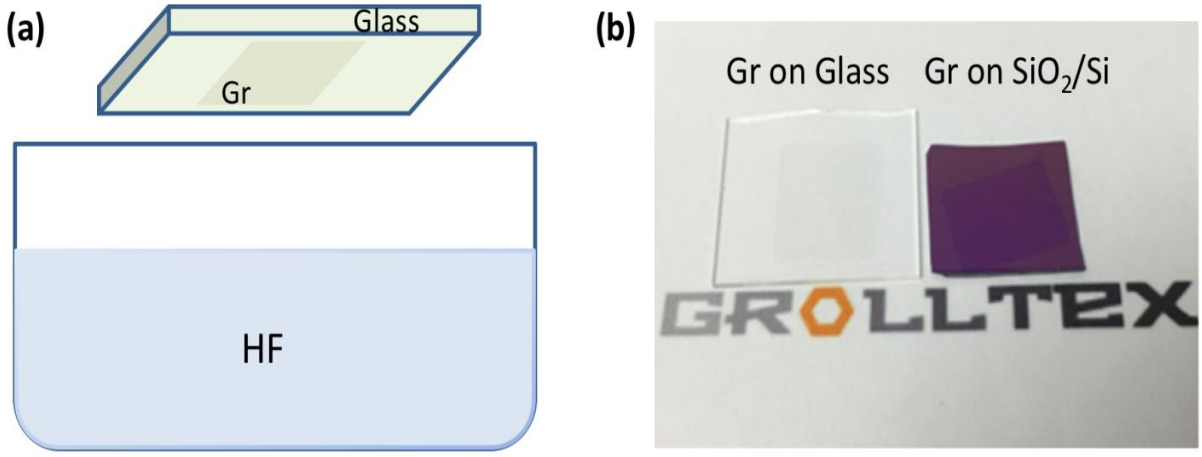

Figure 5.5:(a) A schematic representation of HF treatment. (b) Optical images of single layer graphene on glass and SiO_2(300nm)/Si substrate.

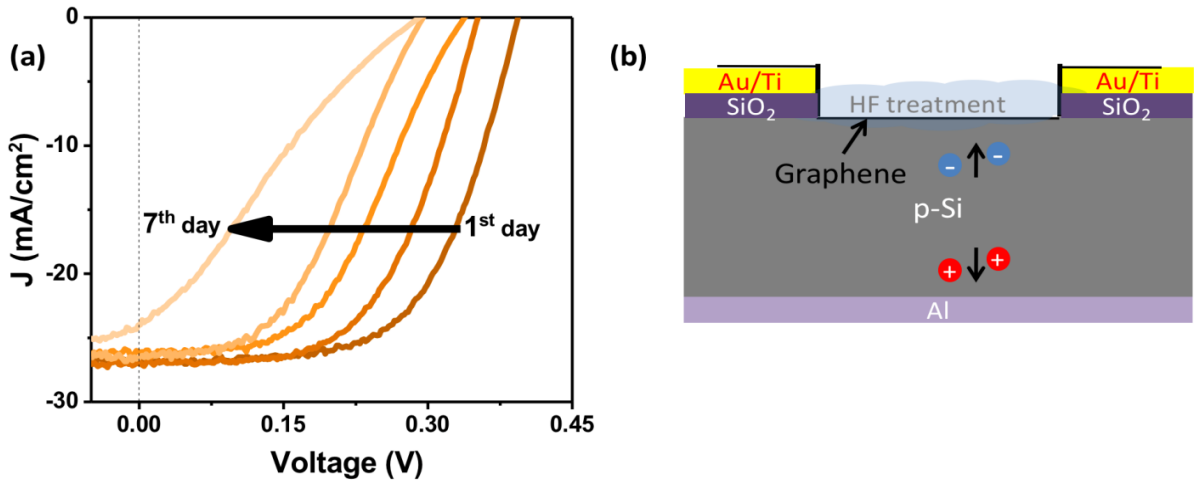

Figure 5.6: (a) Evolution of the *J-V* curve HF treated Gr/p-Si solar cell within the seven day of testing period without encapsulation. Around 65% PCE depredation observed. (b) A schematic cross-section of solar cell at that stage.

While the HF treatment significantly improves the PCE of n-Gr/p-Si solar cell, there was a significant degradation of the solar cell efficiency, due to a counteracting effect of the n-doped Gr on ambient exposure which has been discussed in previous chapter.[82] Figure 5.6a shows the *J-V* characteristic of device along with the cross-sectional schematic of solar cell at that stage. It has been observed around 65% PCE degradation from the original PCE within a week of testing period.

We consequently deployed ALD- AlO_x as an encapsulating layer. Beneq TFS200 Atomic Layer Deposition is used for AlO_x deposition. Trimethylaluminium (TMA) and water (H_2O) used as precursor with N_2 gas flow and deposition temperature set to 200°C. Deposition rate is found to be 1.01A per cycle by using different number of cycles ranging from 50 to 1000 on polished silicon substrate (100). Ellipsometry (Rudolph Auto EL-III) was used to measure the thickness of the deposited AlO_x as well as the refractive index. The refractive index of AlO_x (n_{arc}

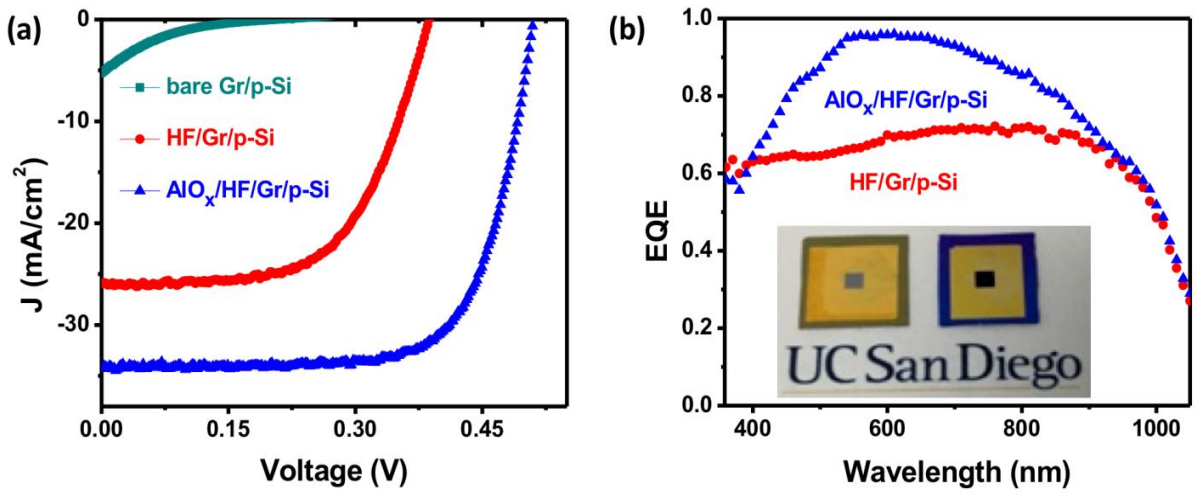

Figure 5.7: Evolution of *J-V* curve with applied methodologies. (b) EQE of HF/Gr/p-Si and AlO_x/ HF/Gr/p-Si solar cells indicates a significant enhancement in visible region upon AlO_x deposition. Inset figure shows the actual devices of without (left) and with (right) ARC.

Table 5.1: Output parameters of solar cells presented in Figure 5.7a

	V_{oc} (V)	J_{sc}(mA/cm^2)	FF	PCE (%)
Gr/p-Si	**0.195**	**6.0**	**0.10**	**0.1**
HF/Gr/p-Si	**0.395**	**26.2**	**0.58**	**6.0**
AlO$_x$/HF/Gr/p-Si	**0.510**	**34.5**	**0.71**	**12.5**

~1.75 at a wavelength λ: 550nm, the peak intensity of the solar spectrum) suggests its possible use as an ARC with an optimum thickness $d_o=\lambda/4n_{arc}$.[63,104] Consequently, we deposited 80nm

AlO_x on top of graphene. As indicated in Figure 5.7a, the J_{sc} of solar cell increased from 26.2mA/cm^2 to 34.5mA/cm^2 indicating a better harvesting of incoming light by reducing the light reflection from Gr/Si surface, due to the ARC. The enhanced J_{sc} was further verified with external quantum efficiency (EQE) measurements shown in Figure 5.7b. A significant EQE enhancement in the visible wavelength region for AlO_x deposited solar cell (AlO_x/HF/Gr/p-Si) compared to the ARC free solar cell (HF/Gr/p-Si) indicates such enhanced current density. By integrating the EQE over the solar spectrum as described in chapter 3, Equation 3.1 we estimated a J_{sc} increase from 25.6mA/cm^2 to 34mA/cm^2 in accord with observed J_{sc} increase brought by *J-V* measurements shown in Figure 5.7a.

We also carried out reflectance measurements on bare p-Si and Si coated with the AlO_x, presented in Figure 5.8a along with the optical images of bare and AlO_x deposited Si substrates in Figure 5.8b. Significantly reduced reflection from 400nm to 1000nm wavelength region has been realized. This can be visually seen from the comparison of silicon wafers in Figure 5.8b that AlO_x deposited sample has a darker color indicating the reduced reflection. The lowest reflectance (of ~3%) obtained in the wavelength range of 550nm to 600nm which is in accord with the highest EQE in the range. In addition, to reveal how the reflection from solar cell correlates with EQE, comparison of reflectance and EQE of AlO_x/HF/Gr/p-Si solar cell as a function of wavelength is presented in Figure 5.9. It can be seen form Figure 5.9 that the reduced EQE at longer wavelength region (λ>800nm) is in accord with the increased reflection at corresponding wavelength. This indicates a possible double layer ARC can address the long wavelength response of our solar cell and subsequently improve the PCE.

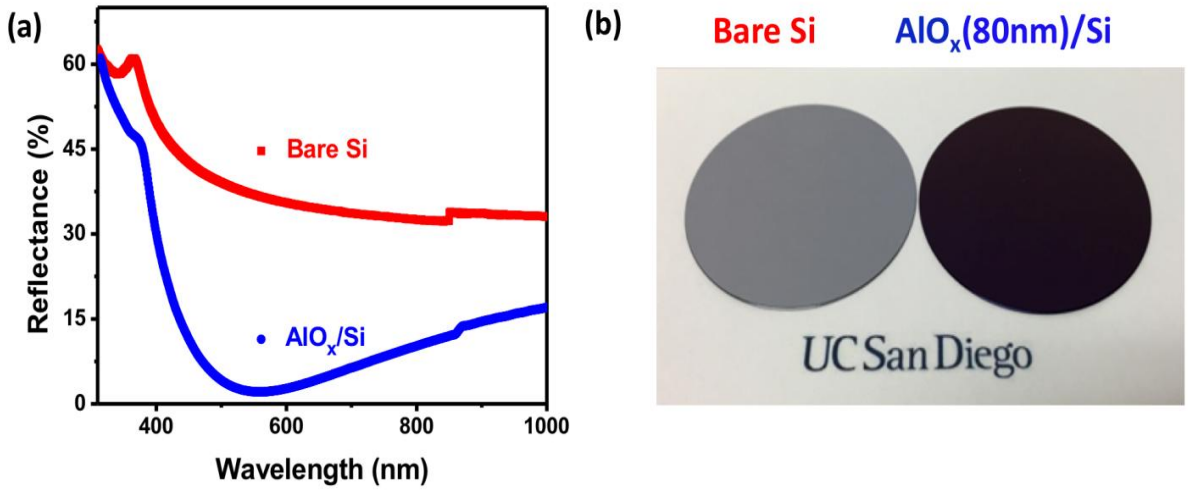

Figure 5.8: (a) Reflectance measurements of bare silicon and AlO_x deposited (80nm) silicon. The lowest reflectance (~3%) obtained at ~550nm corresponds to peak intensity of solar spectrum. (b) Optical images of corresponding wafers

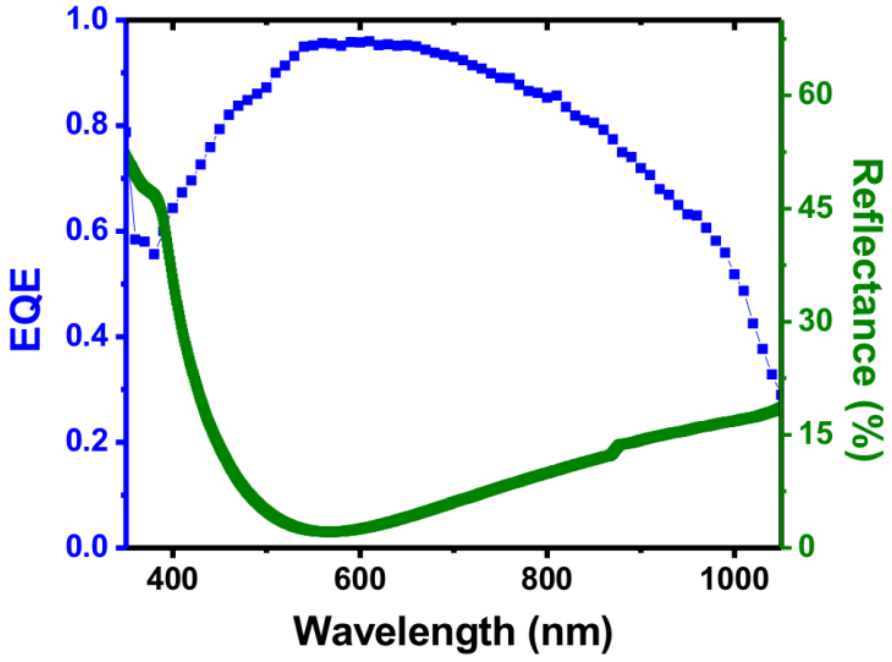

Figure 5.9: EQE and reflectance as a function of wavelength indicates that lowest reflectance is in line with the highest EQE.

The use of ALD-AlO_x also yielded an improved *FF* (from 0.58 to 0.71) as well as the V_{oc} (from 0.390V to 0.510V) indicates that AlO_x may also contribute n-doping of the Gr. We have studied such a possibility by fabricating a Gr based field effect transistor (FET), as indicated in Figure 5.10a. For Gr-FET devices, a 300nm PECVD SiO_2 deposited on p-type Silicon wafer (~1-10Ωcm^{-1}). Au/Ti electrical contacts were sputtered following the lithography process. CVD growth single layer graphene was suspended on contacts using the PMMA assisted transfer process as described in previous chapters. After removing PMMA, a 4nm ALD-AlO_x deposited on top of graphene. The use of thin film of AlO_x was to minimize the contact resistance related issues since ALD is conformal. Gate voltage was applied through the back side of p-Silicon. This four pads contact pattern was also used to measure the sheet resistance of Gr which is found to be ~400$\Omega/\square$ in ambient conditions without any treatment.

In such a FET device, the shift of Dirac point, i.e., upon a chemical treatment, towards a higher positive potential indicates a p-doping while shifting towards negative potential indicates an n-doping.[98,100,105] Figure 5.10b shows the gate-dependent conductivity of graphene FET. It was observed that synthesized graphene shows p-type behavior with a Dirac point around +14V due ambient exposure as reported previously.[82,99] However, a shift to a lower voltage of Dirac point, to +2V, was observed when 4nm AlO_x was deposited on top, indicating the possibility of n-doping due to AlO_x.[105]

We have explored the n-doping possibility further through Raman spectroscopy analysis. For the Raman analysis of ALD-AlO_x, the standard SiO_2(300nm)/Si substrate used with the above mentioned transfer process. A 4nm AlO_x deposited on Gr which forms a AlO_x/Gr/SiO_2/Si while Gr/SiO_2/Si sample used as a control sample for this experiment. Upon AlO_x deposition; (i) a shift to lower wavenumbers (a *red shift*) observed in the G- and 2D- peaks on the

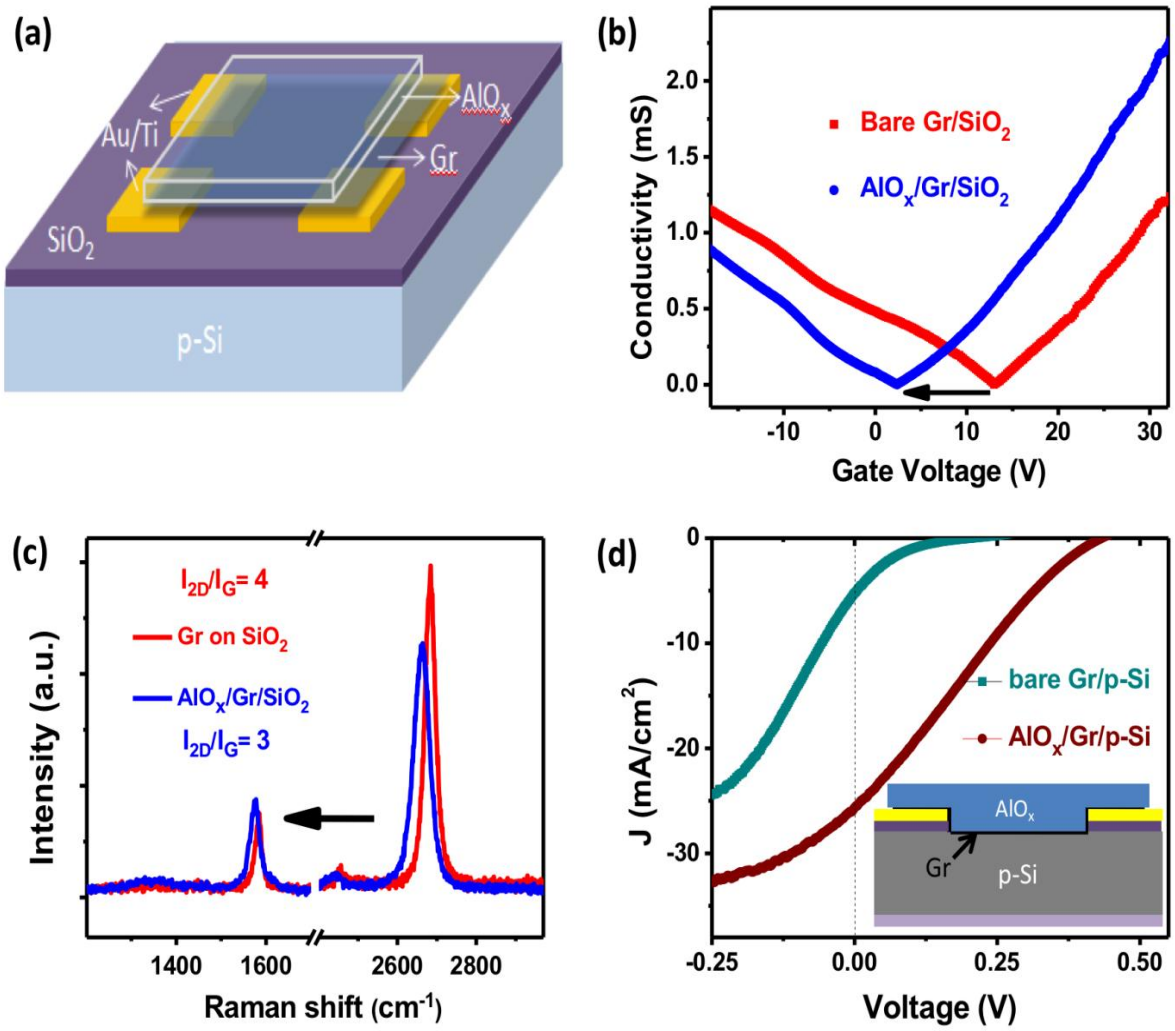

Figure 5.10: (a) A schematic of fabricated Gr-FET device. (b) Gate dependent conductivity of fabricated Gr-FETs. Shift towards negative potential indicates n-type doping upon AlO_x. (c) Raman spectrum of bare Gr on SiO_2 and AlO_x/Gr on SiO_2. (d) *J-V* curve of bare Gr/p-Si and AlO_x/Gr/p-Si solar cells (at the absence of HF treatment).

AlO_x(4nm)/Gr/SiO_x(300nm)/Si, (ii) reduced I_{2D}/I_G ratio from ~4 to~ 3 and (iii) broadening of the 2D peak suggesting such *n*-doping: Figure 5.10c.[34,36] In a comparative AlO_x/Gr/p-Si solar cell was prepared, at the absence of HF treatment. An increased PCE from ~0.1% to 2.6% with an increase of J_{sc}, V_{oc} and *FF* was observed: Figure 5.10d. As indicated earlier, a larger V_{oc} may be

attributed to higher Φ_b, which may also yield efficient carrier collection. Indeed, from the dark ln(*J*)-*V* analysis presented in Figure 4a, the AlO_x/HF/Gr/p-Si solar cell has a higher Φ_b of 704 meV. Such an n-doping may be attributed to the work function difference between Gr and AlO_x, which has been reported to be ~3.7 eV.[106,107]

Ideally, a material with a higher work function than that of Gr is a p-type dopant as previously shown with Au (~5.4eV),[19,25]graphene oxide,(~5.3eV)[21,27] and NiO (~5.4eV-6eV)[28,29]while a material with lower work function than graphene such as polyethylenimineethoxylate (PEIE ~4.1eV),[31,32] TiO_2 (~4.15eV),[33] Ti (4.3eV),[30] n-dopes the graphene. Within that scope, we propose that the low work function of AlO_x reduces the work function of graphene and consequently improves the Schottky barrier height (Φ_b). Indeed from

Table 5.2: Raman spectroscopy analysis of graphene used in this chapter. Bare graphene on glass and bare Gr on SiO_2 samples are used as reference.

	2D peak	**G peak**	**I_{2D}/I_G**	**FWHM (2D)**
Bare Gr on Glass	2673 (±2)	1583 (±2)	2.4	39 (±1)
HF treated Gr on Glass	2660 (±3)	1579 (±2)	2.1	51 (±2)
Bare Gr on SiO_2	2683 (±2)	1583 (±1)	4	32 (±1)
AlO_x coated Gr on SiO_2	2658 (±2)	1575 (±2)	3	47 (±1)

the dark ln(*J*)-*V* analysis presented in Figure 5.11a, it is estimated that Φ_b increases to 704 meV for the AlO_x/HF/Gr/p-Si solar cell as compared to the 572 meV of HF/Gr/p-Si solar cell, in accord with the observed 114mV increase in V_{oc} upon AlO_x coating. It should be noted that compared to the reported Φ_b values for Gr/n-Si solar cells, the highest obtained Φ_b here is significantly lower while the V_{oc} still compatible with Gr/n-Si solar cells. This might indicate that a higher V_{oc} can be obtained in a Gr/p-Si solar cell. Additionally, from Eqn. (1), we can deduce[17]

$$\frac{D(V)}{D(\ln(J))} = R_s A_{eff} J + \frac{n}{\beta} \qquad (3)$$

Where R_s is the series resistance A_{eff} is the diode effective area, n is the ideality factor and β is the q/k_BT. From the slope of Figure 5.11b, we estimate that the R_s of our solar cell reduced from 1.03Ωcm^2 to 0.62Ωcm^2. Such reduced R_s upon AlO_x deposition is attributed the observed *FF* enhancement.

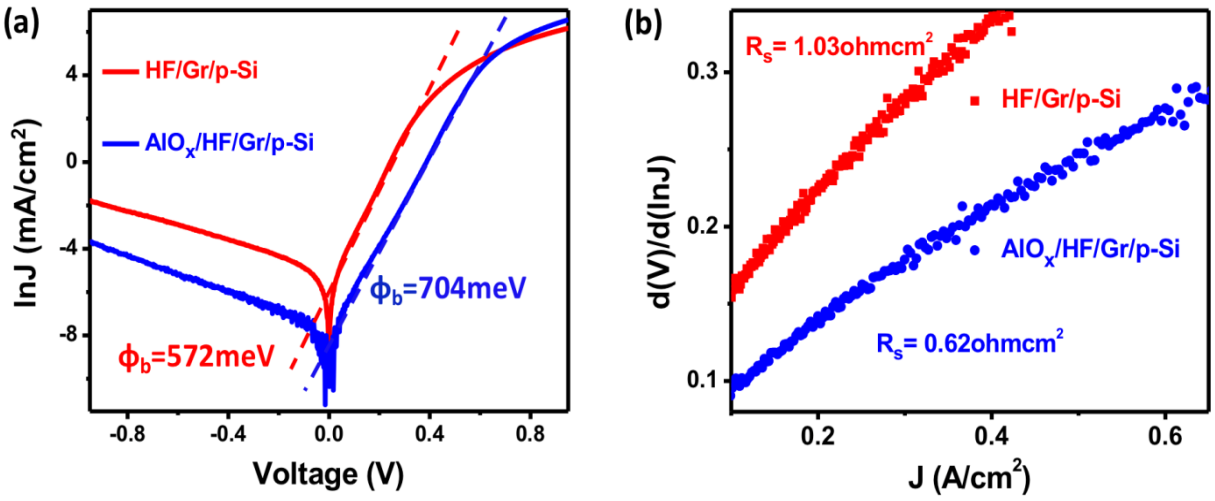

Figure 5.11: (a) Dark ln(*J*)-*V* curve of solar cells ad corresponding Φ_b of solar cells. (b) *dV/d(ln(J))-J* curve indicates the series resistance is reduced upon AlO_x deposition.

Since one of the purposes of AlO_x was to prevent the degradation of solar cell PCE, we tested AlO_x/HF/Gr/p-Si solar cell over the period of two months without any further encapsulation. We did not observe any noticeable degradation for AlO_x encapsulated solar cells (AlO_x/HF/Gr/p-Si) which seem to be a remarkable improvement over previous works which indicated a stability around two weeks.[21,26,49,108] A comparison of the reported stabilities of solar cells, from literature, (in the form of normalized PCE vs time) is presented in Figure 5.12. Compared to reported techniques, such as spin coating, spray coating, the highly conformal, controllable, uniform, non-destructive and air stability of ALD-AlO_x is promising for Gr/Si solar cells as well encapsulation of graphene based electronic devices. Since exposure of graphene with the ambient air significantly changes its electronic structure, carrier type and doping concentration (as discussed in chapter 4), preventing such an exposure through atomically controllable deposition technique may broaden the use of graphene for different electronic applications.

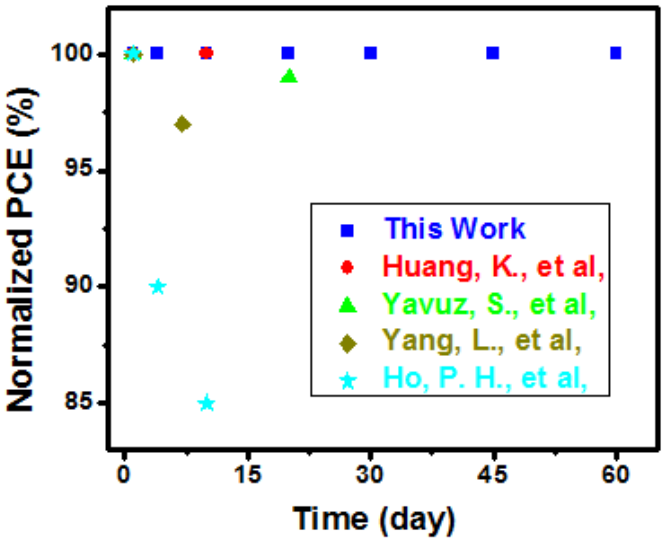

Figure 5.12: A comparison of reported stability for Gr/Si solar cells in the form of normalized PCE versus time is presented.[21,49,79,108]

5.5 Conclusion

In summary, we have reported a record PCE of 12.5% for an n-doped graphene/p-Silicon solar cell, through simple and cost-effective processing. A simple HF treatment was shown to be significantly improves the PCE around 60 times from 0.1% to 6%. The efficiency of deploying an ALD-AlO_x coating for multiple purposes, i.e.,(i) as an ARC, as well as (ii) n-dopant for the Gr is a highlight. The AlO_x coating also confers exceptional stability to the solar cell in ambient conditions, over the period of testing of two months. Further improvement in the V_{oc} as well as PCE of the indicated solar cells may be accomplished through a further reduction of Gr work function, e.g., through use of CsF. As highlighted, the one of the limiting factor of our solar cell is the low Note that there is no intentional front and back surface passivation in our solar cell. Significance of surface passivation on solar cell performance has been investigated recently. Applying such passivation procedures to Gr/p-Si solar cell expected to improve the PCE even further.

Chapter 5, in part, has been submitted to Nano Letters which titled "Improved conversion efficiency and stability, through the use of aluminum oxide, in an n-graphene/p-silicon solar cell" by Serdar Yavuz, Erick M. Loran, Nirjhar Sarkar, David P. Fenning and Prabhakar R. Bandaru. The dissertation/thesis author was the primary investigator and author of this paper.

CHAPTER 6: FUTURE DIRECTIONS FOR GRAPHENE/SILICON SOLAR CELLS

6.1 Introduction

After first demonstration in 2010, the efficiency of Gr/Si solar cell increased more than an order, reaching up to 17%. Such a significant enhancement indicates that a higher PCE can be obtained in Gr/Si solar cells. It is obvious that reducing the sheet resistance of graphene is one of the most critical aspects for its photovoltaic applications. While the sheet resistance as low as 30Ω/□ has been demonstrated for multilayer graphene[109] the sheet resistance of single layer graphene is still high to be used as an effective carrier collector. This chapter will highlight some of the possible directions for possible PCE improvements in Gr/Si solar cells. In addition to addressing the sheet resistance of graphene, applying below mentioned approaches expected to increase PCE even further.

6.2 Effective doping of graphene

Due to the natural p-doping by ambient exposure, Gr is adjusted to on top of n-silicon in early Gr/Si solar cells. This is followed by further p-doping of graphene as discuss in previous Chapters. While theoretical upper limit of the graphene work function (W_{Gr}) is still a discussion, the experimental results obtained so far indicated ~ 5.1eV for p-Gr. Considering the V_{oc} is also a factor of W_{Gr}, a more effective p-doping say through a material that has higher work function (W_m> 5.5eV) can be implemented to Gr/n-Si solar cells. Combined with earlier doping strategies such as air exposure, acidic doping, incorporation of a higher work function material expected to increase the Schottky barrier and enhance the V_{oc} so as the PCE.

Alternatively, a work function of 3.25 eV of Gr upon doping with CsF was experimentally demonstrated.[31]Such a low W_{Gr} indicates a possible Φ_b between the Gr and p-

silicon that is larger than the band gap of Silicon, i.e., Φ_b>1.1 eV. This implies that a built in potential up to 1.1eV can be obtained through a modified doping. In turn, as discussed in Chapter2, a higher V_{oc} can be obtained when Gr incorporated with a p-silicon.

6.3 Surface passivation for graphene silicon solar cells

Progress in characterization techniques revealed the importance of the controlling the surfaces and interfaces of materials for optical and electrical applications. Being able to monitor carriers movement in a material and/or interfaces enable scientists to understand and address the possible loss mechanisms for photo generated carriers in solar cells. In general, created electron-hole pairs in a solar cell either lost inside the material with bulk recombination or at the surface via surface recombination. As briefly discussed in Chapter 4, reducing the losses at the interfaces is one of the key factors for high efficiency solar cells. Along with the precise control of thin film depositions in atomic scale, a significant progress in reducing the interface related losses in solar cells have been studied which brought the PCE of silicon based p-n junction solar cells close to the theoretical limits[88,110,111]

While different surface passivation techniques have been extensively investigated for p-n junction solar cells such as passivated emitter and rear cell (PERC), passivated emitter, rear locally-doped (PERL), and passivated emitter, rear totally-doped (PERT), the Gr/Si solar cells is still suffer from lack of such passivation schemes. As detailed in Chapter 3, a simple SiO_x back surface passivation significantly improved the PCE. However, a more effective passivation schemes and materials can be applied to the back contact of Gr/Si solar cell. For example, PECVD silicon nitrate (SiN_x) which has known to have positive fix charges, can be more

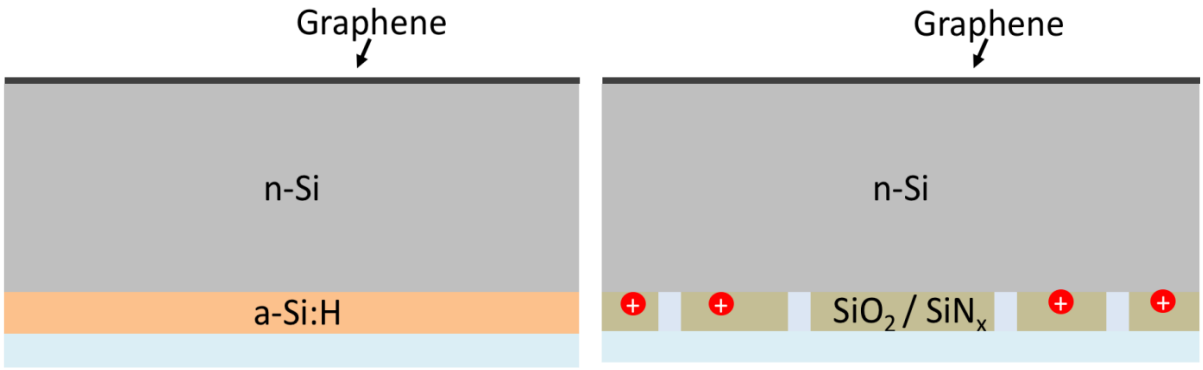

Figure 6.1: Possible back surface passivation schemas for Gr/n-Si solar cells

effective by inducing a field effect passivation in Gr/n-Si solar cell where the photo generated electrons collected through the back contact to silicon. Such a passivation scheme can be applied both as TOPcon[73] and PERL[112,113] approaches.

On the other hand, an ALD-AlO_x can be an effective back surface passivation for Gr/p-Si solar cell. In such an approach, the negative fix charges in ALD-AlO_x can significantly reduce the recombination at the back surface due to field effect passivation. Alternatively, the superior chemical passivation quality of amorphous silicon (a-Si:H), which improved PCE of crystalline silicon solar cell above 26%,[88] can be introduced the Gr/Si solar cells.

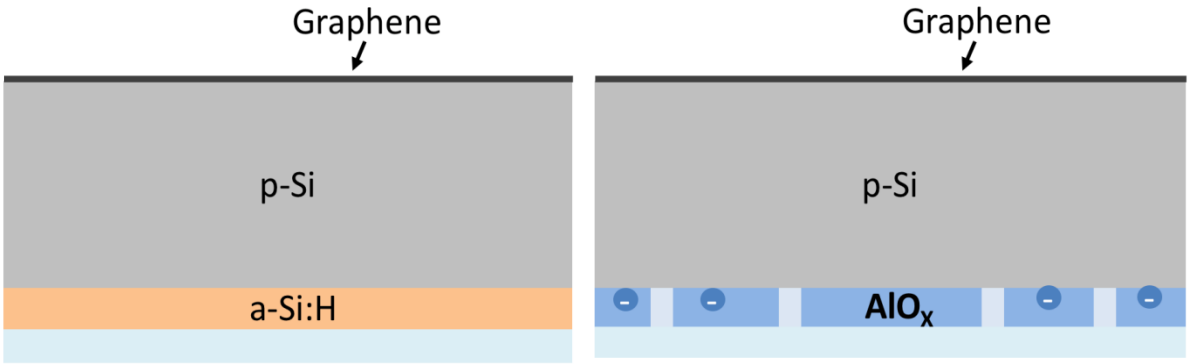

Figure 6.2: Possible back surface passivation schemas for Gr/p-Si solar cells.

Although the back surface passivation can be implemented by following the foot prints of p-n junction solar cells, the front surface passivation needs to be considered carefully. Since Gr is atomically thin, the incorporation of graphene with other materials significantly alters its electrical properties through doping, as discussed in Chapter 4. In the case of Gr/n-Si solar cell a material that can serve both p-doping for Gr as well as an effective passivation for n-silicon should be ideal. Such a material would provide a higher Φ_b as well as passivation benefit. On the other hand, both an n dopant for Gr and a coherent passivation for p-silicon is expected to significantly improve the PCE due to the similar reason.

6.4Impact of wafer quality

Even though understanding and improving the electrical behavior of graphene is the most critical aspect of Gr/Si solar cells, the overall efficiency of solar cell is also depend on the quality of the underlying silicon. Since the PCE of solar cell limited with the recombination of carriers,[38,39,114] a wafer with a longer lifetime such as in the order of ms would expected to improve the reported efficiencies in this thesis. As indicated in chapter 4, the effective lifetime of the carriers is measured as ~75μs which is significantly limits the PCE of reported solar cell. Incorporating graphene with the long lifetime wafers that are used in high efficiency silicon p-n junction counterparts[88,115]can reveal the performance of Gr/Si solar cell.

In addition, the doping concentration of silicon might be relevant topic to investigate. As indicated in chapter 2, equation 2.2, the Schottky barrier height is also depend on the doping concentration of silicon. Within that scope, a systematic study of effect of silicon doping concentration on Gr/Si solar cell efficiency can be helpful to understand the Gr/Si Schottky junction formation.

6.5 Conclusion

While Gr/Si solar cells are still a laboratory based research, the progress achieved less than a decade indicates they can be one of the chains of clean energy production in future. It is, of course, obvious that extensive research is needed to understand the whole nature of graphene. Once this is accomplished, graphene is expected to have much broader application as a transparent conductive electrode as well as many other opti-electrical applications.

In addition to improving the PCE of graphene silicon solar cells to a record efficiency, to date, this thesis led to the following conclusions:

1- Graphene can be used both as a hole extraction layer as well as an electron extraction layer on top of silicon.
2- Graphene oxide can be used as a p-doping of graphene as well as an ARC with a suitable thickness
3- Graphene/silicon solar can have as high fill factor as a p-n junction solar cell when the sheet resistance of graphene is reduced the state-of-art emitters.
4- A stable n-type doped graphene can be obtained for electronic applications through ALD alumina oxide deposition which will broaden the use of graphene in future.

REFERENCES

(1) Green, M. A.; Hishikawa, Y.; Dunlop, E. D.; Levi, D. H.; Hohl-Ebinger, J.; Ho-Baillie, A. W. Y. Solar Cell Efficiency Tables (Version 51). *Prog. Photovoltaics Res. Appl.* **2018**, *26* (1), 3–12.

(2) Shockley, W. The Theory of P-N Junctions in Semiconductors and P-N Junction Transistors. *Bell Syst. Tech. J.* **1948**, *28*, 435–489.

(3) McIntosh, K. Lumps, Humps and Bumps : Three Detrimental Effects in the Current-Voltage Curve of Silicon Solar Cells, University of New South Wales, 2001.

(4) Araujo, G. .; Sánchez, E. Analytical Expressions for the Determination of the Maximum Power Point and the Fill Factor of a Solar Cell. *Sol. Cells* **1982**, *5*, 377–386.

(5) Sanchez, E.; Araojo, G. L. On the Analytical Determination of Solar Cell Fill Factor and Efficiency. *Sol. Cells* **1987**, *20*, 1–11.

(6) Green, M. A. Accurate Expression for Solar Cell Fill Factors Including Series and Shunt Resistance. *Applait Phys. Lett.* **2016**, *108*, 81111-1–5.

(7) Li, X.; Zhu, H.; Wang, K.; Cao, A.; Wei, J.; Li, C.; Jia, Y.; Li, Z.; Li, X.; Wu, D. Graphene-on-Silicon Schottky Junction Solar Cells. *Adv. Mater.* **2010**, *22* (25), 2743–2748.

(8) Geim, A. K.; Novoselov, K. S. The Rise of Graphene. *Nat. Mater.* **2007**, *6* (3), 183–191.

(9) Bae, S.; Kim, H.; Lee, Y.; Xu, X.; Park, J.-S.; Zheng, Y.; Balakrishnan, J.; Lei, T.; Ri Kim, H.; Song, Y. Il; Kim, Y.-J.; Kim, K. S.; Özyilmaz, B.; Ahn, J.-H.; Hong, B. H.; Iijima, S. Roll-to-Roll Production of 30-Inch Graphene Films for Transparent Electrodes. *Nat. Nanotechnol.* **2010**, *5* (8), 574–578.

(10) Anderson, W. A.; Delahoy, A. E.; Milano, R. A. An 8% Efficient Layered Schottky-Barrier Solar Cell. *J. Appl. Phys.* **1974**, *45* (9), 3913–3915.

(11) Mead, C. A.; Spitzer, W. G. Fermi Level Position at Metal Semicondconductor Interfaces. *Phys. Rev. Lett.* **1964**, *134*, 21.

(12) Lillington, D. R.; Townsend, W. G. Effects of Interfacial Oxide Layers on the Performance of Silicon Schottky-Barrier Solar Cells. *Appl. Phys. Lett.* **1976**, *28* (2), 97–98.

(13) Godfrey, R. B.; Green, M. A. 655 mV Open-Circuit Voltage, 17.6% Efficient Silicon MIS Solar Cells. *Appl. Phys. Lett.* **1979**, *34* (11), 790–793.

(14) Hezel, R. High Efficiency Inversion Layer Solar Cells on Polycrystalline Silicon by the Application of Silicon Nitride. *Electron Devices, IEEE Trans.* **1981**, No. 12, 1466–1469.

(15) Hezel, R.; Meyer, R.; Metz, A. New Generation of Crystalline Silicon Solar Cells: Simple Processing and Record Efficiencies for Industrial-Size Devices. *Sol. Energy Mater. Sol. Cells* **2001**, *65* (1), 311–316.

(16) Miao, X.; Tongay, S.; Petterson, M. K.; Berke, K.; Rinzler, A. G.; Appleton, B. R.; Hebard, A. F. High Efficiency Graphene Solar Cells by Chemical Doping. *Nano Lett.* **2012**, *12* (6), 2745–2750.

(17) Cheung, S. K., and Cheung N.W. Extraction of Schottky Diode Parameters from Forward Current-Voltage Characteristics Extraction of Schottky Diode Parameters from Forward Current-Voltage Characteristics. *Appl. Phys. Lett.* **1986**, *85* (49), 85–87.

(18) Jiao, K.; Wang, X.; Wang, Y.; Chen, Y. Graphene Oxide as an Effective Interfacial Layer for Enhanced Graphene/silicon Solar Cell Performance. *J. Mater. Chem. C* **2014**, *2* (37), 7715.

(19) Liu, X.; Zhang, X. W.; Yin, Z. G.; Meng, J. H.; Gao, H. L.; Zhang, L. Q.; Zhao, Y. J.; Wang, H. L. Enhanced Efficiency of Graphene-Silicon Schottky Junction Solar Cells by Doping with Au Nanoparticles. *Appl. Phys. Lett.* **2014**, *105* (18), 183901.

(20) Shi, E.; Li, H.; Yang, L.; Zhang, L.; Li, Z.; Li, P.; Shang, Y.; Wu, S.; Li, X.; Wei, J.; Wang, K.; Zhu, H.; Wu, D.; Fang, Y.; Cao, A. Colloidal Antireflection Coating Improves Graphene-Silicon Solar Cells. *Nano Lett.* **2013**, *13* (4), 1776–1781.

(21) Yavuz, S.; Kuru, C.; Choi, D.; Kargar, A.; Jin, S.; Bandaru, P. R. Graphene Oxide as a P-Dopant and an Anti-Reflection Coating Layer, in Graphene/silicon Solar Cells. *Nanoscale* **2016**, *2* (9), 6473–6478.

(22) Geim, A. K.; Novoselov, K. S. The Rise of Graphene. *Nat. Mater.* **2007**, 183–191.

(23) Ricciardulli, A. G.; Yang, S.; Feng, X.; Blom, P. W. M. Solution-Processable High-Quality Graphene for Organic Solar Cells. *ACS Appl. Mater. Interfaces* **2017**, *9* (30), 25412–25417.

(24) Miao, X.; Tongay, S.; Petterson, M. K.; Berke, K.; Rinzler, A. G.; Appleton, B. R.; Hebard, A. F. High Efficiency Graphene Solar Cells by Chemical Doping. *Nano Lett.* **2012**, *12* (6), 2745–2750.

(25) Lin, Y.; Li, X.; Xie, D.; Feng, T.; Chen, Y.; Song, R.; Tian, H.; Ren, T.; Zhong, M.; Wang, K.; Zhu, H. Graphene/semiconductor Heterojunction Solar Cells with Modulated Antireflection and Graphene Work Function. *Energy Environ. Sci.* **2013**, *6* (1), 108.

(26) Ho, P. H.; Yeh, Y. C.; Wang, D. Y.; Li, S. S.; Chen, H. A.; Chung, Y. H.; Lin, C. C.; Wang, W. H.; Chen, C. W. Self-Encapsulated Doping of N-Type Graphene Transistors with Extended Air Stability. *ACS Nano* **2012**, *6* (7), 6215–6221.

(27) Kim, H.; Kim, H. H.; Jang, J. I.; Lee, S. K.; Lee, G.-W.; Han, J. T.; Cho, K. Doping Graphene with an Atomically Thin Two Dimensional Molecular Layer. *Adv. Mater.* **2014**, *26* (48), 8141–8146.

(28) Wei, B.; Yamamoto, S.; Ichikawa, M.; Li, C.; Fukuda, T.; Taniguchi, Y. High-Efficiency Transparent Organic Light-Emitting Diode with One Thin Layer of Nickel Oxide on a Transparent Anode for See-through-Display Application. *Semicond. Sci. Technol.* **2007**, *22* (7), 788–792.

(29) Kuru, C.; Yavuz, S.; Kargar, A.; Choi, D.; Choi, C.; Rustomji, C.; Jin, S.; Bandaru, P. R. Enhanced Power Conversion Efficiency of Graphene/Silicon Heterojunction Solar Cells Through NiO Induced Doping. *J. Nanosci. Nanotechnol.* **2016**, *16* (1), 1190–1193.

(30) Iqbal, M. W.; Singh, A. K.; Iqbal, M. Z.; Eom, J. Raman Fingerprint of Doping due to Metal Adsorbates on Graphene. *J. Phys. Condens. Matter* **2012**, *24* (33), 335301.

(31) Chang, J. K.; Lin, W. H.; Taur, J. I.; Chen, T. H.; Liao, G. K.; Pi, T. W.; Chen, M. H.; Wu, C. I. Graphene Anodes and Cathodes: Tuning the Work Function of Graphene by Nearly 2 eV with an Aqueous Intercalation Process. *ACS Appl. Mater. Interfaces* **2015**, *7* (31), 17155–17161.

(32) Zhang, Y.; Chen, L.; Hu, X.; Zhang, L.; Chen, Y. Low Work-Function Poly(3,4-Ethylenedioxylenethiophene): Poly(styrene Sulfonate) as Electron-Transport Layer for High-Efficient and Stable Polymer Solar Cells. *Sci. Rep.* **2015**, *5* (August), 1–12.

(33) Imanishi, A.; Tsuji, E.; Nakato, Y. Dependence of the Work Function of TiO2 (Rutile) on Crystal Faces, Studied by a Scanning Auger Microprobe. *J. Phys. Chem. C* **2007**, *111* (5), 2128–2132.

(34) Das, A.; Pisana, S.; Chakraborty, B.; Piscanec, S.; Saha, S. K.; Waghmare, U. V.; Novoselov, K. S.; Krishnamurthy, H. R.; Geim, A. K.; Ferrari, A. C.; Sood, A. K. Monitoring Dopants by Raman Scattering in an Electrochemically Top-Gated Graphene Transistor. *Nat. Nanotechnol.* **2008**, *3* (4), 210–215.

(35) Kalbac, M.; Reina-Cecco, A.; Farhat, H.; Kong, J.; Kavan, L.; Dresselhaus, M. S. The

Influence of Strong Electron and Hole Doping on the Raman Intensity of Chemical Vapor-Deposition Graphene. *ACS Nano* **2010**, *4* (10), 6055–6063.

(36) Bruna, M.; Ott, A. K.; Ijäs, M.; Yoon, D.; Sassi, U.; Ferrari, A. C. Doping Dependence of the Raman Spectrum of Defected Graphene. *ACS Nano* **2014**, *8* (7).

(37) Heydrich, S.; Hirmer, M.; Preis, C.; Korn, T.; Eroms, J.; Weiss, D.; Sch??ller, C.; Iqbal, M. W. Z.; Singh, A. K.; Iqbal, M. W. Z.; Eom, J. Raman Fingerprint of Doping due to Metal Adsorbates on Graphene. *J. Phys. Condens. Matter* **2010**, *97* (4), 2008–2011.

(38) Tiedje, T.; Yablonovitch, E.; Cody, G. D.; Brooks, B. G. Limiting Efficiency of Silicon Solar Cells. *IEEE Trans. Electron Devices* **1984**, *ED-31(5)* (711–716).

(39) Kerr, M. J.; Cuevas, A.; P., C. Limiting Efficiency of Crystalline Silicon Solar Cells Due to Coulomb-Enhanced Auger Recombination. *Prog. Photovoltaics Res. Appl.* **2003**, *11*, 97–104.

(40) Novoselov, K. S.; Geim, A. K.; Morozov, S. V; Jiang, D.; Zhang, Y.; Dubonos, S. V; Grigorieva, I. V; Firsov, A. A. Electric Field Effect in Atomically Thin Carbon Films. *Science* **2004**, *306* (5696), 666–669.

(41) Reddy, A. L. M.; Srivastava, A.; Gowda, S. R.; Gullapalli, H.; Dubey, M.; Ajayan, P. M. Synthesis of Nitrogen-Doped Graphene Films for Lithium Battery Application. *ACS Nano* **2010**, *4* (11), 6337–6342.

(42) Liu, C.; Yu, Z.; Neff, D.; Zhamu, A.; Jang, B. Z. Graphene-Based Supercapacitor with an Ultrahigh Energy Density. *Nano Lett.* **2010**, *10* (12), 4863–4868.

(43) Zhu, Y.; Murali, S.; Cai, W.; Li, X.; Suk, J. W.; Potts, J. R.; Ruoff, R. S. Graphene and Graphene Oxide: Synthesis, Properties, and Applications. *Adv. Mater.* **2010**, *22* (35), 3906–3924.

(44) An, X.; Liu, F.; Jung, Y. J.; Kar, S. Tunable Graphene-Silicon Heterojunctions for Ultrasensitive Photodetection. *Nano Letters*. 2013, pp 909–916.

(45) Fowler, J. D.; Allen, M. J.; Tung, V. C.; Yang, Y.; Kaner, R. B.; Weiller, B. H. Practical Chemical Sensors from Chemically Derived Graphene. *ACS Nano* **2009**, *3* (2), 301–306.

(46) Lv, P.; Zhang, X.; Zhang, X.; Deng, W.; Jie, J. High-Sensitivity and Fast-Response Graphene/crystalline Silicon Schottky Junction-Based near-IR Photodetectors. *IEEE Electron Device Lett.* **2013**, *34* (10), 1337–1339.

(47) Reina, A.; Jia, X.; Ho, J.; Nezich, D.; Son, H.; Bulovic, V.; Dresselhaus, M. S.; Jing, K.;

Kong, J. LETTERS Large Area , Few-Layer Graphene Films on Arbitrary Substrates by Chemical Vapor Deposition. *Nano Lett.* **2009**, *xx* (x), 30–35.

(48) An, X.; Liu, F.; Kar, S. Optimizing Performance Parameters of Graphene–silicon and Thin Transparent Graphite–silicon Heterojunction Solar Cells. *Carbon N. Y.* **2013**, *57*, 329–337.

(49) Yang, L.; Yu, X.; Hu, W.; Wu, X.; Zhao, Y.; Yang, D. An 8.68% Efficiency Chemically-Doped-Free Graphene–Silicon Solar Cell Using Silver Nanowires Network Buried Contacts. *ACS Appl. Mater. Interfaces* **2015**, 150210153736004.

(50) Garnett, E.; Yang, P. Light Trapping in Silicon Nanowire Solar Cells. *Nano Lett.* **2010**, *10* (3), 1082–1087.

(51) Watcharotone, S.; Dikin, D. A.; Stankovich, S.; Piner, R.; Jung, I.; Dommett, G. H. B.; Evmenenko, G.; Wu, S.-E.; Chen, S.-F.; Liu, C.-P.; Nguyen, S. T.; Ruoff, R. S. Graphene-Silica Composite Thin Films as Transparent Conductors. *Nano Lett.* **2007**, *7* (7), 1888–1892.

(52) Marcano, D. C.; Kosynkin, D. V; Berlin, J. M.; Sinitskii, A.; Sun, Z.; Slesarev, A.; Alemany, L. B.; Lu, W.; Tour, J. M. Improved Synthesis of Graphene Oxide. *ACS Nano* **2010**, *4* (8), 4806–4814.

(53) Ruan, K.; Ding, K.; Wang, Y.; Diao, S.; Shao, Z.; Zhang, X.; Jie, J. Flexible Graphene/silicon Heterojunction Solar Cells. *J. Mater. Chem. A* **2015**, *0*, 1–8.

(54) Cheung, S. K.; Cheung, N. W. Extraction of Schottky Diode Parameters from Forward Current-Voltage Characteristics. *Appl. Phys. Lett.* **1986**, *49* (2), 85.

(55) Sinha, D.; Lee, J. U. Ideal Graphene/silicon Schottky Junction Diodes. *Nano Lett.* **2014**, *14*, 4660–4664.

(56) How, G. T. S.; Pandikumar, A.; Ming, H. N.; Ngee, L. H. Highly Exposed {001} Facets of Titanium Dioxide Modified with Reduced Graphene Oxide for Dopamine Sensing. *Sci. Rep.* **2014**, *4*, 5044.

(57) Cui, P.; Lee, J.; Hwang, E.; Lee, H. One-Pot Reduction of Graphene Oxide at Subzero Temperatures. *Chem. Commun.* **2011**, *47* (45), 12370.

(58) Pisana, S.; Lazzeri, M.; Casiraghi, C.; Novoselov, K. S.; Geim, A. K.; Ferrari, A. C.; Mauri, F. Breakdown of the Adiabatic Born-Oppenheimer Approximation in Graphene. *Nat. Mater.* **2007**, *6* (3), 198–201.

(59) Shim, J.; Lui, C. H.; Ko, T. Y.; Yu, Y. J.; Kim, P.; Heinz, T. F.; Ryu, S. Water-Gated Charge Doping of Graphene Induced by Mica Substrates. *Nano Lett.* **2012**, *12*, 648–654.

(60) Becerril, H. A.; Mao, J.; Liu, Z.; Stoltenberg, R. M.; Bao, Z.; Chen, Y. Evaluation of Solution-Processed Reduced Graphene Oxide Films as Transparent Conductors. *ACS Nano* **2008**, *2* (3), 463–470.

(61) Compton, O. C.; Nguyen, S. T. Graphene Oxide, Highly Reduced Graphene Oxide, and Graphene: Versatile Building Blocks for Carbon-Based Materials. *Small* **2010**, *6* (6), 711–723.

(62) Saleh, B. E. A.; Teich, M. C. *Fundamentals of Photonics*, 2nd ed.; Saleh, B. E. A., Ed.; John Wiley & Sons : Hoboken, NJ, 2007.

(63) Raut, H. K.; Ganesh, V. A.; Nair, A. S.; Ramakrishna, S. Anti-Reflective Coatings: A Critical, in-Depth Review. *Energy Environ. Sci.* **2011**, *4* (10), 3779.

(64) Sun, C.-H.; Jiang, P.; Jiang, B. Broadband Moth-Eye Antireflection Coatings on Silicon. *Appl. Phys. Lett.* **2008**, *92* (6), 61112.

(65) Jung, I.; Vaupel, M.; Pelton, M.; Pinery, R.; Dikin, D. A.; Stankovich, S.; An, J.; Ruoff, R. S. Characterization of Thermally Reduced Graphene Oxide by Imaging Ellipsometry. *J. Phys. Chem. C* **2008**, *112* (23), 8499–8506.

(66) Song, Y.; Li, X.; Mackin, C.; Zhang, X.; Fang, W.; Palacios, T.; Zhu, H.; Kong, J. Role of Interfacial Oxide in High-Efficiency Graphene-Silicon Schottky Barrier Solar Cells. *Nano Lett.* **2015**, *15* (3), 2104–2110.

(67) Xie, C.; Zhang, X.; Ruan, K.; Shao, Z.; Dhaliwal, S. S.; Wang, L.; Zhang, Q.; Zhang, X.; Jie, J. High-Efficiency, Air Stable graphene/Si Micro-Hole Array Schottky Junction Solar Cells. *J. Mater. Chem. A* **2013**, *1* (48), 15348.

(68) Das Sharma, S.; Adam, S.; Hwang, E. H.; Rossi, E. Electronic Transport in Two-Dimensional Graphene. *Rev. Mod. Phys.* **2011**, *83*, 407.

(69) Castro Neto, A. H.; Guinea, F.; Peres, N. M. R.; Novoselov, K. S.; Geim, A. K. The Electronic Properties of Graphene. *Rev. Mod. Phys.* **2009**, *81* (1), 109–162.

(70) Li, X.; Zhu, Y.; Cai, W.; Borysiak, M.; Han, B.; Chen, D.; Piner, R. D.; Colomba, L.; Ruoff, R. S. Transfer of Large-Area Graphene Films for High-Performance Transparent Conductive Electrodes. *Nano Lett.* **2009**, *9* (12), 4359–4363.

(71) Oh, J.; Yuan, H.-C.; Branz, H. M. An 18.2%-Efficient Black-Silicon Solar Cell Achieved

through Control of Carrier Recombination in Nanostructures. *Nat. Nanotechnol.* **2012**, *7*, 743–748.

(72) Nelson, J. *The Physics of Solar Cells*; Imperial College Press: London, UK, 2003.

(73) Feldmann, F.; Bivour, M.; Reichel, C.; Steinkemper, H.; Hermle, M.; Glunz, S. W. Tunnel Oxide Passivated Contacts as an Alternative to Partial Rear Contacts. *Sol. Energy Mater. Sol. Cells* **2014**, *131*, 46–50.

(74) Takahashi, A. I.; Kobayashi, H. Nitric Acid Oxidation of Silicon at Electrical Characteristics Nitric Acid Oxidation of Silicon at È 120 ° C to Form 3 . 5-Nm SiO 2 / Si Structure with Good Electrical Characteristics. *Appl. Phys. Lett.* **2004**, *85* (3783), 5–8.

(75) Asuha, H. K.; Maida, O.; Takahashi, M.; Iwasa, H.; Kobayashi, H.; Maida, O.; Takahashi, M.; Iwasa, H. Nitric Acid Oxidation of Si to Form Ultrathin Silicon Dioxide Layers with a Low Leakage Current Density Nitric Acid Oxidation of Si to Form Ultrathin Silicon Dioxide Layers with a Low Leakage Current Density. *J. Appl. Phys.* **2003**, *94* (2003), 7328.

(76) Agostinelli, G.; Delabie, A.; Vitanov, P.; Alexieva, Z.; Dekkers, H. F. W.; De Wolf, S.; Beaucarne, G. Very Low Surface Recombination Velocities on P-Type Silicon Wafers Passivated with a Dielectric with Fixed Negative Charge. *Sol. Energy Mater. Sol. Cells* **2006**, *90* (18–19), 3438–3443.

(77) De, S.; Coleman, J. N. Are There Fundamental Limitations on the Sheet Resistance and Transmittance of Thin Graphene Films? *ACS Nano* **2010**.

(78) Fowles, G. R. *Introduction to Modern Optics*, 2nd ed.; Dover Publications: New York, NY, 1975.

(79) Ho, P.-H.; Lee, W.-C.; Liou, Y.-T.; Chiu, Y.-P.; Shih, Y.-S.; Chen, C.-C.; Su, P.-Y.; Li, M.-K.; Chen, H.-L.; Liang, C.-T.; Chen, C.-W. Sunlight-Activated Graphene-Heterostructure Transparent Cathodes: Enabling High-Performance N-Graphene/p-Si Schottky Junction Photovoltaics. *Energy Environ. Sci.* **2015**, *8*, 2085–2092.

(80) Li, R.; Di, J.; Yong, Z.; Sun, B.; Li, Q. Polymethylmethacrylate Coating on Aligned Carbon Nanotube – Silicon Solar Cells for Performance. *J. Mater. Chem. A* **2014**, *2*, 4140–4143.

(81) Ryu, S.; Liu, L.; Berciaud, S.; Yu, Y.; Liu, H.; Kim, P.; Flynn, G. W.; Brus, L. E. Atmospheric Oxygen Binding and Hole Doping in Deformed Graphene on a SiO 2 Substrate. *Nano Lett.* **2010**, *10*, 4944–4951.

(82) Liu, L.; Ryu, S.; Tomasik, M. R.; Stolyarova, E.; Jung, N.; Hybertsen, M. S.; Steigerwald, M. L.; Brus, L. E.; Flynn, G. W. Graphene Oxidation : Thickness-Dependent Etching and Strong Chemical Doping 2008. *Nano Lett.* **2008**, *8* (7), 1965–1970.

(83) Kerr, M. J.; Cuevas, A.; Kerr, M. J.; Cuevas, A. Recombination at the Interface between Silicon and Stoichiometric Plasma Silicon Nitride. *Semicond. Sci. Technol* **2002**, *17*, 166–172.

(84) Macdonald, D.; Cuevas, A. Reduced Fill Factors in Multicrystalline Silicon Solar Cells due to Injection -Level Dependent Bulk Recombination Lifetimes. *Prog. Photovoltaics Res. Appl.* **2000**, *8*, 363–375.

(85) Larionova, Y.; Mertens, V.; Harder, N.-P.; Brendel, R. Surface Passivation of N-Type Czochralski Silicon Substrates by Thermal-SiO2/plasma-Enhanced Chemical Vapor Deposition SiN Stacks. *Appl. Phys. Lett.* **2010**, *96* (3), 32105.

(86) Bonilla, R. S.; Reichel, C.; Hermle, M.; Senkader, S.; Wilshaw, P. Controlled Field Effect Surface Passivation of Crystalline N - Type Silicon and Its Application to Back - Contact Silicon Solar Cells. *IEEE* **2014**, *978* (1), 571–576.

(87) Battaglia, C.; Cuevas, A.; De Wolf, S.; Manuscript, A. High-Efficiency Crystalline Silicon Solar Cells: Status and Perspectives. *Energy Environ. Sci.* **2016**, *9*.

(88) Yoshikawa, K.; Kawasaki, H.; Yoshida, W.; Irie, T.; Konishi, K.; Nakano, K.; Uto, T.; Adachi, D.; Kanematsu, M.; Uzu, H.; Yamamoto, K. Silicon Heterojunction Solar Cell with Interdigitated Back Contacts for a Photoconversion Efficiency over 26%. *Nat. Energy* **2017**, *2* (17032), 1–8.

(89) Imamura, K.; Takahashi, M.; Hirayama, Y.; Imai, S. Nitric Acid Oxidation of Si Method at Nitric Acid Oxidation of Si Method at 120 ° C : HNO 3 Concentration. *J. Appl. Phys.* **2010**, *107* (54503), 1–6.

(90) Ng, K. K.; Card, H. C. Photocurrent Supprssion and Interface State Recombination in MIS-Schottky Barriers. *IEEE Int. Electron Device Meet* **1977**, 57–61.

(91) Mcgill, J.; Kinmond, J. I. B. W.; Mcgill, J.; Wilson, J. I. B. The Interfacial Layer in MIS Amorphous Silicon Solar Cells. *J. Appl. Phys.* **1979**, *50* (1), 548–555.

(92) Schmidt, J.; Kerr, M.; Cuevas, A. Surface Passivation of Silicon Solar Cells Using Plasma-Enhanced Chemical-Vapour-Deposited SiN Films and Thin Thermal SiO 2 / Plasma SiN Stacks. *Semicond. Sci. Technol* **2001**, *16* (3), 164–170.

(93) Cuevas, A.; Russell, D. A. Co-Optimization of the Emitter Region and the Metal Grid of

Silicon Solar Cells. *Prog. Photovolt Res. Appl* **2000**, *8*, 603–616.

(94) Wu, Y.; Chen, L.; Wu, J.; Yehua, T.; Chunlan, Z.; Wenjing, W.; Wen, L.; Yueqiang, L.; Jianjun, C.; Peters, S.; Ballif, C.; Borchert, D.; Chen, N.; Tate, K.; Ebong, A.; Yupeng, X.; Peide, H.; Yujie, F.; Shuai, W. Optimization of the Emitter Region and the Metal Grid of a Concentrator Silicon Solar Cell. *J. Semicond.* **213AD**, *34* (5), 1–8.

(95) Rodrigues, A. M. Extraction of Schottky Diode Parameters from Current-Voltage Data for a Chemical- Vapor-Deposited Diamond / Silicon Structure over a Wide Temperature Range Extraction of Schottky Diode Parameters from Current-Voltage Data for a Chemical-Vapor-Deposited Di. *J. Appl. Phys.* **2008**, *103* (83708), 1–6.

(96) Zhang, X. X.; Xie, C.; Jie, J.; Wu, Y.; Zhang, W. High-Efficiency graphene/Si Nanoarray Schottky Junction Solar Cells via Surface Modification and Graphene Doping. *J. Mater. Chem. A* **2013**, *1* (22), 6593.

(97) Schroder, D. K. Carrier Lifetimes in Silicon. *IEEE Trans. Electron Devices* **1997**, *44*.

(98) Cha, M.-J.; Song, W.; Kim, Y.; Jung, D. S.; Jung, M. W.; Lee, S. Il; Adhikari, P. D.; An, K.-S.; Park, C.-Y. Long-Term Air-Stable N-Type Doped Graphene by Multiple Lamination with Polyethyleneimine. *RSC Adv.* **2014**, *4* (71), 37849.

(99) Sagade, A. A.; Neumaier, D.; Schall, D.; Otto, M.; Pesquera, A.; Centeno, A.; Elorza, A. Z.; Kurz, H. Highly Air Stable Passivation of Graphene Based Field Effect Devices. *Nanoscale* **2015**, *7* (8), 3558–3564.

(100) Kim, S.; Zhao, P.; Aikawa, S.; Einarsson, E.; Chiashi, S.; Maruyama, S. Highly Stable and Tunable N-Type Graphene Field-Effect Transistors with Poly(vinyl Alcohol) Films. *ACS Appl. Mater. Interfaces* **2015**, *7* (18), 9702–9708.

(101) Kim, D. J.; Kim, G. S.; Park, N. W.; Lee, W. Y.; Sim, Y.; Kim, K. S.; Seong, M. J.; Koh, J. H.; Hong, C. H.; Lee, S. K. Effect of Annealing of Graphene Layer on Electrical Transport and Degradation of Au/graphene/n-Type Silicon Schottky Diodes. *J. Alloys Compd.* **2014**, *612*, 265–272.

(102) Ferrari, A. C.; Meyer, J. C.; Scardaci, V.; Casiraghi, C.; Lazzeri, M.; Mauri, F.; Piscanec, S.; Jiang, D.; Novoselov, K. S.; Roth, S.; Geim, A. K. Raman Spectrum of Graphene and Graphene Layers. *Phys. Rev. Lett.* **2006**, *97* (18), 1–4.

(103) Lee, J.; Novoselov, K. S.; Shin, H. S. Interaction between Metal and Graphene Dependence on the Layer Number of Graphne. *ACS Nano* **2010**, *5* (1), 608–612.

(104) Sun, C.-H.; Jiang, P.; Jiang, B. Broadband Moth-Eye Antireflection Coatings on Silicon.

Cit. Appl. Phys. Lett. Appl. Phys. Lett. Phys. Lett. Appl. Phys. Lett. Phys. Lett. Phys. Lett **2008**, *92* (91), 61112–261102.

(105) Some, S.; Kim, J.; Lee, K.; Kulkarni, A.; Yoon, Y.; Lee, S.; Kim, T.; Lee, H. Highly Air-Stable Phosphorus-Doped N-Type Graphene Field-Effect Transistors. *Adv. Mater.* **2012**, *24* (40), 5481–5486.

(106) Yu. I. Semov. Work Function of Oxidized Metal Surfaces and Estimation of Al2O3 Film Band Stracture Parameters. *Phys. Status Solids - Rapid Res. Lett.* **1969**, *41*, 41–44.

(107) Yeo, Y. C.; King, T. J.; Hu, C. Metal-Dielectric Band Alignment and Its Implications for Metal Gate Complementary Metal-Oxide-Semiconductor Technology. *J. Appl. Phys.* **2002**, *92* (12), 7266–7271.

(108) Huang, K.; Yan, Y.; Yu, X.; Zhang, H.; Yang, D. Graphene Coupled with Pt Cubic Nanoparticles for High Performance, Air-Stable Graphene-Silicon Solar Cells. *Nano Energy* **2017**, *32* (December 2016), 225–231.

(109) Bae, S.; Kim, H.; Lee, Y.; Xu, X.; Park, J.-S.; Zheng, Y.; Balakrishnan, J.; Lei, T.; Ri Kim, H.; Il Song, Y.; Kim, Y.-J.; Kim, K. S.; Zyilmaz, B.; Ahn, J.-H.; Hee Hong, B.; Iijima, S. Roll-to-Roll Production of 30-Inch Graphene Films for Transparent Electrodes. *Nat. Nanotechnol.* **2010**, *5*, 574–578.

(110) Masuko, K.; Shigematsu, M.; Hashiguchi, T.; Fujishima, D.; Kai, M.; Yoshimura, N.; Yamaguchi, T.; Ichihashi, Y.; Mishima, T.; Matsubara, N.; Yamanishi, T.; Takahama, T.; Taguchi, M.; Maruyama, E.; Okamoto, S. Achievement of More Than 25% Conversion Efficiency With Crystalline Silicon Heterojunction Solar Cell. *IEEE J. Photovoltaics* **2014**, *4* (6), 1433–1435.

(111) Richter, A.; Glunz, S. W.; Richter, A.; Hermle, M.; Glunz, S. W. Reassessment of the Limiting Efficiency for Crystalline Silicon Solar Cells. *IEEE J. Phot.* **2013**, *3* (4), 1184–1191.

(112) Wang, A.; Zhao, J.; Green, M. A. 24% Efficient Silicon Solar Cells. *Appl. Phys. Lett.* **1990**, *57* (6), 602–604.

(113) Zhao, J.; Wang, A.; Green, M. A. 24.5% Efficiency Silicon PERT Cells on MCZ Substrates and 24.7% Efficiency PERL Cells on FZ Substrates. *Prog. Photovoltaics Res. Appl.* **1999**, *7* (6), 471–474.

(114) Shockley, W.; Queisser, H. J. Detailed Balance Limit of Efficiency of P-N Junction Solar Cells. *J. Appl. Phys.* **1961**, *32* (3), 510–519.

(115) Feldmann, F.; Bivour, M.; Reichel, C.; Steinkemper, H.; Hermle, M.; Glunz, S. W. Tunnel Oxide Passivated Contacts as an Alternative to Partial Rear Contacts. *Sol. Energy Mater. Sol. Cells* **2014**, *131*, 46–50.